Regularization-Based Fictitious Domain Methods

DISSERTATION
zur Erlangung des Grades eines Doktors
der Naturwissenschaften

vorgelegt von
Dipl.-Math. Torsten Krüger

eingereicht bei der Naturwissenschaftlich-Technischen Fakultät
der Universität Siegen
Siegen 2012

Gutachter der Dissertation: Professor Dr. Franz-Theo Suttmeier
Professor Dr. Robert Plato

Tag der mündlichen Prüfung: 31.10.2012

Gedruckt auf alterungsbeständigem holz- und säurefreiem Papier.

Zusammenfassung

Die vorliegende Arbeit befasst sich mit Methoden aus dem Bereich der sogenannten Fictitious Domain (FD) Techniken bei gleichzeitiger Verwendung von Finiten Elementen. Fictitious Domain Techniken eigenen sich gut, falls das Gebiet, auf dem eine partielle Differenzialgleichung gelöst werden soll, geometrisch komplex oder auch zeitabhängig ist.
Eigene Vorschläge, welche auf Straf- und Regularisierungstechniken basieren, werden vorgestellt und analysiert. Varianten der bekannten Nitsche-Methode zur Aufprägung von Randbedingungen kommen zum Einsatz. Dies wird kombiniert mit Verfahren einer regularisierungs-basierenden FD Methode, ursprünglich erdacht von Glowinski et al.
Die zugrunde liegenden Modellgleichungen zweiter Ordnung sind dabei von nichtlinearer und recht allgemeiner Natur. Eine numerische Analyse findet in Bezug auf die linearisierten Gleichungen statt. So wird neben den resultierenden symmetrischen Problemen insbesondere auch auf Aspekte hinsichtlich dominanter Konvektion eingegangen, sowie auf die Umgehung einer diskreten Inf-Sup-Bedingung im Falle des Oseen-Problems. Der Nutzung von Streamline-Diffusion/Galerkin-Least-Squares Techniken kommt dabei die Schlüsselrolle zu.
Die erforderliche implizite Beschreibung der ursprünglichen Geometrie erfolgt über die Level Set Methode. Dabei wird der eingebettete Rand als Nullmenge einer geeigneten Funktion beschrieben, was eine bequeme und flexible Handhabung der Geometrie erlaubt.
Der Darstellung von zugrunde liegenden algorithmischen Aspekten und einer allgemeinen Überprüfung hinsichtlich der Genauigkeit der neuen Methoden anhand von verschiedenen Beispielen mit bekannter analytischer Lösung wird Platz eingeräumt. Teil der Arbeit ist zudem die Präsentation verschiedener Anwendungen, um das Potenzial der neuen Methoden auf verschiedenen Gebieten auszuloten. Dazu
werden Beispiele aus dem Bereich der planaren stationären und instationären Strömungsprobleme, inklusive einem Beispiel mit bewegtem Rand, sowie die Boussinesq-Gleichungen auf komplexen, mehrfach zusammenhängenden Gebieten, behandelt.

Summary

The work at hand is addressed to methods from the fictitious domain context, combined with the finite element method. Fictitious domain techniques are suitable in case partial differential equations have to be solved on a geometrically complex or time-dependent domain.
Own suggestions based on penalization and regularization, utilizing variants of Nitsches method in order to impose boundary conditions in a weak sense, are introduced and analyzed. The techniques presented are generalizations of methods due to Glowinski et al.
The underlying model equations of order two are non-linear reaction-diffusion-convection equations of rather general type, able to describe a lot of real-world situations. In addition, incompressible Stokes and Navier-Stokes systems are introduced, being special cases of the original model equations in some sense.
The numerical analysis is carried out with respect to linearized versions of the original model equations. Within this process, symmetrical reaction-diffusion, diffusion-convection-reaction and a version of the Oseen equations are treated separately, in order to deal with different typical problems appearing in each case adequately.
Following that, besides symmetrical problems, tasks like dominant convection, as well as the circumvention of a discrete inf-sup condition in case the Oseen problem are discussed. Streamline diffusion/Galerkin least squares techniques playing a key role in that matter.
For implicit description of the embedded boundary the well established level set method is used, describing the boundary as a zero level set of suitable functions. This allows for an easy and flexible handling of the geometrical aspects.
Algorithmic tasks are addressed, followed by tests regarding numerical accuracy. In the end, several applications are presented in order to show the potential of the new methods: Examples regarding plain flow problems, including one with moving boundary, and the Boussinesq equations on complex multi-connected domains.

Contents

1 Introduction

Motivation and Objectives

In many fields, like fluid dynamics and elasticity, problems occur making it necessary to solve problems on domains being geometrically complex or time-dependent. As the generation of boundary-fitted meshes of good quality in such cases is a rather complex, often time consuming task of (not at least from the computational point of view) high cost, the fictitious domain (FD) method (see [Glo03]) and other related methods have been developed in order to overcome the meshing and re-meshing problem. This is done by embedding the original problem stated on a domain $\Omega \subset \mathbb{R}^d$ into a simple shaped domain $\tilde{\Omega}$, in many cases chosen as a parallelepiped of equal dimension. After that, the triangulation is carried out for the larger domain $\tilde{\Omega}$, which has a rather Eulerian character, and is not fitted to the boundary of $\Omega \subset \tilde{\Omega}$ in general. The original problem then is replaced by a new, being related to the original one, with the resulting solution restricted to Ω being at least close to the solution of the original problem in some sense.

The actual work at hand jumps on that bandwagon by presenting new variants of methods in the FD context, based on regularization, to overcome the problems stemming from ill-posedness of the problems on the fictitious domain, and those following from the necessity of imposing additional essential constraints on the solution. The level set method (see [Set99]) is used to describe the domain Ω implicitly rather than explicitly by a boundary-fitted mesh. We follow the papers of Pan and Glowinski et al. [GPWZ96, GP92], in order to develop and analyse methods being generalizations of the one stated in the mentioned papers, to the cases of far more general time-dependent, non-linear reaction-diffusion-convection problems with mixed boundary conditions, as well as the case of Stokes and Navier-Stokes systems describing incompressible fluid flow. Various numerical tests and applications are given in order to demonstrate and evaluate the new methods under consideration.

The aim is to present methods being able to handle problems without introducing

additional degrees of freedom, which is a common way in the fictitious domain community, but just using standard finite element spaces and meshes. Moreover, the philosophy of the methods at hand is to handle the problems in a quit standard way on the domain Ω, employing techniques like Galerkin least squares stabilization (e.g. [RST08]) in order to deal with additional problems like dominant convection and violation of a discrete inf-sub condition in case of saddle point problems and mixed finite elements (cf. [BF91]).

As a first demonstration and motivation, an example of Navier-Stokes flow around multiple obstacles in case of a lid-driven cavity is shown in Figure 1.1. The fictitious domain techniques presented in this work are used for the simulation, with a Cartesian grid covering $(-1, 1)^2$ as a fictitious domain. While it would be standard to generate a triangulation in case of a single inner circle, as such kind of holed domains are contained in every ordinary grid-generator, it would be harder to generate a suitable fitted mesh in case of the multi-obstacle flow. That case would make it necessary to build up a new grid, using a mesh-generator or by hand in an suitable format, if there was not a good soul having already implemented such a structure, which in general would be surprising. Not to mention the case the obstacles would change the number or shape and/or move in time. With the methods at hand handling such problems is not hard in principle, as only an implicit description has to be given for the position of the obstacles, avoiding complicated meshing an re-meshing procedures.

Outline of the thesis

The outline after the introduction is as follows:

- In the *second chapter*, the continuous context, including the nomenclature and basic principles, as well as the underlying general linear and non-linear problems is given. This is done along with a review of FD methods and related ones already existing. The new methods, being generalizations of the one presented in [GPWZ96,GP92], are introduced in the continuous context, based on suitable model problems being linearized versions of the firstly presented non-linear equations. Furthermore, methods fit for describing a domain implicitly are discussed, with the level set method among them.

- The *third chapter* is addressed to the discretization of the continuous case, with special attention on formulating well-posed discrete problems. The latter

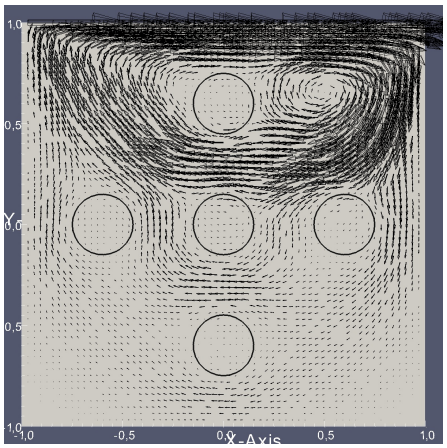

Figure 1.1: Example of a lid-driven cavity flow around multi-obstacles modelled by the Navier-Stokes equations. The regularized fictitious domain methods presented in this work have been used for solving the system of equations.

in general is not an easy task, as one has to deal with grids not fitted to the boundary of the underlying domain. Numerical robustness in case of singularly perturbed equations is discussed. Variants of Nitsches method (see [Nit71]) are the methods of choice in order to enforce essential Dirichlet boundary conditions, while streamline diffusion/Galerkin least squares techniques are brought into play for stabilization. The methods are given and analysed for linear scalar model problems and vectorial Oseen problems, as both types of equations need different treatment to show the methods result in well-posed problems.

- Implementational and algorithmic issues are presented in the *fourth chapter*: Linearization techniques, local quadrature, the solution process and for completeness an additional geometrical regularization. As the basis for implementation, the free finite element C++-library deal.II, see [BHK07], is used. The chapter ends with the presentation of test problems for evaluating the accuracy of the methods.

- The *fifth chapter* gives some practical applications:

  a) Laminar flow around a plain cylinder, which is an essential benchmark problem, as a lot of numerical and experimental data are available, showing that our new methods work accurate, while being able to handle steady flow problems,

b) Unsteady flow around a plain cylinder, another benchmark for testing whether a solver works accurate and is able to resolve non-linear effects, while leaving the laminar regime. As it turns out the solver based on the new FD based methods is able to produce sufficiently good results compared to established boundary-fitted methods,

c) Exploring the capabilities of the new methods to treat with the time-dependent Boussinesq equations on multi-connected domains. Which turns out to give qualitatively good results with respect to physical phenomena, while at the same time the accurate enforcing of strong constraints at the inner boundaries of the domain in the considered laminar regime is ensured. Moreover, the high flexibility regarding geometrical complex stationary domains is shown,

d) Time-dependent incompressible viscous flow around a moving plain cylinder, in order to show the method is able to deal with moving boundary problems in principle. This is another test the new methods pass, while the description of the method is not perfectly adequate from the physical and mathematical point of view with no further modification regarding the time derivative. Nevertheless, from the qualitative side the methods gives sufficient results compared to other FD methods.

Finally, the work is ended by the discussion and outlook section, highlighting pros and cons of the new methods, along with giving hints for further improvements and interesting fields to be explored using the methods developed in this work.

2 Description of the model equations

In this chapter the model equations treated in this work are introduced. We want to deal with systems of non-linear reaction-diffusion-convection (RDC) equations, in order to be able to cover a wide range of problems in a uniform framework. The aim is to give a general background, not to focus on the solvability of this partial differential equation (PDE) systems. Doing so, we present the basic principles and the nomenclature used in this work, as well as the general appearance of the equations and terms we have to deal with. As complicated and maybe time dependent domains have to be considered, furthermore a journey on the treatment of weakly imposed boundary conditions in the case of a mesh not fitted to the boundary of the domain the equations are defined on, is given. Finally we present own ideas in this context, based on regularization techniques first time given in [GP92]. The chapter is ended by discussing techniques for implicit description of a given domain.

2.1 Nomenclature and basic principles

Within this paragraph the basic principles and the nomenclature of this work are presented in a compact fashion. In what follows let $\Omega \subset \mathbb{R}^d$ $(d = 2, 3)$ always be a connected, open and bounded domain with a rectifiable, sufficiently smooth boundary $\Gamma := \partial\Omega$, i.e. Γ being of class $C^{k,1}$ for some integer $k \geq 0$.

Definition 2.1 (see [AH09])**.** *Let V be a function space on $\mathbb{R}^{d-1}$. Γ is of class V, if for each point $x_0 \in \Gamma$ there exists an $r > 0$, as well as a function $g \in V$, such that we have*

$$\Omega \cap \mathbb{B}_r(x_0) = \{\mathbf{x} \in \mathbb{B}_r(x_0) : x_d > g(x_1, \ldots, x_{d-1})\},$$

upon a transformation of the coordinate system if necessary.
Here $\mathbb{B}_r(x_0)$ is the open d-dimensional ball with radius r and center x_0. In particular, if the function space V consists of C^k functions, we say Ω is of class C^k or simply

a C^k domain. If the function space V consists of $C^{k,1}$ functions, that is functions with k-times Lipschitz continuous partial derivatives, we say Ω is of class $C^{k,1}$, or Ω is a Lipschitz domain (of class $C^{k,1}$), or simply a $C^{k,1}$ domain.

The unit normal vector pointing outward in some point x (in what follows not written in bold letters) of the boundary is denoted by $\boldsymbol{n} = \boldsymbol{n}(x)$. Let always be $I := (0,T) \subset \mathbb{R}$ a time interval, $T > 0$ and $t \in I$. In general the domain could be time-dependent ($\Omega = \Omega(t)$) as well.

The normal derivatives $\partial_n u$ and $\partial_n \boldsymbol{u}$ are defined to be

$$\partial_n u := \boldsymbol{n} \cdot \nabla u, \qquad \partial_n \boldsymbol{u} := (\boldsymbol{n} \cdot \nabla)\boldsymbol{u} = (\partial_n \boldsymbol{u}_i)_{i=1,\dots,d}$$

in the vectorial case.

The Lebesgue measure of a subset $X \subset \mathbb{R}^m$ is written as

$$meas(X) := \int_{\mathbb{R}^m} 1_X \, dX, \text{ where } 1_X(x) := \begin{cases} 1 & \text{if } x \in X, \\ 0 & \text{else.} \end{cases}$$

We will denote the standard inner product of the Hilbert space $L^2(X)$ over the real numbers, with elements defined on a bounded domain $X \subset \mathbb{R}^d$, for scalar functions $u, v \in L^2(X)$ by

$$(u,v)_X := \int_X uv \, dx,$$

and

$$(\boldsymbol{u},\boldsymbol{v})_X := \sum_{i=1}^{d} (u_i, v_i)_X \,, \quad (\boldsymbol{U},\boldsymbol{V})_X := \sum_{i,j=1}^{d} (U_{ij}, V_{ij})_X \,,$$

in the case of $\boldsymbol{u}, \boldsymbol{v}$ being elements of $(L^2(X))^d$ and $\boldsymbol{U}, \boldsymbol{V} \in (L^2(X))^{d\times d}$, with the corresponding component functions indexed.

Moreover, in case of $X \subset \mathbb{R}^{d-1}$ the inner product of $L^2(X)$ is denoted by

$$\langle u, v \rangle_X := \int_X uv \, ds, \quad \langle \boldsymbol{u}, \boldsymbol{v} \rangle_X := \sum_{i=1}^{d} \langle u_i, v_i \rangle_X \,,$$

analogous to the former cases. The induced $L^2(X)$-norms are then denoted by

$$\|\cdot\|_{0,X} := (\cdot,\cdot)_X^{\frac{1}{2}} \quad \text{or} \quad \|\cdot\|_{0,X} := \langle \cdot,\cdot \rangle_X^{\frac{1}{2}} \,,$$

depending on the context.

Besides that, for $X \subset \mathbb{R}^d$ and $p \in [1, \infty]$, we denote the $L^p(X)$-norm of a suitable function v (analogous in case of vector or matrix functions) by

$$\|v\|_{L^p(X)} := \left(\int_X |v|^p \right)^{\frac{1}{p}} \quad \text{and} \quad \|v\|_{L^\infty(X)} := \|v\|_{\infty,X} := \inf_{meas(X')=0} \sup_{x \in X \setminus X'} |v(x)|.$$

Following that, it holds $\|v\|_{L^2(X)} = \|v\|_{0,X}$ in case $v \in L^2(X)$.

Definition 2.2. *Let k be a non-negative integer, $p \geq 1$ a real number. The Sobolev space $W^{k,p}(X)$, $X \subset \mathbb{R}^d$ open and bounded, is defined to be*

$$W^{k,p}(X) := \left\{ v \in L^p(X) : \ \partial^\alpha v \in L^p(X), \ |\alpha| \leq k \right\},$$

with α a multi-index. The space shall be equipped with the norm and semi-norm

$$\|v\|_{k,p,X} := \left(\sum_{|\alpha| \leq k} \|\partial^\alpha v\|_{0,X}^2 \right)^{\frac{1}{2}}, \quad |v|_{k,p,X} := \left(\sum_{|\alpha| = k} \|\partial^\alpha v\|_{0,X}^2 \right)^{\frac{1}{2}}.$$

It is a well-known fact that $W^{k,p}(X)$ is a Banach space.

The case $p = 2$ is very important when dealing with second order problems. As it is common practice, we will make use of the Sobolev spaces $H^k(X) := W^{k,2}(X)$, $X \subset \mathbb{R}^d$ open and bounded, for some integer $k > 0$.

Definition 2.3. *Let k be a non-negative integer. The space $H^k(X) := W^{k,2}(X)$ shall be equipped with the norm and semi-norm*

$$\|v\|_{k,X} := \|v\|_{k,2,X}, \quad |v|_{k,X} := |v|_{k,2,X}$$

and the inner product

$$(u, v)_{k,X} := \sum_{|\alpha| \leq k} (\partial^\alpha u, \partial^\alpha v)_{0,X}, \quad u, v \in H^k(X).$$

Another well-known fact is the next theorem, see e.g. [Hac86] and [Bra03].

Theorem 2.1. *Assume $\Omega \subset \mathbb{R}^d$ is a Lipschitz domain. Then there exists a continuous linear operator $\tilde{\gamma} : H^1(\Omega) \to L^2(\Gamma)$ with*

(a) $\tilde{\gamma} v = v|_\Gamma$ *if* $v \in H^1(\Omega) \cap C(\overline{\Omega})$.

(b) $\exists C = C(\Omega) > 0 : \ \|\tilde{\gamma} v\|_{0,\Gamma} \leq C \|v\|_{1,\Omega} \ \forall v \in H^1(\Omega)$.

(c) $\tilde{\gamma}$ *is a compact mapping.*

Using this trace operator, the Sobolev space $H^{\frac{1}{2}}(\Gamma)$ is defined as

$$H^{\frac{1}{2}}(\Gamma) := \{w \in L^2(\Gamma) : \ \exists v \in H^1(\Omega) : w = \tilde{\gamma} v\},$$

equipped with the norm

$$\|w\|_{\frac{1}{2},\Gamma} := \inf\{\|v\|_{1,\Omega} : \ v \in H^1(\Omega), \ \tilde{\gamma} v = w\}.$$

Furthermore, by the trace operator the closed subspace:

$$H_0^1(\Omega) := \left\{v \in H^1(\Omega) : \ \tilde{\gamma}(v) = v|_\Gamma = 0\right\} \subset H^1(\Omega).$$

can be specified.

Let now the boundary be partitioned into Γ_1 and Γ_2, with $\Gamma = \Gamma_1 \cup \Gamma_2$ and $\Gamma_1 \cap \Gamma_2 = \emptyset$, where Γ_1 is relatively closed, Γ_2 relatively open. The cases $\Gamma_1 = \emptyset$ or $\Gamma_2 = \emptyset$ shall be allowed as well. In the case of $\Gamma_1 \neq \emptyset$ it can be shown, that there exists an analogous continuous trace operator $\tilde{\gamma}_1 : H^1(\Omega) \to L^2(\Gamma_1)$ with $\tilde{\gamma}_1 v = v|_{\Gamma_1}$, see [Glo03, QV94].

In this sense, for suitable functions $g, g_i \in C^\infty(\Omega) \cap H^1(\Omega)$ mapping to $\mathbb{R}$, $\boldsymbol{g} = (g_i)_{i=1,\ldots,d}$, we define for frequently usage:

$$\begin{aligned} V_g(\Omega) &:= \left\{v \in H^1(\Omega) : \ v|_{\Gamma_1} = g\right\}, \\ \mathbf{V}_g(\Omega) &:= \left\{\boldsymbol{v} \in \left(H^1(\Omega)\right)^d : \ \boldsymbol{v}|_{\Gamma_1} = \boldsymbol{g}\right\}. \end{aligned}$$

In order to get convergence results for the methods presented later on, it will be necessary to extend the solution of the problems we want to treat onto a domain covering the original one. An interesting and also well known statement, suitable for this purpose, is given in Theorem 2.2. It is a basic result regarding the existence of an extension operator in case of sufficiently smooth functions and domain boundaries.

Theorem 2.2 (see [GT83]). *Let $k \geq 0$ be an integer and $\Omega \subset \mathbb{R}^d$ be a bounded $C^{k,1}$ domain with $\overline{\Omega} \subset \tilde{\Omega}$, $\tilde{\Omega}$ being an open set in $\mathbb{R}^d$. Then there exists a bounded linear extension operator $E_{k+1} : H^{k+1}(\Omega) \to H^{k+1}(\tilde{\Omega})$ such that $E_{k+1}v|_\Omega = v$ and*

$$\|E_{k+1}u\|_{k+1,\Omega} \leq C(k, \Omega, \tilde{\Omega})\|u\|_{k+1,\tilde{\Omega}} \quad \forall v \in H^{k+1}(\Omega). \tag{2.1}$$

2.2 Reaction-Diffusion-Convection (RDC) equations

Motivated by physical processes and applications like reactive flow, droplet evaporation and other complex systems, we want to model the transport of one or several quantities w_i within an open, time-dependent domain, driven by diffusion and/or a flow field. Reactions between these quantities should be allowed as well.

As we will specify the terms for special cases in the application parts later on, we will now state the general type of non-linear coupled second order partial differential equation systems with possibly mixed Dirichlet and Neumann boundary data we want to deal with.

2.2.1 Classical formulation

Splitting the boundary $\Gamma = \partial\Omega$ into the disjoint sets $\Gamma = \Gamma_D \cup \Gamma_N$, with $\Gamma_D \cap \Gamma_N = \emptyset$, the classical formulation of the problems we want to treat is stated to be:

$$\begin{aligned}
\partial_t w_i - \nabla \cdot \mathbf{j}_i + \boldsymbol{\beta} \cdot \nabla w_i &= r_i + f_i \text{ in } \Omega \times I, && (2.2)\\
w_i &= g_D^i \text{ on } \Gamma_D \times I, && (2.3)\\
j_i\, \partial_n w_i &= g_N^i \text{ on } \Gamma_N \times I, && (2.4)\\
w_i(x, 0) &= w_0^i \text{ on } \Omega. && (2.5)
\end{aligned}$$

The cases $\Gamma_D = \emptyset$ or $\Gamma_N = \emptyset$ are allowed as well.

The index i runs from 1 to N, with N being the total number of quantities w_i under consideration. For the vector valued flux functions $\mathbf{j}_i$ we suppose that there holds

$$\mathbf{j}_i = j_i \nabla w_i.$$

In this general formulation r_i, j_i are sufficiently smooth scalar functions, typically depending on

$$\mathbf{w} = (w_i)_{i=1,\dots,n}$$

and/or the space coordinate x and time coordinate t:

$$r_i = r_i(x, t, \mathbf{w}), \quad j_i = j_i(x, t, \mathbf{w}).$$

Neumann and Dirichlet data are supposed to be functions in space and time, but in general could be depending on $\mathbf{w}$ as well:

$$g_N^i = g_N^i(x, t, \mathbf{w}), \quad g_D^i = g_D^i(x, t, \mathbf{w}).$$

Physically the j_i stands for the individual diffusive flux of the ith quantity, and so the term including the j_i stands for the diffusive part, also taking into account the influence of the remaining quantities on the diffusive processes of ith quantity. The r_i-terms model the reactions between the ith quantity and the rest of the system. The f_i represents an external force, taking effect on the ith quantity, this functions sufficiently smooth as well.

The data $\boldsymbol{\beta} : \Omega \times I \to \mathbb{R}^d$ is an external velocity field which models convection within the system. This velocity field will be calculated from a Stokes or Navier-Stokes system (see next subsection) in many cases, but it could be of complete external origin. In many cases the convective part will dominate the equations.

2.2.2 Weak formulation

Testing with appropriate functions from $V_0(\Omega)$ and integrating by parts yields the weak form corresponding to our problem (1.2)-(1.5). Our weak formulation thus reads:

For $i = 1, \dots, N$ and $t \in I$ find $w_i(t) \in V_{g_D^i}(\Omega)$, with $w_i(\cdot, 0) = w_0^i(\cdot)$, such that:

$$(\partial_t w_i, v)_\Omega + a_i(\mathbf{w}; v) = (h_i(\mathbf{w}); v) \tag{2.6}$$

for all $v \in V_0(\Omega)$.

The semi-linear forms are defined as:

$$a_i(\mathbf{w}; v) := (\mathbf{j}_i, \nabla\varphi)_\Omega + (\boldsymbol{\beta} \cdot \nabla w_i, v)_\Omega, \tag{2.7}$$

$$(h_i(\mathbf{w}); v) := (r_i, v)_\Omega + (f_i, v)_\Omega + \langle g_N^i, v\rangle_{\Gamma_N}. \tag{2.8}$$

Clearly, this system in general does not have a solution, we will focus on such cases a solution exists.

In particular we will have to treat linearized versions of the system under the typical assumptions ensuring the solvability due to the Lax-Milgram theorem in the linear case. These assumptions will be discussed in another section, which treats a (linear) model problem closely related to the general (stationary) system, and we will assume that analogue and directly transferable assumptions always hold in the considered problems.

Remark 2.1. In case the diffusion coefficient depends on derivatives of $\mathbf{w}$, it may be necessary to substitute the underlying $H^1(\Omega)$-space by $W^{1,p}(\Omega)$, with suitable p in the definition of $V_{g_D^i}(\Omega)$, in order to match the smoothness properties of the solution. An example for this is the well known p-Laplace problem and other akin ones. Similar will be true in case of the Stokes and Navier-Stokes problem later on.

2.3 Stokes and Navier-Stokes equations

In order to handle flow problems as well and compute velocity fields driving the physical processes mentioned above, in particular for the calculation of the field $\boldsymbol{\beta}$ from (2.2) if necessary, we treat variants of the incompressible Stokes and Navier-Stokes equations as well. This equations are effectively variants of the PDE systems of the former paragraph, but with an additional constraint to ensure incompressibility.

2.3.1 Classical formulation

Let the boundary be partitioned into the disjoint subsets Γ_D and Γ_N covering the overall boundary in order to state the essential and the natural boundary conditions of the problems we want to include.

The system of equations for the velocity $\boldsymbol{u} : \Omega \to \mathbb{R}^d$ in case of the (dimensionless) Stokes problem to be estimated is written as follows:

$$\begin{aligned} -\nabla \cdot (\nu \nabla \boldsymbol{u}) + \nabla p &= \boldsymbol{f} \text{ in } \Omega, && (2.9)\\ \nabla \cdot \boldsymbol{u} &= 0 \text{ in } \Omega, && (2.10)\\ \boldsymbol{u} &= \boldsymbol{g}_D \text{ on } \Gamma_D, && (2.11)\\ \nu \partial_n \boldsymbol{u} - \boldsymbol{n} p &= \boldsymbol{g}_N \text{ on } \Gamma_N. && (2.12) \end{aligned}$$

In this system p stands for the pressure, being the Lagrangian parameter to ensure the constraint (2.10), while $\boldsymbol{f}$ is an external forcing distribution. Furthermore, $\nu > 0$ is the kinematic viscosity, in some cases being dependent on $\boldsymbol{u}$ as well. All the equation data are supposed to be sufficiently smooth.

Now for a full version of the Navier-Stokes equations:

$$\begin{aligned} \partial_t \boldsymbol{u} - \nabla \cdot (\nu \nabla \boldsymbol{u}) + (\boldsymbol{u} \cdot \nabla)\boldsymbol{u} + \nabla p &= \boldsymbol{f} \text{ in } \Omega \times I, && (2.13)\\ \nabla \cdot \boldsymbol{u} &= 0 \text{ in } \Omega \times I, && (2.14)\\ \boldsymbol{u} &= \boldsymbol{g}_D \text{ on } \Gamma_D \times I, && (2.15)\\ \nu \partial_n \boldsymbol{u} - \boldsymbol{n} p &= \boldsymbol{g}_N \text{ on } \Gamma_N \times I, && (2.16)\\ \boldsymbol{u}(x, 0) &= \boldsymbol{u}_0 \text{ on } \Omega. && (2.17) \end{aligned}$$

The initial data $\boldsymbol{u}_0$ is supposed to meet the constraint $\nabla \cdot \boldsymbol{u}_0 = 0$. $I = (0, T)$ is a given time interval.

2.3.2 Weak formulation

Lets assume $meas(\Gamma_N) > 0$. First we handle the weak formulation, originating from (2.9)-(2.12). The corresponding weak formulation of the Stokes system reads:

Find $(\boldsymbol{u}, p) \in \mathbf{V}_{\boldsymbol{g}_D}(\Omega) \times L^2(\Omega)$ such that

$$S((\boldsymbol{u}, p); (\boldsymbol{v}, q)) = L(\boldsymbol{v}) \quad \forall (\boldsymbol{v}, q) \in \mathbf{V}_0(\Omega) \times L^2(\Omega), \tag{2.18}$$

where

$$\begin{aligned} S((\boldsymbol{u},p);(\boldsymbol{v},q)) &:= (\nu\nabla\boldsymbol{u},\nabla\boldsymbol{v})_\Omega - (p,\nabla\cdot\boldsymbol{v})_\Omega + (\nabla\cdot\boldsymbol{u},q)_\Omega, \\ L(\boldsymbol{v}) &:= (\boldsymbol{f},\boldsymbol{v})_\Omega + \langle \boldsymbol{g}_N,\boldsymbol{v}\rangle_{\Gamma_N} \quad \forall v \in \left(H^1(\Omega)\right)^d, \end{aligned}$$

for all $\boldsymbol{u},\boldsymbol{v} \in \left(H^1(\Omega)\right)^d, p,q \in L^2(\Omega)$.

For the full version of the Navier-Stokes equations (2.13)-(2.17) the resulting weak formulation is:

For $t \in I$ find $(\boldsymbol{u}(t),p(t)) \in \mathbf{V}_{\boldsymbol{g}_D}(\Omega) \times L^2(\Omega)$ with $\boldsymbol{u}(\cdot,0) = \boldsymbol{u}_0(\cdot)$ such that

$$(\partial_t\boldsymbol{u},\boldsymbol{v})_\Omega + N((\boldsymbol{u},p);(\boldsymbol{v},q)) = L(\boldsymbol{v}) \tag{2.19}$$

for all $(\boldsymbol{v},q) \in \mathbf{V}_0(\Omega) \times L^2(\Omega)$. The semi-linear form N is defined to be

$$N((\boldsymbol{u},p);(\boldsymbol{v},q)) := S((\boldsymbol{u},p);(\boldsymbol{v},q)) + ((\boldsymbol{u}\cdot\nabla)\boldsymbol{u},\boldsymbol{v})_\Omega. \tag{2.20}$$

Providing the case the corresponding classical formulations are solvable, both the saddle point problem (2.18) and the non-linear problem (2.19) are well posed, as there holds the inf-sup condition, see e.g. [BF91]:

$$\exists\gamma > 0 : \inf_{q\in L^2(\Omega)} \sup_{\boldsymbol{v}\in\mathbf{V}_0(\Omega)} \frac{(q,\nabla\cdot\boldsymbol{v})_\Omega}{\|\boldsymbol{v}\|_{(H^1(\Omega))^d}\|q\|_{L^2(\Omega)}} \geq \gamma. \tag{2.21}$$

Closing with this kind of weak formulation, it shall be pointed out that in the case $meas(\Gamma_N) = 0$ the pressure space $L^2(\Omega)$ often is replaced by $L^2_0(\Omega)$, defined as:

$$L^2_0(\Omega) := \left\{ q \in L^2(\Omega) : \ (q,1)_\Omega = 0 \right\}.$$

This additional constraint ensures the unique solvability of the problem, as the pressure variable is only defined up to a real constant if not doing so. Additionally the compatibility condition

$$\langle \boldsymbol{g}_D,\boldsymbol{n}\rangle_{\Gamma_D} = 0$$

has to be fulfilled by the essential boundary data due to the divergence theorem.

We will give a second possible form of a weak formulation of the linear Stokes

problem. Let's define the following subspace of divergence-free vector functions:

$$\mathbf{V}_{\boldsymbol{g},div}(\Omega) := \{\boldsymbol{v} \in \mathbf{V}_{\boldsymbol{g}}(\Omega) : \ \nabla \cdot \boldsymbol{v} = 0 \ \ a.e.\}\,.$$

That is the condition of the velocity being incompressible is already incorporated into the function space. The weak form of the Stokes problem in this case simply reads, see e.g. [BF91] or [GR94]:

$$\boldsymbol{u} \in \mathbf{V}_{\boldsymbol{g}_D,div}(\Omega) : \quad B_{div}(\boldsymbol{u},\boldsymbol{v}) = (\boldsymbol{f},\boldsymbol{v})_\Omega + \langle \boldsymbol{g}_N, \boldsymbol{v}\rangle_{\Gamma_N} \quad \forall \boldsymbol{v} \in \mathbf{V}_{0,div}(\Omega), \tag{2.22}$$

with

$$B_{div}(\boldsymbol{u},\boldsymbol{v}) := (\nu\nabla\boldsymbol{u}, \nabla\boldsymbol{v})_\Omega \quad \forall \boldsymbol{u},\boldsymbol{v} \in \left(H^1(\Omega)\right)^d,$$

and $\nu\partial_n\boldsymbol{u}|_{\Gamma_N} = \boldsymbol{g}_N$.

Analogous the resulting weak formulation of the Navier-Stokes problem can be deduced. The advantage of this formulation is the fact, that it leads to a convex minimization problem, which can be employed to bring the tools developed for the scalar model equations in the next paragraph into play. As in practice it is quite hard to achieve the incompressibility constraint in the construction of the underlying function space, and as it is more natural and sometimes even necessary to treat the weak formulation (2.18), stemming from the original strong formulation, the latter one is to be preferred.

2.4 Fictitious Domain (FD) method

Problems like those we want to handle may include a domain being time dependent and may have a complicated curved boundary as well. As boundary fitted meshes may be of poor quality and/or their computation may be a hard and expensive task, in areas like computational fluid dynamics a lot of techniques have been developed to overcome those problems. The idea is to replace the original problem posed on a complicated domain $\Omega \subset \mathbb{R}^d$, to one posed on a very simple domain $\tilde{\Omega}$ of equal dimension, which includes the complicated one, see Figure 2.1. After embedding the complicated domain of interest Ω into the bigger and simpler one, in most cases being a parallelepiped, the original function space the potentially solution will be an

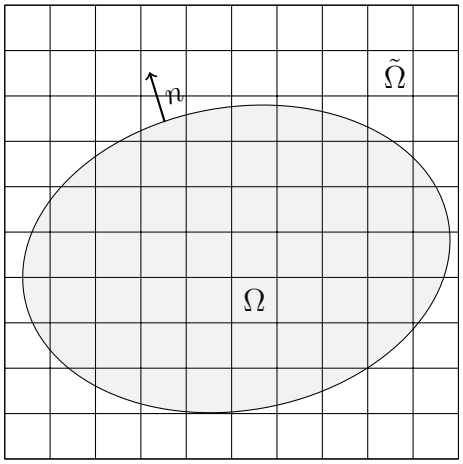

Figure 2.1: Example of a rectangular hold all domain $\tilde{\Omega}$, triangulated by a Cartesian grid, and the domain of interest Ω being embedded.

element of, is embedded into a space defined in a natural way on $\tilde{\Omega}$. Methods based on this idea therefore are called Domain Embedding methods sometimes. Then the original problem is replaced by one defined on the covering domain. More plastically:

Let the original problem of interest defined on Ω be of the form:

$$u \in V: \quad a_\Omega(u, v) = l_\Omega(v) \quad \forall v \in V,$$

where $V = V(\Omega)$. This problem then is replaced by an alternative problem defined on $\tilde{\Omega}$:

$$\tilde{u} \in \tilde{V}: \quad a_{\tilde{\Omega}}(\tilde{u}, \tilde{v}) = l_{\tilde{\Omega}}(\tilde{v}) \quad \forall \tilde{v} \in \tilde{V},$$

where $\tilde{V} = \tilde{V}(\tilde{\Omega})$ or based on such a space. Providing the new problem has been chosen well, it holds $\tilde{u}|_\Omega = u$, with $u \in V$ the solution of the original problem, or a function close to it with respect to a suitable norm.

Following this idea, the concept of fictitious domain methods and other closely related ones is "embed and conquer" instead of "divide and conquer", which is the guiding one in general domain decomposition methods, see e.g. [QV05].

2.4.1 General concept of FD and related methods

This subsection deals with a collection of common methods in order to handle problems with complicated and/or moving boundaries, using fictitious domain and related methods. A little bit anticipating on what is coming up below in the next chapter, continuous and discrete concepts will be mixed up within this subsection. This is due to the fact, that several formulations regarding FD methods and related ones only make sense after migrating to a discrete setting, using a mesh to launch an FEM on the problem. Also the full range of problems and advantages of the methods can only be shown this way.

For ease of presentation, a simple Cartesian grid with cell diameter $h > 0$, covering a rectangular hold all domain $\tilde{\Omega}$, which includes the original domain Ω, is employed as a stationary grid, while the boundary conditions on $\partial\Omega$ are imposed in an approximative sense, see Figure 2.1. This overall methodology for handling boundary value problems is often called Cartesian grid methods.

As a simple model for describing the resulting methods consider the problem

$$-\triangle u + u \;=\; f \text{ in } \Omega, \tag{2.23}$$

with Dirichlet conditions

$$u \;=\; g_D \text{ on } \partial\Omega, \tag{2.24}$$

as well as the associated elliptical bilinear form

$$a_\Omega(u,v) := (\nabla u, \nabla v)_\Omega + (u,v)_\Omega \qquad \forall\, u, v \in H^1(\Omega).$$

Boundary penalty One method for describing the essential Dirichlet boundary conditions, fitting into the context, is the Boundary penalty method, see [BE86] and [Bab73b]. After replacing (2.24) by the Robin type condition

$$\epsilon\partial_n u + u = g \text{ on } \partial\Omega, \tag{2.25}$$

where $\epsilon > 0$ is a penalty parameter, and testing in (2.23) with $v \in C^\infty(\tilde{\Omega})$, the resulting weak formulation writes

$$u^\epsilon \in H^1(\tilde{\Omega}): \quad a_\Omega(u^\epsilon, v) + \epsilon^{-1}\langle u^\epsilon, v\rangle_{\partial\Omega} = (f,v)_\Omega + \epsilon^{-1}\langle g, v\rangle_{\partial\Omega}\, \forall v \in H^1(\tilde{\Omega}). \tag{2.26}$$

Indeed, the solution of this problem is not unique in $H^1(\tilde{\Omega})$, but $u^\epsilon|_\Omega$ is unique in $H^1(\Omega)$, and it is shown in the mentioned papers that it holds $u^\epsilon|_\Omega \to u$ strongly as ϵ tends to zero. In order to ensure the best possible convergence results for this nonconforming method after discretization by an FEM, the penalty parameter has to be coupled to the grid parameter. If optimal order of convergence in the L^2-norm has to be achieved (if possible at all), this has to be done in such a way that the original behaviour from the conforming discrete method, regarding the condition number of the resulting matrix, in general is not preserved. Furthermore, it has to be taken into account that $meas(K \cap \Omega)$, K an element of the underlying triangulation, can be arbitrarily small, as we have to deal with an unfitted mesh. This fact causes additional stability problems, as the system gets ill conditioned due to the potentially existence of several matrix rows with a vector-norm being arbitrarily small, see [Hei08].

Lagrange multiplier Very popular are the boundary and volume supported Lagrange multiplier methods due to Glowinski et al. [Glo03] and variants of it. In case of boundary supported methods, the idea is the same as in case of the boundary Lagrange multiplier method due to Babuška [Bab73a]. A Lagrangian multiplier, being an element of a suitable function space, is introduced in order to impose the boundary condition approximately. Defining the elliptic bilinear form

$$a_{\tilde{\Omega}}(u, v) := (\nabla \tilde{u}, \nabla v)_{\tilde{\Omega}} + (\tilde{u}, v)_{\tilde{\Omega}} \quad \forall u, v \in H^1(\tilde{\Omega}),$$

the following saddle point problem to be solved results:

Find $(\tilde{u}, \lambda) \in H^1(\tilde{\Omega}) \times H^{-\frac{1}{2}}(\partial\Omega)$:

$$\begin{aligned} a_{\tilde{\Omega}}(\tilde{u}, v) + \langle \lambda, v \rangle_{\partial\Omega} &= (\tilde{f}, v)_{\tilde{\Omega}} \qquad \forall v \in H^1(\tilde{\Omega}), & (2.27)\\ \langle \tilde{u}, \mu \rangle_{\partial\Omega} &= \langle g, \mu \rangle_{\partial\Omega} \qquad \forall \mu \in H^{-\frac{1}{2}}(\partial\Omega), & (2.28) \end{aligned}$$

where $\tilde{f}$ is a suitable extension of the load. Certainly, the choice of $\tilde{f}$ is crucial for the smoothness of the resulting solution.
As pointed out in [GG95], in the continuous setting the above saddle point problem is well posed. Passing to the discrete setting, the interaction of data living on two (or possibly more) different meshes (for primal solution on the fictitious domain and Lagrange multiplier on the embedded boundary) have to be coordinated. In general this leads to a rather expensive searching problem (from the computational

point of view) when combining the data from the different grids. The boundary grid parameter $\eta > 0$ has to be chosen carefully in order to get a discrete inf-sup condition satisfied. In [GG95] a mixed FEM employing a P_1/P_0 pairing was studied, and the compatibility condition

$$3h < \eta < Lh$$

has been deduced to make the discrete spaces compatible.
Different ways of avoiding such rather vague compatibility conditions and get the resulting saddle point problem well posed are given e.g. in [HY09] and [BH10a]. In [HY09], inspired by XFEM methods (see below), the discrete inf-sup condition is circumvented by a stabilization method in the spirit of Barbosa and Hughes [BH91]. Cut elements and stabilization are used in [BH10a].

In addition to the boundary Lagrange multiplier methods, having the drawback of being not well suited in case of an a priori unknown evolution of Ω, the volume based Lagrange multiplier methods have been developed, see e.g. [Glo03] and the literature therein. The idea: Let $\omega \subset \Omega$ be an open domain and $\tilde{\Omega} = \Omega \cup \overline{\omega}$, extend the resulting weak problem to $\tilde{\Omega}$, and augment the formulation by a suitable scalar-product over $H^1(\omega)$ in order to get to an appropriate saddle point problem. Variants of this methods have been widely used for simulation of incompressible viscous flow around rigid bodies as well as fluid particle interaction, see e.g. [GPH+99, Bön06].

Variants of Nitsches method In [Nit71] Nitsche presented a method for imposing the essential Dirichlet boundary conditions in a weak sense by applying the discrete weak formulation:

Find $u_h \in V_h \subset H^1(\Omega)$:

$$\begin{aligned} a_\Omega(u_h, v_h) - \langle \partial_n u_h, v_h \rangle_{\partial\Omega} - \langle u_h, \partial_n v_h \rangle_{\partial\Omega} + \langle \gamma_D h^{-1} u_h, v_h \rangle_{\partial\Omega} \\ = (f, v_h)_\Omega + \langle g_D, \gamma_D h^{-1} v_h - \partial_n v_h \rangle_{\partial\Omega} \quad \forall v_h \in V_h \end{aligned}$$

for discretization of problem (2.23)-(2.24) within a discrete space of functions not satisfying constraint (2.24) in case of a mesh fitted to the domain Ω by an FEM. An extensive review on Nitsches method can be found in [Han05]. The parameter $\gamma_D > 0$ can in principle be estimated by solving an eigenvalue problem, see also [Han05].

This kind of penalty method turns out to be of optimal order in the H^1- and

L^2-sense, while maintaining the condition of the original discrete problem with boundary conditions already incorporated into the discrete function space. Nitsches method and its variants have been employed and studied extensively in the context of different fields like fluid-structure interaction (e.g. [BF09, HH03]), optimization (e.g. [Bec02, Düc10]), domain decomposition (e.g. [BHS01, Ste98]) and FD methods (e.g. [CB09, BH10b]). It is directly related to a stabilized boundary Lagrange multiplier method on the one hand, and the boundary penalty method on the other hand, see [JS08] and [Ste95]. In this work other regularized variants of Nitsches method are given and analyzed in order to impose boundary conditions approximately in the case of an unfitted mesh.

Immersed boundary Another popular family of methods are the so called Immersed Boundary methods due to Peskin et al., see e.g. [Pes72, Pes02] and the literature therein. The key component is the imposition of the boundary conditions by appropriate delta distributions, describing suitable punctual penalty forces on the embedded inner boundary. As this kind of method is very popular in the context of fluid-structure interaction, this forcing terms often are interpreted as and stem from a feedback control of the physical forces acting on a structure. First order accuracy can be granted in the original version, although higher order accuracy has been reached, see for example [LP00].

Extended FEM (XFEM) In order to handle different kinds of discontinuities like cracked and holed domains (e.g. [MDB99,SCMB01]), interface problems (e.g. [CB03, GR07]) and later on in FD and related methods (e.g. [HY09, BBH10]), the XFEM has been introduced. A basis is the partition of unity method due to Babuška et al. [BM97]. The principle of the original extended FEM is the enrichment of a standard continuous FE space with suitable local FE functions, while the set of the enriched functions gives a partition of unity. The enriched space allows to handle the physical forces/conditions in an adequate and more elegant way compared to standard FE methods without complicated meshing. Existing discontinuities and other troublemakers are resolved by means of the enriched function space.

Discontinuous Galerkin (DG) methods In [LB08] an example of an FE method, using continuous elements on the part of the mesh not being intersected by the boundary, and elementwise discontinuous functions on elements intersected by the boundary, is proposed. In the interface zone, a geometry dependent local FE basis of discontinuous functions, fulfilling zero boundary conditions exactly on the embedded boundary described by a level set function is used. The method was analyzed in [LN11] and turns out to be of almost optimal order.
Another approach using a set of discontinuous FE basis functions on the overall grid meshing the fictitious domain is presented in [EB05]. In this method first the parts of the domain lying within each element of the covering grid are detected, using a two-dimensional bisection if necessary. The advantage of this method is that it can handle very complex domains, but the bisection procedure is not a cheap one from the computational point of view, and the shape of the artificial elements possibly violates the cone condition.

Composite FE Originally created as an effective geometrical multigrid preconditioner in the case of complicated domains, the composite FE method and its variants have been fully developed to handle boundary value problems like the Poisson problem, and also the Stokes problem, in the case of arbitrarily mixed boundary conditions, while the mesh does not resolve the geometrical details in a direct way, see [HS97, Rec06, PS08, PS09]. A container-grid, covering the original domain, is departed into standard degrees of freedom and the so called slave nodes, being associated to the degrees of freedom on elements cut by the domain boundary. On the part of the mesh including the slave nodes, the essential and natural boundary conditions are imposed approximately by extending the shape functions in the inner part of the original domain under consideration, and projecting this extension in a suitable way. So the shape of the finite element functions is adapted to fulfill the boundary constraints in order to impose the boundary conditions.

2.4.2 Scalar problem with mixed boundary conditions

Now we will formulate a linear scalar model problem being closely related to a linearized version of the (stationary) subproblems for the individual species treated above. Due to this latter fact, and in order to demonstrate the principles of the fictitious domain approach we will present here, we focus on the solution of

$$-\nabla \cdot (D\nabla u) + \boldsymbol{\beta} \cdot \nabla u + cu = f \text{ on } \Omega, \tag{2.29}$$

$$u = g_D \text{ on } \Gamma_D, \tag{2.30}$$

$$D\partial_n u = g_N \text{ on } \Gamma_N. \tag{2.31}$$

It shall be pointed out, that there are different ways to linearize the non-linear subproblems, but in almost every case this leads to a similar problem of solving an equation like the given one.

In order to guarantee the unique solvability of this model problem, we make the following assumptions on the equation data to bring the Lax-Milgram theorem into play:

$$D, \beta_i, c \in L^\infty(\Omega); \tag{2.32}$$

$$\exists\, \theta > 0 :\ D \geq \theta \text{ a.e. in } \Omega; \tag{2.33}$$

$$f \in L^2(\Omega); \tag{2.34}$$

$$g_D \in L^2(\Gamma_D); \tag{2.35}$$

$$g_N \in L^2(\Gamma_N); \tag{2.36}$$

$$\boldsymbol{\beta} \cdot \boldsymbol{n} \geq 0 \text{ a.e. on } \Gamma_N; \tag{2.37}$$

$$\exists\, c_0 > 0 :\ c - \frac{1}{2}\nabla \cdot \boldsymbol{\beta} \geq c_0 \text{ a.e. in } \Omega. \tag{2.38}$$

The velocity field $\boldsymbol{\beta} = (\beta_i)_{i=1,\ldots,d}$ and the rest of the data are supposed to be sufficiently smooth to match these assumptions.

In [GPWZ96] and [GP92] a regularized/penalized fictitious domain method for linear reaction-diffusion equations with Neumann boundary conditions was presented. We will adapt the ideas presented in the mentioned papers to this more general problem with a non-symmetric operator, including an additional convection term and mixed boundary conditions. In order to do so, we embed the domain Ω into the larger rectangular domain $\tilde{\Omega}$, where $\overline{\Omega} \subset \tilde{\Omega}$ (see figure 2.2). Following Glowinski et al.

[GP92] let Ω be of class $C^{0,1}$.

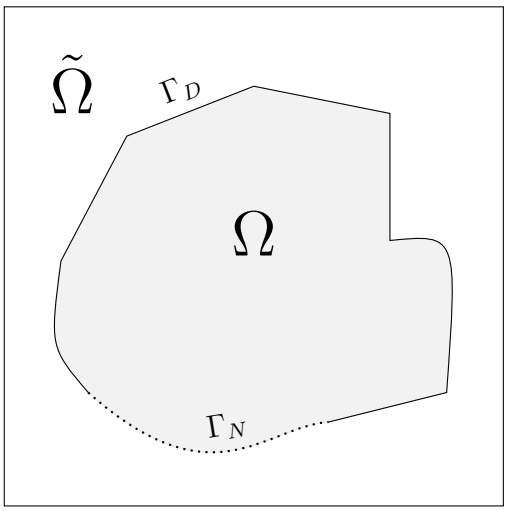

Figure 2.2: An example for a fictitious hold all domain $\tilde{\Omega}$ with original domain Ω embedded. The boundary $\partial\Omega$ being decomposed into a Neumann part Γ_N and a Dirichlet part Γ_D.

We concentrate on the case $g_D = 0$ on Γ_D, respectively we make the standard assumption that there exists a suitable $u_0 \in C^2(\Omega) \cap H^1(\Omega)$, with $u_0|_{\Gamma_D} = g_D$ in the sense of traces, and replace $l(v)$ by $l'(v) := l(v) - a(u_0, v)$ if necessary. Equivalently the corresponding variational formulation now reads:

$$\begin{aligned} &u \in V_0(\Omega) : \\ &a(u,v) = l(v) \quad \forall v \in V_0(\Omega), \end{aligned} \tag{2.39}$$

where

$$\begin{aligned} a(u,v) &:= (D\nabla u, \nabla v)_\Omega + (\boldsymbol{\beta} \cdot \nabla u + cu, v)_\Omega \quad \forall u, v \in H^1(\Omega) \times H^1(\Omega), \\ l(v) &:= (f, v)_\Omega + \langle g_N, v \rangle_{\Gamma_N} \quad \forall v \in H^1(\Omega). \end{aligned}$$

are a continuous, elliptic bilinear form, and a continuous linear form.

Now let us define the following spaces/subsets:

$$\begin{aligned} V &:= H^1(\tilde{\Omega}) \text{ or } V := H_0^1(\tilde{\Omega}), \\ V_{\Gamma_D} &:= \{v \in V : v|_{\Gamma_D} = 0\}, \\ H &:= \{v \in V_{\Gamma_D} : a(v,\mu) = l(\mu)\ \forall \mu \in V_{\Gamma_D}\}, \\ H_0 &:= \{v \in V_{\Gamma_D} : a(v,\mu) = 0\ \forall \mu \in V_{\Gamma_D}\}. \end{aligned}$$

Note that

$$H^1(\Omega) = \{v : v = \tilde{v}|_\Omega,\ \tilde{v} \in V\}, \tag{2.40}$$

$$V_0(\Omega) = \{v : v = \tilde{v}|_\Omega,\ \tilde{v} \in V_{\Gamma_D}\}, \tag{2.41}$$

i.e. $H^1(\Omega)$ is embedded in V and $V_0(\Omega)$ is embedded in V_{Γ_D}. The assumption on Ω to be of class $C^{0,1}$ was used for this kind of embedding of the function spaces.

As the problem (2.39) under consideration has a unique solution due to the Lax-Milgram theorem, the subsets H, H_0 thus are non-empty closed convex subsets of $H^1(\tilde{\Omega})$. It follows that the variational inequality

$$\begin{aligned} &\tilde{u} \in H : \\ &b(\tilde{u}, v - \tilde{u}) \geq 0 \quad \forall v \in H, \end{aligned} \tag{2.42}$$

where $b : V \times V \to \mathbb{R}$ is the continuous, V-elliptic bilinear form

$$b(v,w) := (\nabla v, \nabla w)_{\tilde{\Omega}} + \alpha (v,w)_{\tilde{\Omega}} \quad \forall v, w \in V, \tag{2.43}$$

has a unique solution, see e.g. [LGT81]. Here $\alpha \geq 0$ is a constant, and $\alpha > 0$ in case of $V = H^1(\tilde{\Omega})$. We consider then the regularized problem

$$\begin{aligned} &u^\rho \in V_{\Gamma_D} : \\ &\rho b(u^\rho, v) + a(u^\rho, v) = l(v) \quad \forall v \in V_{\Gamma_D}. \end{aligned} \tag{2.44}$$

In this formulation the parameter $\rho > 0$ is a penalty/regularization parameter.

While the mentioned papers treat the case of a linear reaction-diffusion equation with Neumann boundary conditions, in our case there are mixed boundary conditions and an additional, probably dominant, convective term included as well. Thus, the

equations under consideration are not symmetric anymore, and hence this is true for the corresponding bilinear forms, also.

An analysis of the proof of Theorem 3.1 in [GPWZ96] shows that the resulting statement is still true in the considered case. So we get the following theorem:

Theorem 2.3. *Let $\Omega \subset \mathbb{R}^d$ $(d = 2, 3)$ be a $C^{0,1}$ domain and $\rho > 0$ a parameter. Let $u, \tilde{u}$ and u^ρ be the solutions of the problems (2.39), (2.42) and (2.44), respectively. Then there holds:*

$$\begin{aligned} \lim_{\rho \to 0} \|u^\rho - \tilde{u}\|_{H^1(\tilde{\Omega})} &= 0, \\ \lim_{\rho \to 0} \rho^{-\frac{1}{2}} \|u^\rho - u\|_{H^1(\Omega)} &= 0. \end{aligned} \tag{2.45}$$

Proof. The proof closely follows the one from [GPWZ96], which is a typical convergence proof for regularization problems. We will show the result in three steps.
(1) Boundedness of the family $\{u^\rho\}_{\rho>0}$.
As there holds $\tilde{u}|_\Omega = u$ and $\tilde{u}|_{\Gamma_D} = 0$ we get the relation

$$a(\tilde{u}, v) = l(v) \quad \forall v \in V_{\Gamma_D}. \tag{2.46}$$

By taking $v = u^\rho - \tilde{u} \in V_{\Gamma_D}$ in (2.46) and by (2.44) we get

$$\begin{aligned} & b(u^\rho - \tilde{u}, u^\rho - \tilde{u}) + \frac{1}{\rho} a(u^\rho - \tilde{u}, u^\rho - \tilde{u}) \\ = \; & -b(\tilde{u}, u^\rho - \tilde{u}) + \frac{1}{\rho} \left\{ l(u^\rho - \tilde{u}) - a(\tilde{u}, u^\rho - \tilde{u}) \right\} \\ = \; & -b(\tilde{u}, u^\rho - \tilde{u}). \end{aligned} \tag{2.47}$$

From the latter relation, the continuity and ellipticity of b over $V \times V$ and the ellipticity of a over $V_0(\Omega) \times V_0(\Omega)$ it follows:

$$C \left(\|u^\rho - \tilde{u}\|^2_{1,\tilde{\Omega}} + \rho^{-1} \|u^\rho - u\|^2_{1,\Omega} \right) \leq \|b\| \|\tilde{u}\|_{1,\tilde{\Omega}} \|u^\rho - \tilde{u}\|_{1,\tilde{\Omega}} \quad \forall \rho > 0, \tag{2.48}$$

where $C > 0$ is an appropriate constant. This implies the boundedness

$$\|u^\rho\|_{1,\tilde{\Omega}} \leq \tilde{C} \quad \forall \rho > 0, \tag{2.49}$$

as $\tilde{u}$ is fixed.

(2) Weak convergence of the family $\{u^\rho\}_{\rho>0}$.
From the boundedness of $\{u^\rho\}_{\rho>0}$ there exists a subsequence $\{u^{\rho_k}\}_{\rho_k>0}$, such that

$$\lim_{\rho_k \to 0} u^{\rho_k} = u^* \tag{2.50}$$

weakly in $H^1(\tilde{\Omega})$. Hence by taking the limit $\rho_k \to 0$ in (2.44) we obtain:

$$a(u^*, v) = l(v) \quad \forall v \in V_{\Gamma_D},$$

and thus we have

$$u^* \in H. \tag{2.51}$$

Taking into account that $v|_\Omega = u$ and $v|_{\Gamma_D} = 0$ $\forall v \in H$ we get:

$$a(v, v - u^\rho) = l(v - u^\rho) \quad \forall v \in H. \tag{2.52}$$

After replacing v by $v - u^\rho \in V_{\Gamma_D}$ in (2.44), using the $V_0(\Omega)$-ellipticity of a and combining with the latter relation, we obtain (setting $\rho_k = \rho$)

$$\begin{aligned} b(u^\rho, v) &= b(u^\rho, u^\rho) + \frac{1}{\rho}\{-a(u^\rho, v - u^\rho) + l(v - u^\rho)\} \\ &\geq b(u^\rho, u^\rho) + \frac{1}{\rho}\{-a(v - u^\rho, v - u^\rho) - a(u^\rho, v - u^\rho) + l(v - u^\rho)\} \\ &= b(u^\rho, u^\rho) + \frac{1}{\rho}\{-a(v, v - u^\rho) + l(v - u^\rho)\} \\ &= b(u^\rho, u^\rho) \quad \forall v \in H. \end{aligned} \tag{2.53}$$

Combining this result with the continuity and ellipticity properties of b we have:

$$b(u^*, v) \geq b(u^*, u^*) \quad \forall v \in H. \tag{2.54}$$

Hence u^* is a solution of problem (2.42). As problem (2.42) has a unique solution $\tilde{u}$, the weak convergence of the whole family to $\tilde{u}$ follows.

(3) Strong convergence of the family $\{u^\rho\}_{\rho>0}$.
From equation (2.47), using the ellipticity properties of the bilinear forms under consideration, the weak convergence of the family $\{u^\rho\}_{\rho>0}$ to $\tilde{u}$ and that there holds

$\tilde{u}|_\Omega = u$ we obtain:

$$\lim_{\rho \to 0} \left(\|u^\rho - \tilde{u}\|^2_{1,\tilde{\Omega}} + \frac{1}{\rho} \|u^\rho - u\|^2_{1,\Omega} \right) = 0.$$

Which implies the desired result. □

An analysis of the last proof shows that the bilinear form a and linear form l only have to fulfill the standard assumptions regarding coercivity and continuity. So other linear forms standing in context to the model problem, or problems close to it, are included within the statement of an analogous theorem as well.

In the case of a pure Neumann problem, or by substituting the essential Dirichlet conditions, or both of the given boundary conditions, by Robin conditions, there would be no need to incorporate the corresponding boundary constraints into the underlying function space. The latter would be necessary when providing the penalty problem to a numerical method, in order to get an advantage over a standard method in case the mesh can or is not fitted to the inner boundary. As a consequence, the method is not intended for direct usage.

The real advantage, as will be shown later on, is the combination with Nitsches method (see [Nit71]) in order to impose the essential boundary condition accurately in a weak sense. Other methods based on a kind of boundary penalty, see e.g. [BE86] and [Bab73b], would fit into the context, too.

One word on pure Neumann problems: The mixed case is set back to the original one handled in the mentioned papers by simply setting $\Gamma_D = \emptyset$ and substituting V_{Γ_D} by V.

2.4.3 Fictitious Domain Oseen problem

After providing the theoretical background for a fictitious domain method in case of a scalar model problem, the same thing will be done with the help of a model problem being close to linearized versions of the stationary Navier-Stokes equations in the vector valued case. For ease of presentation we keep the focus on homogeneous Dirichlet conditions on the whole boundary, but the case of Neumann conditions also included is not far away.

A vector valued model problem, well suited for this goal, is the Oseen problem with sufficiently smooth data analogously to the scalar case:

$$\begin{aligned} -\nabla \cdot (\nu \nabla \boldsymbol{u}) + (\boldsymbol{\beta} \cdot \nabla)\boldsymbol{u} + \sigma \boldsymbol{u} + \nabla p &= \boldsymbol{f} \text{ in } \Omega && (2.55)\\ \nabla \cdot \boldsymbol{u} &= 0 \text{ in } \Omega && (2.56)\\ \boldsymbol{u} &= 0 \text{ on } \Gamma_D. && (2.57) \end{aligned}$$

As already done in the case of the Stokes problem above, in this theoretical part we give the weak formulation using divergence-free spaces and keeping the notation of paragraph 2.3.2:

$$\boldsymbol{u} \in \mathbf{V}_{0,div}(\Omega) : \; A(\boldsymbol{u}, \boldsymbol{v}) = (\boldsymbol{f}, \boldsymbol{v})_\Omega \quad \forall \boldsymbol{v} \in \mathbf{V}_{0,div}(\Omega), \tag{2.58}$$

where

$$A(\boldsymbol{u}, \boldsymbol{v}) := B_{div}(\boldsymbol{u}, \boldsymbol{v}) + ((\boldsymbol{\beta} \cdot \nabla)\boldsymbol{u}, \boldsymbol{v})_\Omega + (\sigma \boldsymbol{u}, \boldsymbol{v})_\Omega \quad \forall \boldsymbol{u}, \boldsymbol{v} \in \left(H^1(\Omega)\right)^d. \tag{2.59}$$

Clearly, it is possible to generalize the theoretical framework of the scalar case using the underlying function spaces, as each of the components of this system is of the form (2.29)-(2.30). Hence the regularized/penalized problem prepared for handling the original problem on a suitable fictitious domain $\tilde{\Omega}$ reads:

$$\boldsymbol{u}^{\boldsymbol{\rho}} \in \mathbf{V}_{\Gamma_D,div} : \; \rho(\boldsymbol{\nabla} \boldsymbol{u}^{\boldsymbol{\rho}}, \nabla \boldsymbol{v})_{\tilde{\Omega}} + A(\boldsymbol{u}^{\boldsymbol{\rho}}, \boldsymbol{v}) = (\boldsymbol{f}, \boldsymbol{v})_\Omega \quad \forall \boldsymbol{v} \in \mathbf{V}_{\Gamma_D,div}, \tag{2.60}$$

where in this case

$$\mathbf{V}_{\Gamma_D,div} := \left\{ \boldsymbol{v} \in \left(H^1(\tilde{\Omega})\right)^d : \; \boldsymbol{v}|_{\Gamma_D} = 0, \; \nabla \cdot \boldsymbol{v} = 0 \; a.e. \right\},$$

and $\rho > 0$ again is a penalty parameter.

2.5 Description of domain geometries

A survey and comparison on suitable methods for describing geometries in flow problems, applicable for a wider class of problems also, is given e.g. in [Jim04]. As always let $\Omega \subset \mathbb{R}^d$ be a domain with sufficiently smooth boundary $\Gamma = \partial\Omega$, and $\tilde{\Omega} \subset \mathbb{R}^d$, with $\Omega \subset \tilde{\Omega}$, be a covering domain. One way of treating the boundary of an embedded complex or time dependent domain is to interpret the boundary as a front between two different chemical/physical species, while only the behaviour of one species (the one contained in Ω) is of relevance for the original problem. Two general concepts of describing complex or time dependent domains in this sense can be distinguished:

- *Front tracking methods*, describing the boundary/interface Γ as the boundary of a (in general) time-dependent subdomain explicitly, using a boundary-fitted mesh for numerical methods.
- *Front capturing methods*, describing the underlying geometry in an implicit way on a fixed covering domain $\tilde{\Omega}$, without a boundary-fitted grid on the resulting discrete level.

We will concentrate on the second concept, being a kind of Eulerian framework, in order to describe the underlying geometry in an implicit way by a scalar field $\phi : \tilde{\Omega} \times I \to \mathbb{R}$, where as always I is a time interval. We will now discuss popular and common ways of describing a co-dimension one surface implicitly, needed for our purpose.

The transport equation

$$\partial_t \phi + \boldsymbol{v} \cdot \nabla \phi = 0 \quad \text{on } \tilde{\Omega} \times (0, T], \tag{2.61}$$

$$\phi(x, 0) = \phi_0(x) \quad \text{on } \tilde{\Omega}, \tag{2.62}$$

in many cases plays a key role in order to get the scalar field, for it can be interpreted as describing the evolution of the zero level set of a function ϕ in time with respect to a given (or estimated) velocity field $\boldsymbol{v}$.

Phase Field Method One kind of implicit description utilizes the so called phase field function ϕ, see for example [EGK08], which covers the boundary of the domain Ω, being the surface or curve to describe, in a diffusive sense. Depending on whether the function value is one or zero in a given point, this point is within or out of Ω. Moreover, the interface-zone, covering Γ, has typically the form of a tube of maximal-width $\epsilon > 0$. In this zone ϕ behaves like a regularized step-function. The parameter ϵ typically is proportional to the grid width of a covering triangulation on the numerical level. The phase field function can be calculated by solving the Cahn-Hillard equation, be constructed from a signed distance function, for example after solving the transport equation (2.61)-(2.62), or from external data. This kind of description is well suited if the boundary has to be smeared out, see [Jim04].

Volume of Fluid Another common way of implicit description, somewhat akin to the phase field method, often used in multi-physical interface problems of fluids, is the volume of fluid method, see [HN81]. ϕ is a (ideally) cellwise constant function, where $\phi(x,t) \in [0,1]$ gives the volume fraction of the fluids and thus provides a way of giving information regarding the position with respect to the domain Ω and $\tilde{\Omega} \setminus \Omega$, both filled by different fluids. Again an equation of the form (2.61)-(2.62) often is employed in order to get a suitable scalar field ϕ.

Level Set Method The way of implicit description chosen in this work is the so called level set framework, see e.g. [Set99] and [OS88]. A level set function is a (smooth) scalar field $\phi : \tilde{\Omega} \times (0,T] \to \mathbb{R}$, which is often calculated from the first order hyperbolic transport equation (2.61)-(2.62).
Ideally the level set function is a signed distance function, that is it holds $\|\nabla\phi\| = 1$. This is for reason of mass conservation, see [Set99, SFSO97], and for a good and geometrically intuitive description of the co-dimension one surface either, because as the name already says, the function just gives the signed distance of a point in $x \in \mathbb{R}^d$ to the surface; the sign depends on the local orientation of the latter. It allows for the construction of an oriented normal vector field, needed in various calculations in an adequate and easy way as well. Moreover, a sharp description of the boundary can be obtained.

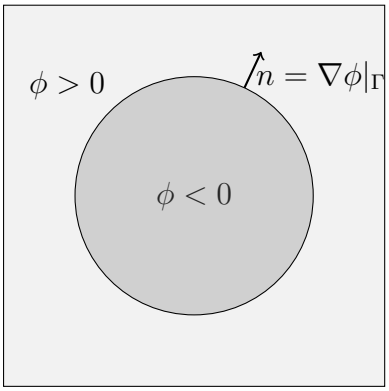

Figure 2.3: Example of the implicit description of a circle $\mathbb{B}_r(x_m, y_m)$ within a covering domain $\tilde{\Omega}$. The level set function in this case is given by $\phi(x, y) := \sqrt{(x - x_m)^2 + (y - y_m)^2} - r$.

The implicit description of Ω embedded in a larger domain $\Omega \subset \tilde{\Omega}$ is very intuitive and works like that:

$$\begin{cases} \phi(x) < 0 & \text{if } x \in \Omega, \\ \phi(x) = 0 & \text{if } x \in \partial\Omega, \\ \phi(x) > 0 & \text{if } x \in \tilde{\Omega} \setminus \overline{\Omega}. \end{cases}$$

So a simple evaluation of ϕ gives information regarding the surface at time t, see Figure 2.3.

3 Discretization

In this chapter the discretization of the coupled systems of equations from Chapter 2 will be described. More precise, we will deal with appropriate linear prototypes, being closely related to linearizations of the original systems of equations from Section 2.2 and 2.3. We will focus on the two-dimensional case, but the methods can be extended to the three-dimensional case as well.
As we potentially have to handle complex and time-dependent domains, and we do not want to employ a re-meshing algorithm, which may produce a very poor grid (see for discussion within the previous chapter), we will use a fictitious domain method. In order to respond to these goal we focus on numerical aspects like stability and the weak incorporation of boundary conditions on implicitly given domains.

We start by formulating assumptions on the relation between covering grid and domain Ω in general. Next an adequate discrete weak formulation of the linear model problems, using the penalty/regularized/FD framework already described in Chapter 2, is developed. This is done for scalar model problems first, followed by another related one for an Oseen model problem. After that we deal with accurate techniques of semi-discretization in time in case of non stationary problems.

In general the model equations and the non-linear RDC-Systems will be convection dominated. So we will have to take care about choosing a robust numerical scheme, being able to handle the resulting problems due to stability and spurious non-physical oscillations, while fitting into the overall framework at the same time.

The discretization of the Stokes and Navier-Stokes systems, based on the Oseen model problem stated below, is given similar to the scalar model equations, but under the additional aspect of the pressure, to be understood as a Lagrangian parameter to ensure the incompressibility condition. Thus, a discrete saddle point problem has to be solved, using Galerkin least squares stabilization techniques to circumvent a discrete inf-sup condition, which is not fulfilled in case of the FE spaces defined below.

While in the standard case a polygonal boundary is given which is part of the closure of a triangulation, we will have to deal with an only implicitly given boundary which cuts an unfitted mesh (see also [BH10a, BH10b] for example). Thus, we will employ the utilities from Section 2.4.2. Whereas in the latter the incorporation of Dirichlet boundary conditions is an essential part of the considered function spaces, we will describe this conditions in an adequate weak sense using Nitsches method, see [Nit71].

3.1 Assumptions on domain and triangulation

Let $\tilde{\Omega}$ be a suitable rectangular domain in $\mathbb{R}^2$, see Section 2.4.2, with $\overline{\Omega} \subset \tilde{\Omega}$. We will make the additional assumption on Ω to be of class C^2, which makes it possible, among other things, to define the boundary of the domain by a locally smooth level set function being a signed distance function (see [LN11] and the literature therein). Furthermore, the following assumptions and definitions regarding the domain Ω, its boundary Γ and the triangulations of the fictitious domain $\tilde{\Omega}$ are made:

A1: Let $\{T_h\}_h$ be a shape regular family of triangulations of $\tilde{\Omega}$, each of them consisting of open quadrilateral elements K with bounded maximal diameter h_K being less or equal to the grid-parameter $h > 0$, where

$$h_K := \operatorname{diam}(K) \quad \text{and} \quad h := \max_{K \in T_h} h_K > 0.$$

One hanging node per element face or quad shall be allowed. In what follows let $h > 0$ always be given and fixed.

A2: The boundary shall be well approximated by piecewise polygons without self-intersections. To be more precise: There exists a domain Ω_h with piecewise polygonal boundary, such that $dist(\Omega \cap K, \Omega_h \cap K) \leq C h_K^2$ holds on each cell. Moreover, the cut $\partial\Omega \cap \partial K$ with each element boundary is either empty, a complete face or exactly two points on different faces of ∂K.

A3: There exists a $\gamma_0 > 0$, such that for each triangulation T_h the diameter d_K of the largest circle contained in $\Omega \cap K$ is limited away from zero by $d_K \geq \gamma_0 h_K$.

Assumption A1 enables the usage of the finite element library deal.II, used for the implementations in this work, which only supports quadrilateral-based elements.

The hanging nodes give rise for efficient and easy to implement local refinement algorithms. In the case of continuous FE the additional constraints to be fulfilled on a side shared by three elements is ensured by elimination/condensation before solving the resulting system, see [BHK].

Assumption A2 represents the wish for the boundary of the domain to be resolved sufficiently good enough by the underlying mesh in some sense, as well as to use an adequate polygonal approximation of it in the concrete implementation, see Section 4.1. If necessary it would be possible to reach this state by local refinements and/or local geometrical smoothing. The methods under consideration thus treats boundaries without self-intersection and local protuberances with respect to the grid. Moreover, the boundary should be sufficiently smooth. Methods better suited for the direct treatment of complex rough boundaries, like the composite FE method, are discussed in Subsection 2.4.1.

In [DBDV10] a domain and the underlying grid are called compatible, if a slight variation of Assumption A3 is valid. This clearly is well founded, as with A1-A3 being valid, the following proposition, being a variant of Proposition 4.1 in [DBDV10], can be given, bringing the roundedness of a local element $K \cap \Omega$ in case $meas(K \cap \Omega) > 0$ into play (see also the discussion in the next section).

Proposition 3.1. *Let Assumptions A1-A3 be true in case of Ω, with $\overline{\Omega} \subset \tilde{\Omega}$ and the triangulation T_h of $\tilde{\Omega}$. Let (K, P, Σ) be an associated finite element and k, m nonnegative integers such that $m < k$. Assume that $\Pi \in \mathcal{L}(H^{k+1}(K), P)$ is a bounded projection and $P \subset H^m(K \cap \Omega)$, where P is a polynomial finite dimensional subspace. Then there exists a constant $C > 0$, not depending on $u \in H^{k+1}(K)$ and h, such that*

$$|u - \Pi u|_{m,K\cap\Omega} \leq C h^{k+1-m} |u|_{k+1,K\cap\Omega}. \tag{3.1}$$

Proof. Due to the assumed kind of shape regularity, the standard techniques of interpolation theory, based on the Bramble-Hilbert lemma, can be utilized in order to get the result. □

The last proposition now opens the gate for analyzing FEMs in the context of the purposed FD methods. Moreover, Assumption A3 will be a key to the error analysis in the next two sections.

3.2 FD discretization for the scalar model equation

The regularized/penalized fictitious domain method of Section 2.4.2, based on the ideas of [GP92] and [GPWZ96] for the model equation (2.29)-(2.31), is now adapted to variants of Nitsches method, see [Nit71]. The reason for doing so is the ability of this methods to impose the essential Dirichlet boundary conditions accurately in a weak sense. In the original formulation of Section 2.4.2 adjusted function spaces for considering the Dirichlet boundary conditions have been used. As the boundary is given only implicitly and the mesh will in general not be fitted to Γ, those spaces are not available. Thus, Nitsches method is an accurate way for imposing essential boundary conditions in a weak sense, when passing over to a discretization of the model equations or the non-linear RDC system.

In what follows let $C > 0$ always be a generic constant if not stated otherwise. Let

$$\Gamma_{D,K} := \Gamma_D \cap K \text{ and } \Gamma_{N,K} := \Gamma_N \cap K,$$

if $K \cap \Gamma \neq \emptyset$. We will describe and analyze the methods at hand under the premise of the absence of variational crimes in the form of approximating a smooth boundary by an appropriate polygonal set, which in fact is done in the concrete implementation. For the details on that see Section 4.2. Using the finite-dimensional space

$$V_h = \{v \in C^0(\overline{\tilde{\Omega}}) : \ v|_K \in Q_1(K) \ \forall K \in T_h, \ v = 0 \text{ on } \partial\tilde{\Omega}\} \subset H_0^1(\tilde{\Omega})$$

of picewise bilinear elements, the discrete weak formulation can be stated as:
Find $u_h^\rho \in V_h$ such that

$$a_h^{\mp}(u_h^\rho, v_h) + \rho b(u_h^\rho, v_h) = l_h^{\mp}(v_h) \tag{3.2}$$

for all $v_h \in V_h$ and $\rho > 0$. The discrete bilinear forms $a_h^{\mp}(\cdot,\cdot)$, $b(\cdot,\cdot)$ respectively the linear form $l_h^{\mp}(\cdot)$ are defined as:

$$\begin{aligned} a_h^{\mp}(u,v) \ := \ & a(u,v) - \langle D\partial_n u, v\rangle_{\Gamma_D} \mp \langle Du, \partial_n v\rangle_{\Gamma_D} + \\ & + \sum_{\Gamma_{D,K}} \frac{\gamma_D^{\mp}}{h_K} \langle Du, v\rangle_{\Gamma_{D,K}} - \langle (\boldsymbol{\beta}\cdot\boldsymbol{n})^- u, v\rangle_{\Gamma_D}, \end{aligned}$$

$$
\begin{aligned}
b(u,v) &:= (\nabla u, \nabla v)_{\tilde{\Omega}}, \\
l_h^{\mp}(v) &:= l(v) \mp \langle Dg_D, \partial_n v\rangle_{\Gamma_D} + \sum_{\Gamma_{D,K}} \frac{\gamma_D^{\mp}}{h_K} \langle Dg_D, v\rangle_{\Gamma_{D,K}} \\
&\quad -\langle (\boldsymbol{\beta}\cdot\boldsymbol{n})^- g_D, v\rangle_{\Gamma_D} + \langle g_N, v\rangle_{\Gamma_N},
\end{aligned}
$$

where $\gamma_D^{\mp} > 0$ is a stabilization parameter, being a sufficiently large real number. In what follows we often refer to those two different FE formulations as $(3.2)^-$ and $(3.2)^+$. Furthermore, let

$$
(y)^- := \begin{cases} y & \text{if } y < 0, \\ 0 & \text{else,} \end{cases}
$$

and

$$
(y)^+ := \begin{cases} y & \text{if } y > 0, \\ 0 & \text{else.} \end{cases}
$$

Before coming to the proof of the well-posedness of the two discrete problems $(3.2)^{\mp}$, a short briefing on the terms appearing in this formulation is given, see also [JS08]:

- The first boundary integral in the definition of $a_h^{\mp}(\cdot,\cdot)$ stems from testing the model PDE and integrating by parts, splitting the boundary into Γ_D and Γ_N.
- The third term in the definition of $a_h^{\mp}(\cdot,\cdot)$ is added in order to preserve symmetry in $H^1(\Omega)$ in case the minus is chosen, while else with the plus the resulting method has better stability properties, see next subsection.
- In general choosing the symmetry preserving version $(3.2)^-$ results in a more accurate method, at least in case of boundary fitted shape regular meshes, see [ABCM02]. But the latter has drawbacks when using unfitted meshes, which will be discussed later on.
- The sum over the cellwise parts of Γ_D is added for stability reason, as well as the last term, which allows a better control of the convection term, see [RST08].
- In all cases a counterpart on the right hand side is added in order to guarantee consistency, taking into account the boundary conditions of the model problem in strong formulation.

So far so classical, but in order to assure stability, care has to be taken when dealing with the roundedness of a local element $K \cap \Omega$ next to Γ_D, similar to the case of the original Nitsche method, see [Han05]. For demonstration a cellwise constant parameter $h_{\Gamma_{D,K}}$ is defined, giving a measure of shape regularity of the involved implicitly given elements $\Omega \cap K$ in case of $K \cap \Gamma_D \neq \emptyset$:

$$h_{\Gamma_{D,K}} := \begin{cases} h_K & \text{if three nodes are in } \overline{K} \cap \overline{\Omega}, \\ \min(h_{K,1}, h_{K,2}) & \text{if two nodes are in } \overline{K} \cap \Omega, \\ \min(h_{K,1}, h_{K,2}) & \text{if one node is in } \overline{K} \cap \Omega, \end{cases} \tag{3.3}$$

where $h_{K,1}, h_{K,2} > 0$ are the Euclidean distances between the two intersections $\partial\Omega \cap \partial K$ and the in each case closest vertex inside Ω, see Figure 3.1.

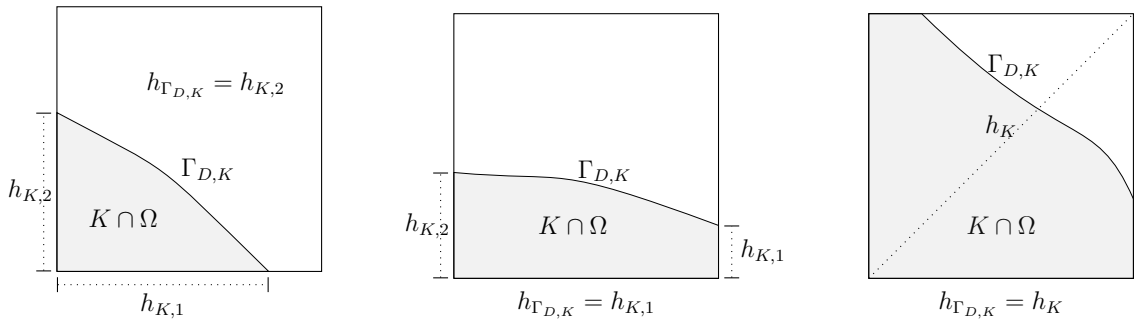

Figure 3.1: The pictures visualize the definition of the parameter $h_{\Gamma_{D,K}}$. In the left situation it is $h_{\Gamma_{D,K}} = h_{K,2}$, while in the middle we set $h_{\Gamma_{D,K}} = h_{K,1}$. In the right picture $h_{\Gamma_{D,K}}$ can be set to the cell-diameter.

Especially the definition of the second and the last case in (3.3) depends on the existence of a minimal diameter $d_K > 0$ of a circle completely within the local cut $K \cap \Omega$, as pointed out in [Han05] and [BH10b] as well. While this is obvious for the third case, in the second case this is due to the fact that the local cut with the mesh has the form of a (deformed) rectangle (small sliver cut). Even if $meas(\Gamma_{D,K})$ has a finite value, $meas(K \cap \Omega)$ does not have to be bounded away from zero, causing $h_{\Gamma_{D,K}}$ to tend to zero.

However, providing Assumption A3 holds, there will be a constant $\gamma_K \in (0, 1]$ with $h_{\Gamma_{D,K}} = \gamma_K h_K$ and a circle with diameter $h_{\Gamma_{D,K}}/2 = \gamma_K h_K/2 \geq \gamma_0 h_K$ bounded away from zero.

In order to analyze the method we will need the following versions of trace/inverse inequalities.

Proposition 3.2. *Let Assumptions A1-A3 be true. Then there holds*

$$\begin{aligned} h_K^{\frac{1}{2}}\|v\|_{0,\Gamma_K} &\leq C(\|v\|_{0,K\cap\Omega} + h_K|v|_{1,K}) \quad \forall v \in H^1(K), && (3.4)\\ h_K^{\frac{1}{2}}\|\partial_n v\|_{0,\Gamma_K} &\leq C(|v|_{1,K\cap\Omega} + h_K|v|_{2,K}) \quad \forall v \in H^2(K), && (3.5)\\ h_K^{\frac{1}{2}}\|\partial_n v_h\|_{0,\Gamma_K} &\leq C\|\nabla v_h\|_{0,K\cap\Omega} \quad \forall v_h \in V_h, && (3.6) \end{aligned}$$

with a bounded constant $C > 0$ and $\Gamma_K := \Gamma \cap K$.

Proof. These inequalities follow by using the trace Theorem (2.1) from [Bra03], and a scaling argument. In more detail, and similar to the proof of Lemma 4.1 in [DBDV10]:

Let $v \in H^1(K)$, $\hat{K} := (0,1)^2$, $\varphi_K : K \to \hat{K}$ be the corresponding affine-linear mapping and $\hat{v} := v \circ \varphi_K \in H^1(\hat{K})$. Due to the made assumptions $\varphi_K(K \cap \Omega) \subset \hat{K}$ is a Lipschitz domain. According to that we find:

$$\int_{\Gamma\cap K} v^2 \, d\Gamma \leq \int_{\hat{K}\cap\varphi_K(\partial\Omega)} \hat{v}^2 \, |J_{\varphi_K}| \, d\hat{\Gamma} \leq \|\hat{v}\|^2_{0,\partial(\varphi_K(K\cap\Omega))} \leq C_K\|\hat{v}\|^2_{1,\varphi_K(K\cap\Omega)},$$

where C_K is the Lipschitz constant of the local cut geometry, depending heavily on the assumed roundedness of $K \cap \Omega$. Writing out the definitions of the norms and by scaling we get

$$\begin{aligned} \|v\|^2_{0,\Gamma\cap K} &\leq C_K\left(\|\hat{v}\|^2_{0,\varphi_K(K\cap\Omega)} + |\hat{v}|^2_{1,\varphi_K(K\cap\Omega)}\right)\\ &\leq \tilde{C}_K\left(h_K^{-1}\|v\|^2_{0,K\cap\Omega} + h_K|v|^2_{1,K\cap\Omega}\right) \end{aligned}$$

from which the the inequalities (3.4) and (3.5) follow again by using the assumed roundedness by setting $C := \max\{\tilde{C}_K : \ K \in T_h, \, K \cap \Gamma \neq \emptyset\}$. Taking into account the norm-equivalence on finite-dimensional spaces inequality (3.6) follows, too.

□

Remark 3.1. Note that as Assumption A3 does not hold for every pair of triangulation and embedded domain, the constant C from the last statement does not have to be moderate or even is not bounded as γ_0 does not have to be bounded away from zero in general. In order to get around this problem, a slight additional geometrical regularization might be necessary to ensure a minimal roundedness of the $K \cap \Omega$ in any case, see Section 4.2 for a possible strategy.

3.2.1 Stability of the discrete form

In order to make things clear, the case of a convection dominated problem, i.e. $|D| \ll |\boldsymbol{\beta}|$, is omitted for the moment. For ease of presentation the diffusion coefficient is supposed to be constant within this section. The presentation is similar to the analogous in the standard case, see e.g. [RST08].

Lemma 3.1. *Assuming A1-A3 and (2.32)-(2.38) hold, for all $v_h \in V_h$ the bilinear form $\rho b(\cdot,\cdot) + a_h^{\mp}(\cdot,\cdot)$ satisfies*

$$\begin{aligned} \rho b(v_h, v_h) + a_h^{\mp}(v_h, v_h) &\geq C\Big\{\rho\|\nabla v_h\|^2_{0,\tilde{\Omega}} + D\|\nabla v_h\|^2_{0,\Omega} + c_0\|v_h\|^2_{0,\Omega} + \\ &+ \||\boldsymbol{n}\cdot\boldsymbol{\beta}|^{\frac{1}{2}} v_h\|^2_{0,\Gamma_D} + \sum_{\Gamma_{D,K}} \frac{D}{h_K}\|v_h\|^2_{0,\Gamma_{D,K}}\Big\}, \end{aligned} \tag{3.7}$$

with sufficiently large $\gamma_D^{\mp} \geq \gamma_0 > 0$ and $C > 0$ being independent of h, ρ and u.

Proof. By the identity

$$\frac{1}{2}\langle(\boldsymbol{n}\cdot\boldsymbol{\beta}), v^2\rangle_{\Gamma_D} + \frac{1}{2}\langle(\boldsymbol{n}\cdot\boldsymbol{\beta}), v^2\rangle_{\Gamma_N} = \frac{1}{2}(\nabla\cdot(\boldsymbol{\beta}v^2), 1)_\Omega = \frac{1}{2}(\nabla\cdot\boldsymbol{\beta}, v^2)_\Omega + (\boldsymbol{\beta}\cdot\nabla v, v)_\Omega,$$

being valid for all $v \in H^1(\tilde{\Omega})$ ($H^1(\Omega)$ is embedded in this larger space), we find:

$$\begin{gathered} (\boldsymbol{\beta}\cdot\nabla v_h + c v_h, v_h)_\Omega - \langle(\boldsymbol{n}\cdot\boldsymbol{\beta})^- v_h, v_h\rangle_{\Gamma_D} = \\ (\underbrace{c - \frac{1}{2}\nabla\cdot\boldsymbol{\beta}}_{\geq c_0}, v_h^2)_\Omega + \tfrac{1}{2}\langle(\boldsymbol{n}\cdot\boldsymbol{\beta}), v_h^2\rangle_{\Gamma_D} + \tfrac{1}{2}\langle\underbrace{(\boldsymbol{n}\cdot\boldsymbol{\beta})}_{\geq 0}, v_h^2\rangle_{\Gamma_N} - \langle(\boldsymbol{n}\cdot\boldsymbol{\beta})^- v_h, v_h\rangle_{\Gamma_D} \geq \\ c_0\|v_h\|^2_{0,\Omega} + \tfrac{1}{2}\langle|\boldsymbol{n}\cdot\boldsymbol{\beta}|, v_h^2\rangle_{\Gamma_D} = c_0\|v_h\|^2_{0,\Omega} + \tfrac{1}{2}\||\boldsymbol{n}\cdot\boldsymbol{\beta}|^{\frac{1}{2}} v_h\|^2_{0,\Gamma_D}. \end{gathered}$$

Consider now the terms $2D\langle\partial_n v_h, v_h\rangle_{\Gamma_{D,K}}$ appearing in case $a_h^-(\cdot,\cdot)$ is chosen. We find by applying the Cauchy-Schwarz and Young's inequality, using inequality (3.6)

$$\begin{aligned} |2D\langle\partial_n v_h, v_h\rangle_{\Gamma_{D,K}}| &\leq 2DCh_K^{-\frac{1}{2}}\|\nabla v_h\|_{0,K\cap\Omega}\|v_h\|_{0,\Gamma_{D,K}} \\ &\leq \frac{D}{2}\|\nabla v_h\|^2_{0,K\cap\Omega} + \frac{2DC^2}{h_K}\|v_h\|^2_{0,\Gamma_{D,K}}. \end{aligned}$$

Hence summation over all elements lying within Ω or including the artificial edges

$\Gamma_{D,K}$ yields:

$$\begin{aligned}\rho b(v_h, v_h) + a_h^-(v_h, v_h) &= \rho\|\nabla v_h\|^2_{0,\tilde{\Omega}} + D\|\nabla v_h\|^2_{0,\Omega} + (\boldsymbol{\beta}\cdot\nabla v_h + cv_h, v_h)_\Omega + \\ &- 2D\langle\partial_n v_h, v_h\rangle_{\Gamma_D} + \sum_{\Gamma_{D,K}} D\frac{\gamma_D^-}{h_K}\|v_h\|^2_{0,\Gamma_{D,K}} - \langle(\boldsymbol{n}\cdot\boldsymbol{\beta})^- v_h, v_h\rangle_{\Gamma_D} \\ &\geq \rho\|\nabla v_h\|^2_{0,\tilde{\Omega}} + \frac{D}{2}\|\nabla v_h\|^2_{0,\Omega} + c_0\|v_h\|^2_{0,\Omega} \\ &+ \sum_{\Gamma_{D,K}} D(\frac{\gamma_D^-}{h_K} - \frac{2C^2}{h_K})\|v_h\|^2_{0,\Gamma_{D,K}} + \frac{1}{2}\||\boldsymbol{n}\cdot\boldsymbol{\beta}|^{\frac{1}{2}} v_h\|^2_{0,\Gamma_D}\end{aligned}$$

for each function $v_h \in V_h$.

After all coercivity of the discrete bilinear form $b(\cdot,\cdot) + a_h^-(\cdot,\cdot)$ is ensured by the choice $\gamma_D^- \geq \gamma_0 \geq \frac{1}{2} + 2C^2$, where C from Proposition 3.2.

In case $a_h^+(\cdot,\cdot)$ is employed, simply setting $\gamma_D^+ > 0$ suffices, as the boundary terms containing the normal derivatives erase each other. □

It follows that problem (3.2) is well posed. Note that by choosing $a_h^+(\cdot,\cdot)$ in place of $a_h^-(\cdot,\cdot)$ ones is far less dependent on Assumption A3 regarding the roundedness of the local cut $K \cap \Omega$ next to Γ_D.

Another relation, taking effectively the place of the Galerkin orthogonality in this case, see also [GP92], and will be used frequently in this work, comes from the following lemma. The value of the penalty parameter $\rho > 0$ may change in different situations.

Lemma 3.2. *Let $u \in H^2(\Omega)$ be the solution of the model problem (2.39), u_h^ρ is the solution of the regularized discrete problem (3.2), then*

$$a_h^\mp(E_2 u - u_h^\rho, v_h) = \rho b(u_h^\rho, v_h) \quad \forall v_h \in V_h. \tag{3.8}$$

Proof. Due to the consistency arguments in the former paragraph (for further details see e.g. [JS08]), using (2.29)-(2.31), and the properties of the extension operator we can write

$$a_h^\mp(E_2 u, v_h) = l_h^\mp(v_h) \quad \forall v_h \in V_h,$$

using the fact that $H^1(\Omega)$ is embedded in $H_0^1(\tilde{\Omega})$. Substracting from this equation (3.2) yields the relation. □

3.2.2 Stabilization in the convection dominated case

In order to give an analysis in case of a convection dominated problem, and for ease of presentation, the diffusion coefficient in (2.39) is assumed to be a constant value ε, being small compared to the norm of $\boldsymbol{\beta}$ at least in some part of the underlying domain. It is well known, see for example [Joh90], that the discretization scheme resulting from the standard Galerkin method gets unstable in case a dominating convective term is added to the symmetrical part of the equation.
This is due to the weak ellipticity of the problem, with respect to its resulting ε-weighted natural norm. In the numerical solution after lauching an FEM based on standard Galerkin, non-physical oscillations can be observed in many cases.
Besides of these nonphysical features, this is a cause of trouble, especially when the numerical solutions are of temporal nature, needed during an overall solution process. The poor quality can lead to a breakdown of the superior task.

In order to stabilize a scheme, which often may have to treat with a dominating convective part for the problems we have to deal with, a standard procedure is the addition of consistency preserving terms (with respect to the original problem) of the form

$$\sum_{K \in T_h} \delta_K (Lu - f, \psi(u))_{\Omega \cap K},$$

see e.g. [RST08]. The mesh dependent parameters $\delta_K > 0$ will be chosen in a suitable manner in order to ensure stability of the resulting scheme, covering the cases of a reaction, diffusion or convection dominated problem, as will be shown later on.

Typical choices for ψ can be $\psi(v) = \boldsymbol{\beta} \cdot \nabla v$ (streamline diffusion, SD) or $\psi(v) = Lv$ (Galerkin least squares, GLS), with L being the underlying linear operator, or an operator close to it. Other choices would be possible, depending on the nature of the underlying problem. We will concentrate on the case $\psi(v) = \boldsymbol{\beta} \cdot \nabla v$, that is the streamline diffusion method. However, the basic principles stay the same for many stabilization methods of this kind and thus the analysis further down can be extended analogously.

The stabilized discrete weak formulation using the SD method with penalty parameter $\rho > 0$ now writes: Find $u_h^\rho \in V_h$, such that

$$A_h^{\mp}(u_h^\rho, v_h) + \rho b(u_h^\rho, v_h) = F_h^{\mp}(v_h) \quad \forall v_h \in V_h, \tag{3.9}$$

where the linear forms are given by

$$\begin{aligned} A_h^{\mp}(u,v) &:= a_h^{\mp}(u,v) + \sum_{K\in T_h} \delta_K(-\varepsilon\triangle u + \boldsymbol{\beta}\cdot\nabla u + cu, \boldsymbol{\beta}\cdot\nabla v)_{\Omega\cap K}, \\ F_h^{\mp}(v) &:= l_h^{\mp}(v) + \sum_{K\in T_h} \delta_K(f, \boldsymbol{\beta}\cdot\nabla v)_{\Omega\cap K}, \end{aligned}$$

defined for all $u, v \in H^1(\tilde{\Omega})$.

Note that due to the local consistency on Ω there holds

$$A_h^{\mp}(E_2 u - u_h^{\rho}, v_h) = \rho b(u_h^{\rho}, v_h) \quad \forall v_h \in V_h \tag{3.10}$$

by the same argument used in the case of the non-stabilized method.

Lemma 3.3. *Suppose the assumptions of Lemma 3.1 hold true. Let δ_K be an elementwise constant function satisfying*

$$0 < \delta_K \leq \frac{c_0}{c_K^2}, \quad \textit{where } c_K := \|c\|_{\infty, K\cap\Omega},$$

on $K \cap \Omega \neq \emptyset$. Then the discrete bilinear form $A_h^{\mp}(\cdot,\cdot) + \rho b(\cdot,\cdot)$ satisfies

$$\begin{aligned} A_h^{\mp}(v_h, v_h) + \rho b(v_h, v_h) &\geq C\Big\{\rho\|\nabla v_h\|^2_{0,\tilde{\Omega}} + \varepsilon\|\nabla v_h\|^2_{0,\Omega} + c_0\|v_h\|^2_{0,\Omega} + \\ &+ \||\boldsymbol{n}\cdot\boldsymbol{\beta}|^{\frac{1}{2}} v_h\|^2_{0,\Gamma_D} + \sum_{K\cap\Omega} \delta_K\|\boldsymbol{\beta}\cdot\nabla v_h\|^2_{K\cap\Omega} + \\ &+ \sum_{\Gamma_{D,K}} \frac{D}{h_K}\|v_h\|^2_{0,\Gamma_{D,K}}\Big\}, \end{aligned} \tag{3.11}$$

with sufficiently large $\gamma_D \geq \gamma_0 > 0$ and $C > 0$ being independent of h.

Proof. Due to (3.7) we only have to focus on the additional stabilization part. For each function $v_h \in V_h$ there holds:

$$\begin{aligned} \sum_K \delta_K(-\varepsilon \underbrace{\triangle v_h}_{=0} + \boldsymbol{\beta}\cdot\nabla v_h + cv_h, \boldsymbol{\beta}\cdot\nabla v_h)_{K\cap\Omega} = \\ \sum_{K\cap\Omega} \delta_K(cv_h, \boldsymbol{\beta}\cdot\nabla v_h)_{K\cap\Omega} + \sum_{K\cap\Omega} \delta_K\|\boldsymbol{\beta}\cdot\nabla v_h\|^2_{K\cap\Omega}. \end{aligned} \tag{3.12}$$

Note that contributions from Laplacians are canceled out, as we effectively use bilinear finite elements on Cartesian grids. We will give an upper bound for the

absolute value of the first term resulting from stabilization, using the given constraint on the parameter δ_K on each element/subelement.

$$\begin{aligned}\left|\sum_{K\cap\Omega}\delta_K(cv_h,\boldsymbol{\beta}\cdot\nabla v_h)_{K\cap\Omega}\right| &\leq \sum_{K\cap\Omega}\left[\delta_K\frac{c_K^2}{2}\|v_h\|_{0,K\cap\Omega}^2+\frac{\delta_K}{2}\|\boldsymbol{\beta}\cdot\nabla v_h\|_{K\cap\Omega}^2\right]\\ &\leq \sum_{K\cap\Omega}\left[\frac{c_0}{2}\|v_h\|_{0,K\cap\Omega}^2+\frac{\delta_K}{2}\|\boldsymbol{\beta}\cdot\nabla v_h\|_{K\cap\Omega}^2\right]\\ &\leq \frac{c_0}{2}\|v_h\|_{0,\Omega}^2+\sum_{K\cap\Omega}\frac{\delta_K}{2}\|\boldsymbol{\beta}\cdot\nabla v_h\|_{K\cap\Omega}^2.\end{aligned}$$

This upper bound together with (3.7) yields the statement. □

As can be seen from the statement of the last lemma, the SD adds artificial diffusion in streamline direction resulting in a more of stability. But there still can be observed over- and undershots in the finite element solution in the presence of sharp layers. Thus, it can be necessary to augment the formulation by suitable shock capturing stabilization terms, in order to add a good amount of artificial diffusion not only in streamline direction. All this is due to the fact that the SD method does not satisfy a discrete maximum principle by itself, which is not addressed in more detail in this work.

Following [RST08], an alternative stabilized method for numerical solution of the regularized/penalized problem, using additional local consistency preserving shock-capturing terms, writes:

$$u_h^\rho\in V_h:\ \rho b(u_h^\rho,v_h)+A_h^{\mp}(u_h^\rho,v_h)+a_{sc}(u_h^\rho;v_h)=F_h(v_h)\quad\forall v_h\in V_h. \tag{3.13}$$

As an example in this formulation the new terms are defined to be of the form

$$\begin{aligned}a_{sc}(u;v) &:= \sum_{K\cap\Omega\neq\emptyset}(\tau_K(u)\nabla u,\nabla v)_{K\cap\Omega},\\ \tau_K(u) &:= \tau^*(R_K^*(u)),\\ R_K^*(u) &:= \frac{\|Lu-f\|_{0,K}}{\kappa_K+\|u\|_{1,K}},\end{aligned}$$

where κ_K is a regularization parameter to ensure the well-posedness of the underlying non-linear problem. $\tau_K^*=\mathcal{O}(h_K^\gamma)$ has to be chosen in such a way, that the order of convergence of the overall scheme is preserved. Note that the consistency with respect to the original problem is still preserved and thus the method fits into the

overall FD framework.

3.2.3 A priori error in the symmetric case

The symmetric case, i.e. $\boldsymbol{\beta} = \mathbf{0}$ in (2.29), is treated first and separately, as it is the easier one and as it is a special case often needed in applications as well.
As there will be given an a priori error bound for the error $u - u_h^\rho$ in a suitable norm, controlling both the $L^2(\Omega)$- and $H^1(\Omega)$-norms of the latter, later on, we first want to give the result of Glowinski et al. from [GP92] for the case of $\Gamma_D = \emptyset$ and $\boldsymbol{\beta} = \mathbf{0}$. Note that V_{Γ_D} has to be replaced by V when using the nomenclature of Section 2.4.2, as $\Gamma_D = \emptyset$.

Clearly, assuming Ω is a $C^{1,1}$ domain in $\mathbb{R}^d$ $(d = 2, 3)$, $f \in H^2(\Omega)$, $g \in H^{\frac{1}{2}}(\Gamma)$, the solution u of problem (2.29)/(2.31) in the considered case will be an element of $H^2(\Omega)$.

Theorem 3.1 (see [GP92])**.**

Let $\Omega \subset \mathbb{R}^d$ $(d = 2, 3)$ be a bounded $C^{k,1}$ domain, where $k > \max\{0, d/2 - 1\}$ and $\overline{\Omega} \subset \tilde{\Omega}$, with $\tilde{\Omega}$ being a rectangular domain. If the solution u of problem (2.39) with $\Gamma_D = \emptyset$, $\boldsymbol{\beta} = \mathbf{0}$ is in $H^{k+1}(\Omega)$, then there holds

$$\|u_h^\rho - u\|_{1,\Omega} \leq C_1 \left(h^k \|u\|_{k+1,\Omega} + \sqrt{\rho} \|u\|_{k+1,\Omega} \right), \tag{3.14}$$

$$\begin{aligned} \|u_h^\rho - u\|_{0,\Omega} \leq\ & C_2 \left(h + \sqrt{\varepsilon} \right) \left(h^k + \sqrt{\rho} \right) \|u\|_{k+1,\Omega} + \\ & + \rho \left(\frac{h}{\sqrt{\varepsilon}} + 1 \right) \left(\frac{h^k}{\sqrt{\rho}} + 1 \right) \|u\|_{k+1,\Omega}, \end{aligned} \tag{3.15}$$

where $C_1, C_2 > 0$ are constants independent of h, u, the solution of problem (2.44) u_h^ρ and ρ, $\varepsilon > 0$.

The ε is the regularization parameter coming from solving and analyzing the auxiliary regularized problem to (2.44):

Find $\phi^\varepsilon \in H_0^1(\tilde{\Omega})$ such that:

$$a(\phi^\varepsilon, v) + \varepsilon b(\phi, v) = ((u - u_h^\rho), v)_\Omega \quad \forall v \in H_0^1(\tilde{\Omega}), \tag{3.16}$$

due to get the $L^2(\Omega)$-error estimate (3.15).

Thus, the regularization/penalty parameters ρ and ε are chosen to be of the form $\rho = Ch^{2s}$, where s is an integer greater or equal to k, as the optimal error estimate for $\|u - u_h^\rho\|_{L^2(\Omega)}$ is of order h^{k+1}.

Following [BH10b] and [GP92], the operator $I^* : H^1(\Omega) \to V_h$ is defined by $I^* := I_h E$, where I_h is an appropriate projection onto the approximation space V_h. We will take the nodewise bilinear interpolant, E is the extension operator from Theorem (2.2) with $k = 2$.

In order to quantify the different error contributions we define

$$\xi_h^\rho := I^* u - u_h^\rho, \qquad \eta^\rho := Eu - I^* u$$

and

$$e^\rho := Eu - u_h^\rho = \underbrace{(Eu - I^* u)}_{\eta^\rho} + \underbrace{(I^* u - u_h^\rho)}_{\xi_h^\rho},$$

which are the approximation and method error regarding the regularized solution and the extended solution of problem (2.39) with respect to the space $H_0^1(\tilde{\Omega})$. Note that it holds $\|\eta^\rho\|_{1,\tilde{\Omega}} \leq ch\|u\|_{2,\Omega}$ for sufficiently smooth u due to the properties of the operators E and I^*. The parameter ρ is always assumed to be bounded away from zero and shall be fixed.

For the error analysis the following mesh dependent discrete quantities, being semi-norms, are introduced. Note that these are norms due to the Poincaré inequality. In the case $\rho \to 0$ the norm properties are only fulfilled on suitable subspaces of V.

$$\begin{aligned} \|v\|_{h,\rho,sym}^2 &:= \rho|v|_{1,\tilde{\Omega}}^2 + |v|_{1,\Omega}^2 + \|v\|_{0,\Omega}^2 + \sum_{K \in T_h} h_K^{-1} \|v\|_{0,\Gamma_{D,K}}^2 \quad \forall v \in V, \\ |||v|||_{h,\rho,sym}^2 &:= \|v\|_{h,\rho,sym}^2 + \sum_{K \in T_h} h_K \|\partial_n v\|_{0,\Gamma_{D,K}}^2 \quad \forall v \in V. \end{aligned}$$

Clearly, these quantities are related to the stabilized discrete bilinear form $(\rho b + a_h^{\mp})(\cdot,\cdot)$ with $\boldsymbol{\beta} = 0$, while the first turns out to be equivalent to the second one on the space V_h:

Lemma 3.4. *Providing A3 holds, there exists a bounded constant $C > 0$, not depending on local grid-widths, such that*

$$\sum_{\Gamma_{D,K}} h_K \|\partial_n v_h\|_{0,\Gamma_{D,K}}^2 \leq C|v_h|_{1,\Omega}^2 \quad \forall v_h \in V_h. \tag{3.17}$$

Proof. Immediately from (3.6). □

This feature is also well established and used in the standard case, see [JS08]. Moreover, this paragraph has been inspired by the techniques used in [BH10b].

Lemma 3.5. *Providing Assumption A3 holds, $u, v \in H^1(\tilde{\Omega})$, $v_h \in V_h$, then*

$$\rho b(u,v) + a_h^{\mp}(u,v) \leq C|||u|||_{h,\rho,sym}|||v|||_{h,\rho,sym}, \tag{3.18}$$

$$\rho b(u,v_h) + a_h^{\mp}(u,v_h) \leq C|||u|||_{h,\rho,sym}\|v_h\|_{h,\rho,sym}, \tag{3.19}$$

with a constant $C > 0$ not depending on h, ρ and u.

Proof. The first bound is an immediate consequence of the Cauchy-Schwarz inequality. The second one follows again by the Cauchy-Schwarz inequality taking the norm equivalence proved by (3.17) into account. □

Lemma 3.6. *Let z be an element of $H^2(\Omega)$, then*

$$|||Ez - I^*z|||_{h,\rho,sym} \leq Ch\sqrt{\rho + 1 + h^2}\|z\|_{2,\Omega}, \tag{3.20}$$

with $C > 0$ not depending on h, ρ and z.

Proof. Simply writing out the definition yields

$$\begin{aligned}|||Ez - I^*z|||^2_{h,\rho,sym} \leq \rho|Ez - I^*z|^2_{1,\tilde{\Omega}} + |Ez - I^*z|^2_{1,\Omega} + \|Ez - I^*z\|^2_{0,\Omega} + \\ + \sum_{K\in T_h} h_K\|\partial_n(Ez - I^*z)\|^2_{0,\Gamma_{D,K}} + \sum_{K\in T_h} h_K^{-1}\|Ez - I^*z\|^2_{0,\Gamma_{D,K}}.\end{aligned}$$

The individual terms can be handled in the following way to bring the approximation properties of the underlying discrete space into play:

$$\begin{aligned}\rho|Ez - I^*z|^2_{1,\tilde{\Omega}} &\leq C\rho h^2\|Ez\|^2_{2,\tilde{\Omega}} \leq C\rho h^2\|z\|^2_{2,\Omega}, \\ |Ez - I^*z|^2_{1,\Omega} &\leq Ch^2\|Ez - I^*z\|^2_{2,\tilde{\Omega}} \leq Ch^2\|z\|^2_{2,\Omega}, \\ \|Ez - I^*z\|^2_{0,\Omega} &\leq Ch^4\|z\|^2_{2,\Omega}.\end{aligned}$$

The boundary terms are treated cell by cell, frequently using the trace inequalities

and an inverse inequality (3.4)-(3.6) following from Assumption A3.

$$\begin{aligned} h_K^{\frac{1}{2}}\|\partial_n(Ez - I^*z)\|_{0,\Gamma_{D,K}} \leq \quad & C\left(|Ez - I^*z|_{1,K} + h_K|Ez - I^*z|_{2,K}\right) \leq Ch_K\|Ez\|_{2,K}, \\ h_K^{-\frac{1}{2}}\|(Ez - I^*z)\|_{0,\Gamma_{D,K}} \leq \quad & C\left(h_K^{-1}\|Ez - I^*z\|_{0,K} + |Ez - I^*z|_{1,K}\right) \leq Ch_K\|Ez\|_{2,K}. \end{aligned}$$

Hence by squaring and summing these contributions we get

$$\begin{aligned} \sum_{K\in T_h} h_K\|\partial_n(Ez - I^*z)\|^2_{0,\Gamma_{D,K}} &\leq Ch^2\|z\|^2_{2,\Omega}, \\ \sum_{K\in T_h} \gamma_D h_K^{-1}\|Ez - I^*z\|^2_{0,\Gamma_{D,K}} &\leq Ch^2\|z\|^2_{2,\Omega}. \end{aligned}$$

and the statement follows. □

Corollary 3.1. *For the error $e^\rho = Eu - u_h^\rho$, u, u_h^ρ being the solutions of the symmetric versions of (2.39) and (2.44) it holds:*

$$|||e^\rho|||_{h,\rho,sym} \leq C(h\sqrt{\rho + 1 + h^2} + \sqrt{\rho})\|u\|_{2,\Omega}. \tag{3.21}$$

Proof. By (3.7), setting $\boldsymbol{\beta} = \mathbf{0}$, we get:

$$\begin{aligned} & C\|\xi_h^\rho\|^2_{h,\rho,sym} \leq \rho b(\xi_h^\rho, \xi_h^\rho) + a_h^\mp(\xi_h^\rho, \xi_h^\rho) \\ = \;& \rho b(I^*u - Eu, \xi_h^\rho) + a_h^\mp(I^*u - Eu, \xi_h^\rho) + \rho b(Eu - u_h^\rho, \xi_h^\rho) + a_h^\mp(Eu - u_h^\rho, \xi_h^\rho) \\ = \;& -\rho b(\eta^\rho, \xi_h^\rho) - a_h^\mp(\eta^\rho, \xi_h^\rho) + \rho b(Eu - u_h^\rho, \xi_h^\rho) + \rho b(u_h^\rho, \xi_h^\rho) \\ = \;& -\rho b(\eta^\rho, \xi_h^\rho) - a_h^\mp(\eta^\rho, \xi_h^\rho) + \rho b(Eu, \xi_h^\rho). \end{aligned}$$

Bringing Lemma 3.5 and Lemma 3.6 into play one gets on the one hand

$$\begin{aligned} \rho b(\eta^\rho, \xi_h^\rho) + a_h^\mp(\eta^\rho, \xi_h^\rho) \;&\leq\; C|||\eta^\rho|||_{h,\rho,sym}|||\xi_h^\rho|||_{h,\rho,sym} \\ &\leq\; Ch\sqrt{\rho + 1 + h^2}\|\xi_h^\rho\|_{h,\rho,sym}\|u\|_{2,\Omega}. \end{aligned}$$

And on the other hand

$$\rho b(Eu, \xi_h^\rho) \leq C\rho^{\frac{1}{2}}\|Eu\|_{2,\tilde{\Omega}}\rho^{\frac{1}{2}}|\xi_h^\rho|_{1,\tilde{\Omega}} \leq C\rho^{\frac{1}{2}}\|Eu\|_{2,\tilde{\Omega}}\|\xi_h^\rho\|_{h,\rho,sym}.$$

Hence combining the last relations, dividing by $\|\xi_h^\rho\|_{h,\rho,sym}$ and employing the norm equivalence on the discrete subspace yields

$$|||\xi_h^\rho|||_{h,\rho,sym} \leq C\left(h\sqrt{\rho + 1 + h^2} + \sqrt{\rho})\right)\|u\|_{2,\Omega}.$$

Applying a triangle inequality finally yields

$$|||e^\rho|||_{h,\rho,sym} \leq |||\eta^\rho|||_{h,\rho,sym} + |||\xi_h^\rho|||_{h,\rho,sym} \leq C\left(h\sqrt{\rho+1+h^2}+\sqrt{\rho}\right)\|u\|_{2,\Omega}.$$

□

Following this statement and as the quantity $|||u-u_h^\rho|||_{h,\rho,sym}$ controls the error $\|u-u_h^\rho\|_{1,\Omega}$ as well, $\rho = Ch^2$ is the optimal choice for the penalty parameter, as it was in the case of the pure Neumann problem either.

3.2.4 A priori error for the stabilized method

We will use the error contributions $e^\rho, \eta^\rho, \xi_h^\rho$ defined in the previous section and concentrate on the SD method without additional shock-capturing term. For the error analysis the following mesh dependent quantities are defined, analogously to the symmetric case:

$$\begin{aligned}
\|v\|_{h,\rho}^2 &:= \rho|v|_{1,\tilde{\Omega}}^2 + \varepsilon|v|_{1,\Omega}^2 + c_0\|v\|_{0,\Omega}^2 + \||\boldsymbol{\beta}\cdot\boldsymbol{n}|^{\frac{1}{2}}v\|_{0,\Gamma_D}^2 + \sum_{\Gamma_{D,K}}\frac{\varepsilon}{h_K}\|v\|_{0,\Gamma_{D,K}}^2.\\
|||v|||_{h,\rho}^2 &:= \|v\|_{h,\rho}^2 + \sum_{K\in T_h}\delta_K\|\boldsymbol{\beta}\cdot\nabla v\|_{K\cap\Omega}^2.
\end{aligned}$$

Lemma 3.7. *Let u be the solution of the original problem (2.39), u_h^ρ the solution of the problem (3.9). Then for the error $e^\rho = Eu - u_h^\rho$ holds*

$$|||e^\rho|||_{h,\rho} \leq C\left(\sum_{K\in T_h}\left\{h_K\lambda(\varepsilon,\boldsymbol{\beta},c,h_K,\delta_K,\rho)+\sqrt{\rho}\right\}\|Eu\|_{2,K}\right), \tag{3.22}$$

where

$$\begin{aligned}
\lambda(\varepsilon,\boldsymbol{\beta},c,h_K,\delta_K,\rho) := \;& \rho^{\frac{1}{2}} + \varepsilon^{\frac{1}{2}} + (1+\delta_K^{-\frac{1}{2}})h_K + h_K^{\frac{1}{2}} + \\
&+\delta_K^{\frac{1}{2}}(\varepsilon h_K^{-1} + \|\boldsymbol{\beta}\|_{\infty,K\cap\Omega} + \|c\|_{\infty,K\cap\Omega}h_K)
\end{aligned}$$

and $C>0$ does not depend on ε, ρ, h and u.

Proof. By (3.7) it holds analogously to the symmetric case

$$\begin{aligned} C|||\xi_h^\rho|||_{h,\rho}^2 &\leq \rho b(\xi_h^\rho,\xi_h^\rho) + A_h^\mp(\xi_h^\rho,\xi_h^\rho) \\ &= \rho b(I^*u - Eu,\xi_h^\rho) + A_h^\mp(I^*u - Eu,\xi_h^\rho) + \\ &+ \rho b(Eu - u_h^\rho,\xi_h^\rho) + A_h^\mp(Eu - u_h^\rho,\xi_h^\rho) \\ &= -\rho b(\eta^\rho,\xi_h^\rho) - A_h^\mp(\eta^\rho,\xi_h^\rho) + \\ &+ \rho b(Eu - u_h^\rho,\xi_h^\rho) + \rho b(u_h^\rho,\xi_h^\rho) \\ &= -\rho b(\eta^\rho,\xi_h^\rho) - A_h^\mp(\eta^\rho,\xi_h^\rho) + \rho b(Eu,\xi_h^\rho). \end{aligned}$$

The last term on the right hand side can be bounded in the usual way by

$$\rho b(Eu,\xi_h^\rho) \leq \rho^{\frac{1}{2}}|Eu|_{1,\tilde{\Omega}}\rho^{\frac{1}{2}}|\xi_h^\rho|_{1,\tilde{\Omega}} \leq C\rho^{\frac{1}{2}}\|Eu\|_{2,\tilde{\Omega}}|||\xi_h^\rho|||_{h,\rho}.$$

The first two terms on the right hand side write

$$\begin{aligned} A_h^\mp(\eta^\rho,\xi_h^\rho) + \rho b(\eta^\rho,\xi_h^\rho) &= \rho(\nabla\eta^\rho,\nabla\xi_h^\rho)_{\tilde{\Omega}} + \varepsilon(\nabla\eta^\rho,\nabla\xi_h^\rho)_\Omega + (\boldsymbol{\beta}\cdot\nabla\eta^\rho + c\eta^\rho,\xi_h^\rho)_\Omega + \\ &\quad -\varepsilon\langle\partial_n\eta^\rho,\xi_h^\rho\rangle_{\Gamma_D} \mp \varepsilon\langle\eta^\rho,\partial_n\xi_h^\rho\rangle_{\Gamma_D} + \\ &\quad + \varepsilon\sum_{\Gamma_{D,K}}\frac{\gamma_D^\mp}{h_K}\langle\eta^\rho,\xi_h^\rho\rangle_{\Gamma_{D,K}} - \langle(\boldsymbol{n}\cdot\boldsymbol{\beta})^-\eta^\rho,\xi_h^\rho\rangle_{\Gamma_{D,K}} + \\ &\quad + \sum_{K\in T_h}\delta_K(-\varepsilon\triangle\eta^\rho + \boldsymbol{\beta}\cdot\nabla\eta^\rho + c\eta^\rho,\boldsymbol{\beta}\cdot\nabla\xi_h^\rho)_{K\cap\Omega} \\ &= \rho(\nabla\eta^\rho,\nabla\xi_h^\rho)_{\tilde{\Omega}} + \varepsilon(\nabla\eta^\rho,\nabla\xi_h^\rho)_\Omega + \\ &\quad + ((c - \nabla\cdot\boldsymbol{\beta})\eta^\rho,\xi_h^\rho)_\Omega - (\eta^\rho,\boldsymbol{\beta}\cdot\nabla\xi_h^\rho)_\Omega + \\ &\quad + \langle(\boldsymbol{\beta}\cdot\boldsymbol{n})^+\eta^\rho,\xi_h^\rho\rangle_{\Gamma_D} + \langle(\boldsymbol{\beta}\cdot\boldsymbol{n})\eta^\rho,\xi_h^\rho\rangle_{\Gamma_N} + \\ &\quad - \varepsilon\langle\partial_n\eta^\rho,\xi_h^\rho\rangle_{\Gamma_D} \mp \varepsilon\langle\eta^\rho,\partial_n\xi_h^\rho\rangle_{\Gamma_D} + \varepsilon\sum_{\Gamma_{D,K}}\frac{\gamma_D^\mp}{h_K}\langle\eta^\rho,\xi_h^\rho\rangle_{\Gamma_{D,K}} + \\ &\quad + \sum_{K\in T_h}\delta_K(-\varepsilon\triangle\eta^\rho + \boldsymbol{\beta}\cdot\nabla\eta^\rho + c\eta^\rho,\boldsymbol{\beta}\cdot\nabla\xi_h^\rho)_{K\cap\Omega}. \end{aligned}$$

Now we estimate the error contributions element by element. An upper bound for local contributions of the first two terms in this expression can be estimated the following way

$$\begin{aligned} \rho(\nabla\eta^\rho,\nabla\xi_h^\rho)_K &\leq \rho^{\frac{1}{2}}|\eta^\rho|_{1,K}\rho^{\frac{1}{2}}|\xi_h^\rho|_{1,K} \leq C\rho^{\frac{1}{2}}h_K\|Eu\|_{2,K}|||\xi_h^\rho|||_{h,\rho}, \\ \varepsilon(\nabla\eta^\rho,\nabla\xi_h^\rho)_K &\leq \varepsilon^{\frac{1}{2}}|\eta^\rho|_{1,K\cap\Omega}\varepsilon^{\frac{1}{2}}|\xi_h^\rho|_{1,K\cap\Omega} \\ &\leq \varepsilon^{\frac{1}{2}}|\eta^\rho|_{1,\tilde{\Omega}}|||\xi_h^\rho|||_{h,\rho} \leq \varepsilon^{\frac{1}{2}}h_K\|Eu\|_{2,K}|||\xi_h^\rho|||_{h,\rho}. \end{aligned}$$

Now for the remaining contributions from the regular weak formulation:

$$\begin{aligned}
& ((c-\nabla\cdot\boldsymbol{\beta})\eta^\rho,\xi_h^\rho)_{\Omega\cap K} - (\eta^\rho,\boldsymbol{\beta}\cdot\nabla\xi_h^\rho)_{\Omega\cap K} \\
\leq\ & C\left(\|\eta^\rho\|_{0,K\cap\Omega}\|\xi_h^\rho\|_{0,K\cap\Omega} + \delta_K^{-\frac{1}{2}}\|\eta^\rho\|_{0,K\cap\Omega}\delta_K^{\frac{1}{2}}\|\boldsymbol{\beta}\cdot\nabla\xi_h^\rho\|_{0,K\cap\Omega}\right) \\
\leq\ & C\left(1+\delta_K^{-\frac{1}{2}}\right)\|\eta^\rho\|_{0,K}|||\xi_h^\rho|||_{h,\rho} \\
\leq\ & C\left(1+\delta_K^{-\frac{1}{2}}\right)h_K^2\|Eu\|_{2,K}|||\xi_h^\rho|||_{h,\rho}.
\end{aligned}$$

The next terms stem from stabilization:

$$\begin{aligned}
& \delta_K(-\varepsilon\triangle\eta^\rho+\boldsymbol{\beta}\cdot\nabla\eta^\rho+c\eta^\rho,\boldsymbol{\beta}\cdot\nabla\xi_h^\rho)_{K\cap\Omega} \\
\leq\ & \delta_K^{\frac{1}{2}}\|-\varepsilon\triangle\eta^\rho+\boldsymbol{\beta}\cdot\nabla\eta^\rho+c\eta^\rho\|_{0,K\cap\Omega}\delta_K^{\frac{1}{2}}\|\boldsymbol{\beta}\cdot\nabla\xi_h^\rho\|_{0,K\cap\Omega} \\
\leq\ & \delta_K^{\frac{1}{2}}(\|-\varepsilon\triangle\eta^\rho\|_{0,K\cap\Omega}+\|\boldsymbol{\beta}\|_{\infty,K\cap\Omega}|\eta^\rho|_{1,K\cap\Omega}+\|c\|_{\infty,K\cap\Omega}\|\eta^\rho\|_{0,K\cap\Omega})|||\xi_h^\rho|||_{h,\rho} \\
\leq\ & C\delta_K^{\frac{1}{2}}h_K(\varepsilon h_K^{-1}+\|\boldsymbol{\beta}\|_{\infty,K\cap\Omega}+\|c\|_{\infty,K\cap\Omega}h_K)\|Eu\|_{2,K}|||\xi_h^\rho|||_{h,\rho}.
\end{aligned}$$

Now we handle the terms from boundary integration. The trace inequalities (3.4)-(3.6) will be used frequently to estimate an upper bound for the error contributions:

$$\begin{aligned}
\langle(\boldsymbol{\beta}\cdot\boldsymbol{n})^+\eta^\rho,\xi_h^\rho\rangle_{\Gamma_{D,K}} &\leq C\|\eta^\rho\|_{0,\Gamma_{D,K}}|||\xi_h^\rho|||_{h,\rho} \leq Ch_K^{\frac{3}{2}}\|Eu\|_{2,K}|||\xi_h^\rho|||_{h,\rho}, \\
\langle(\boldsymbol{\beta}\cdot\boldsymbol{n})\eta^\rho,\xi_h^\rho\rangle_{\Gamma_{N,K}} &\leq C\|\eta^\rho\|_{0,\Gamma_{N,K}}|||\xi_h^\rho|||_{h,\rho} \leq Ch_K^{\frac{3}{2}}\|Eu\|_{2,K}|||\xi_h^\rho|||_{h,\rho}, \\
\varepsilon\langle\partial_n\eta^\rho,\xi_h^\rho\rangle_K &\leq Ch_K^{\frac{1}{2}}\varepsilon^{\frac{1}{2}}\|\partial_n\eta^\rho\|_{0,\Gamma_{D,K}}h_K^{-\frac{1}{2}}\varepsilon^{\frac{1}{2}}\|\xi_h^\rho\|_{0,\Gamma_{D,K}} \\
&\leq Ch_K\varepsilon^{\frac{1}{2}}\|Eu\|_{2,K}|||\xi_h^\rho|||_{h,\rho}, \\
\varepsilon\langle\eta^\rho,\partial_n\xi_h^\rho\rangle_{\Gamma_{D,K}} &\leq C\varepsilon^{\frac{1}{2}}\|\eta^\rho\|_{0,\Gamma_{D,K}}\varepsilon^{\frac{1}{2}}\|\partial_n\xi_h^\rho\|_{0,\Gamma_{D,K}} \\
&\leq C\varepsilon^{\frac{1}{2}}\|\eta^\rho\|_{0,\Gamma_{D,K}}h_K^{-\frac{1}{2}}\varepsilon^{\frac{1}{2}}|\xi_h^\rho|_{1,\Omega\cap K} \\
&\leq C\varepsilon^{\frac{1}{2}}(h_K^{-1}\|\eta^\rho\|_{0,K}+|\eta^\rho|_{1,K})|||\xi_h^\rho|||_{h,\rho} \\
&\leq C\varepsilon^{\frac{1}{2}}h_K\|Eu\|_{2,K}|||\xi_h^\rho|||_{h,\rho}, \\
\varepsilon\frac{\gamma_D^{\mp}}{h_K}\langle\eta^\rho,\xi_h^\rho\rangle_{\Gamma_{D,K}} &\leq C\frac{\varepsilon^{\frac{1}{2}}}{h_K^{\frac{1}{2}}}\|\eta^\rho\|_{0,\Gamma_{D,K}}\frac{\varepsilon^{\frac{1}{2}}}{h_K^{\frac{1}{2}}}\|\xi_h^\rho\|_{0,\Gamma_{D,K}} \\
&\leq C\varepsilon^{\frac{1}{2}}h_K\|Eu\|_{2,K}|||\xi_h^\rho|||_{h,\rho}.
\end{aligned}$$

Summation of all these terms together with the triangle inequality

$$|||e^\rho|||_{h,\rho} \leq |||\eta^\rho|||_{h,\rho} + |||\xi_h^\rho|||_{h,\rho}$$

and an analogous error bound for the error η^ρ yields the statement. □

In order to guarantee the best possible convergence rates in the case of dominant convection, diffusion or reaction either, while the conditions of Lemma 3.3 are still fulfilled, the elementwise term $\delta_K^{-\frac{1}{2}} h_K + \delta_K^{\frac{1}{2}} \left(\varepsilon h_K^{-1} + \|\boldsymbol{\beta}\|_{\infty,K\cap\Omega} + \|c\|_{\infty,K\cap\Omega} h_K\right)$, being part of the expression λ, has to be minimized.

This is done by the choice

$$\delta_K = \frac{\delta_0}{\varepsilon/h_K^2 + \|\boldsymbol{\beta}\|_{\infty,K\cap\Omega}/h_K + \|c\|_{\infty,K\cap\Omega}}, \tag{3.23}$$

where $\delta_0 > 0$ is another constant parameter. Note that this choice leads to the following desirable asymptotic behaviour:

$$\begin{cases} \delta_K \sim \frac{h}{\|b\|_{\infty,K\cap\Omega}} & \|\boldsymbol{\beta}\|_{\infty,K\cap\Omega} \gg \varepsilon, \|c\|_{\infty,K\cap\Omega} \text{ (convection dominance)}, \\ \delta_K \sim \frac{h^2}{\varepsilon} & \varepsilon \gg \|\boldsymbol{\beta}\|_{\infty,K\cap\Omega}, \|c\|_{\infty,K\cap\Omega} \text{ (diffusion dominance)}, \\ \delta_K \sim \|c\|_{\infty,K\cap\Omega}^{-1} & \|c\|_{\infty,K\cap\Omega} \gg \|\boldsymbol{\beta}\|_{\infty,K}, \varepsilon \text{ (reaction dominance)}, \end{cases} \tag{3.24}$$

on the domain Ω without further loss of accuracy. This choice coincides with the one in [Bra98] for the case of a reactive flow system in an analogous problem. Other choices would be possible, see e.g. [RST08].

3.3 FD discretization of the Oseen problem

As divergence-free discrete spaces are very hard to construct and are not at hand in most cases, including ours, we want to handle the more physical formulation including the pressure, which guarantees the divergence-free condition in a weak sense.

The presence of a Lagrange multiplier makes it necessary to show a discrete inf-sup condition for the underlying bilinear form to be fulfilled, since simply showing mere coercivity of the bilinear form is not sufficient to guarantee the unique discrete solution converging to the continuous one in an admissible norm controlling both the $(H^1(\Omega))^d$- and $(H^1(\tilde{\Omega}))^d$-norm of the primal variable, being the velocity in this case, as well as the $L^2(\Omega)$- and $L^2(\tilde{\Omega})$-norm of the pressure.

The outline of this section is as follows: First a suitable FE formulation of the considered problem is derived, with a stability proof given. After that, an a priori

error analysis is presented, as it was done in the scalar case. In this error analysis we will focus on the symmetric case only, again by setting $\boldsymbol{\beta} = \mathbf{0}$. This is done, because the error analysis in the asymmetrical case would not bring a fundamental new perception, as the resulting new parts from dealing with the convection-term would be treated similar to the asymmetrical scalar case.

3.3.1 Stability of the discrete form

In order to show a discrete inf-sup condition, necessary for proving the stability in the case of a saddle point problem, or better said a resulting mixed FE method, the following lemma will be useful.

Lemma 3.8. *Let $p \in L^2(\tilde{\Omega})$ and $\Omega^C := \tilde{\Omega} \setminus \Omega$ be sufficiently smooth, e.g. a Lipschitz domain. Then there exists a $\boldsymbol{w} \in (H^1(\tilde{\Omega}))^d$ and constants $C_1, C_2 > 0$ not depending on p, such that:*

$$\begin{aligned} \|\boldsymbol{w}\|_{1,\tilde{\Omega}} &\leq C_1 \|p\|_{0,\tilde{\Omega}}, && (3.25)\\ \|\boldsymbol{w}\|_{1,\Omega} &\leq C_2 \|p\|_{0,\Omega}, && (3.26)\\ -(\nabla \cdot \boldsymbol{w}, p)_\Omega &= \|p\|^2_{0,\Omega}. && (3.27) \end{aligned}$$

Moreover, if $meas(\Gamma_D) > 0$, the related velocity $\boldsymbol{w}$ can be chosen such that $\boldsymbol{w}|_{\Gamma_D} = \mathbf{0}$ in the sense of traces.

Proof. As $p \in L^2(\tilde{\Omega})$, $p|_\Omega$ is an element of $L^2(\Omega)$ and $p|_{\Omega^C} \in L^2(\Omega^C)$ as well. Let first $meas(\Gamma_N) > 0$. It follows for the restriction of the pressure to Ω that there exists a $\boldsymbol{v}_1 \in (H^1(\Omega))^d$, with $\boldsymbol{v}_1|_{\Gamma_D} = \mathbf{0}$ in case $meas(\Gamma_D) > 0$, and a constant $M_1 > 0$, such that

$$\|\boldsymbol{v}_1\|_{1,\Omega} \leq M_1 \|p\|_{0,\Omega}, \qquad -\nabla \cdot \boldsymbol{v}_1 = p \text{ in } \Omega.$$

In case $meas(\Gamma_N) = 0$, causing $\Gamma = \Gamma_D$, $p|_\Omega$ can be identified as a member of the equivalence-class $[p] \in L^2(\Omega)/\mathbb{R}$ being isometric to $L^2_0(\Omega)$. Again it follows the existence of a velocity $\boldsymbol{v}_1 \in (H^1_0(\Omega))^d$ and a constant $M_1 > 0$ with

$$\|\boldsymbol{v}_1\|_{1,\Omega} \leq M_1 \inf_{c \in \mathbb{R}} \|p + c\|_{0,\Omega} \leq M_1 \|p\|_{0,\Omega}, \qquad -\nabla \cdot \boldsymbol{v}_1 = p \text{ in } \Omega.$$

The existence of $\boldsymbol{v}_1 \in (H^1(\Omega))^d$ in both cases is ensured by the surjectivity of the divergence operator, see e.g. [Glo03].

Let now $\mathbf{E}_1 : (H^1(\Omega))^d \to (H_0^1(\tilde{\Omega}))^d$ be a proper, continuous, linear extension operator. Setting $\tilde{\boldsymbol{v}}_1 := \mathbf{E}_1 \boldsymbol{v}_1 \in (H_0^1(\tilde{\Omega}))^d$ we find with $M_0(\Omega, \tilde{\Omega}) > 0$

$$\|\tilde{\boldsymbol{v}}_{1,\tilde{\Omega}}\| \leq M_0(\Omega, \tilde{\Omega}) \|\boldsymbol{v}_1\|_{1,\Omega}.$$

The pressure $p|_{\Omega^C} \in L^2(\Omega^C)$ can be decomposed and written as

$$p|_{\Omega^C} = p_2 + p_3 : \qquad p_2 \in L_0^2(\Omega^C),\ p_3 = c_3 \in \mathbb{R}.$$

It follows, again due to the surjectivity of the divergence operator, using the condition of Ω^C being sufficiently smooth, that there exists a $\boldsymbol{v}_2 \in (H_0^1(\Omega^C))^d$ and a $M_2 > 0$, such that:

$$\|\boldsymbol{v}_2\|_{1,\Omega^C} \ \leq \ M_2 \|p_2\|_{0,\Omega^C}, \quad -\nabla \cdot \boldsymbol{v}_2 = p_2 \text{ in } \Omega^C.$$

Let now $\tilde{\boldsymbol{v}}_2 \in (H_0^1(\tilde{\Omega}))^d$ be the extension by zero of $\boldsymbol{v}_2$ to the whole domain $\tilde{\Omega}$.

Furthermore, let $\tilde{p}_3 \in L^2(\tilde{\Omega})$ be the extensions by zero of p_3 to $\tilde{\Omega}$. Similar as before there exists $\tilde{\boldsymbol{v}}_3 \in (H^1(\tilde{\Omega}))^d$, $M_3 > 0$, such that:

$$\|\tilde{\boldsymbol{v}}_3\|_{1,\tilde{\Omega}} \ \leq \ M_3 \|\tilde{p}_3\|_{0,\tilde{\Omega}}, \quad -\nabla \cdot \tilde{\boldsymbol{v}}_3 = \tilde{p}_3 \text{ in } \tilde{\Omega}.$$

With that in mind, setting $\boldsymbol{w} := \tilde{\boldsymbol{v}}_1 + \tilde{\boldsymbol{v}}_2 \in (H^1(\tilde{\Omega}))^d$, remembering the choices of the individual velocities $\tilde{\boldsymbol{v}}_i$, it follows:

$$\begin{aligned}
\|\boldsymbol{w}\|_{1,\tilde{\Omega}} &\leq \|\tilde{\boldsymbol{v}}_1\|_{1,\tilde{\Omega}} + \|\tilde{\boldsymbol{v}}_2\|_{1,\tilde{\Omega}} + \|\tilde{\boldsymbol{v}}_3\|_{1,\tilde{\Omega}} \\
&\leq M_0 \|\boldsymbol{v}_1\|_{1,\Omega} + \|\tilde{\boldsymbol{v}}_2\|_{1,\tilde{\Omega}} + M_3 \|\tilde{p}_3\|_{0,\tilde{\Omega}} \\
&\leq M_0 M_1 \|p\|_{0,\Omega} + M_2 \|p_2\|_{0,\Omega^C} + M_3 \|p_3\|_{0,\Omega^C} \\
&\leq M_0 M_1 \|p\|_{0,\Omega} + (M_2 + M_3) \|p\|_{0,\Omega^C} \\
&\leq C_1 \|p\|_{0,\tilde{\Omega}},
\end{aligned}$$

where $C_1 := (M_0 M_1 + M_2 + M_3) > 0$ and we used the fact that

$$(p_2, p_3)_{\Omega^C} = 0.$$

Moreover, the definition of $\boldsymbol{w}$ yields:

$$\begin{aligned}\|\boldsymbol{w}\|_{1,\Omega} &\leq \|\tilde{\boldsymbol{v}}_1\|_{1,\Omega} + \underbrace{\|\tilde{\boldsymbol{v}}_2\|_{1,\Omega}}_{=0,\text{ as } \tilde{\boldsymbol{v}}_2|_\Omega=0} \\ &\leq M_0 M_1 \|p_1\|_{0,\Omega}\end{aligned}$$

by setting $C_2 := M_0 M_1 > 0$.

The last relation to proof then follows by the fact that $\tilde{\boldsymbol{v}}_2|_\Omega = 0$ and thus $\nabla\cdot\tilde{\boldsymbol{v}}_2|_\Omega = 0$:

$$\begin{aligned}-(\nabla\cdot\boldsymbol{w}, p)_\Omega &= -(\nabla\cdot\tilde{\boldsymbol{v}}_1, p)_\Omega - (\nabla\cdot\tilde{\boldsymbol{v}}_2, p)_\Omega \\ &= (p,p)_\Omega \\ &= \|p\|^2_{0,\Omega}.\end{aligned}$$

Finally, as $\boldsymbol{w}|_\Omega = \boldsymbol{v}_1 \in (H^1(\Omega))^d$ and $\boldsymbol{v}_1|_{\Gamma_D} = 0$, the statement follows. □

Following a similar task as in case of the scalar model problem (2.29)-(2.31), we proceed with giving a discrete, regularized weak formulation convenient to handle the boundary conditions to be imposed weakly, too. Consequently, the same assumptions regarding the equation-data, the triangulation, how the boundary cuts the mesh and so on are being made.

Especially it is assumed that a relation of the form

$$\exists \sigma_0 > 0 : \ \sigma - \frac{1}{2}\nabla\cdot\boldsymbol{\beta} \geq \sigma_0 \text{ a.e. in } \Omega$$

is valid.

As already said, we have to handle a saddle point problem, due to the presence of the pressure variable. Clearly, this changes the nature of the underlying problem compared to the scalar one in an essential way. Remembering the discrete formulation of the scalar problem one could use a regularized version of Nitsches method. Additionally, for ease of presentation, we concentrate on the case $\Gamma = \Gamma_D$, i.e. the pure Dirichlet case.

Keeping the idea of the scalar case, the weak formulation is enriched by a bilinear form corresponding to the natural norm on the corresponding continuous product-space in order to ensure coercivity on the discrete space.

The subspaces used for discretization are defined to be:

$$\begin{aligned}\mathbf{V}_h &:= \left\{\boldsymbol{v}_h \in \left(C^0\big(\overline{\tilde{\Omega}}\big)\right)^d : \ \boldsymbol{v}_h|_K \in \ (Q_1(K))^d \ \forall K \in T_h\right\} \cap \left(H_0^1\big(\tilde{\Omega}\big)\right)^d, \\ Q_h &:= \left\{q_h \in C^0\big(\overline{\tilde{\Omega}}\big) : \ \ q_h|_K \in Q_1(K) \ \forall K \in T_h\right\} \cap H_0^1(\tilde{\Omega}).\end{aligned}$$

With that in mind, we now state the underlying discrete formulation for the Oseen problem.

Let $\rho > 0$ be a regularization parameter. Then find $(\boldsymbol{u}_h^\rho, p_h^\rho) \in \mathbf{W}_h := \mathbf{V}_h \times Q_h$:

$$(\rho B + A_h^\mp)((\boldsymbol{u}_h^\rho, p_h^\rho), (\boldsymbol{v}_h, q_h)) = L_h^\mp(\boldsymbol{v}_h, q_h) \quad \forall (\boldsymbol{v}_h, q_h) \in \mathbf{W}_h, \tag{3.28}$$

with the linear forms defined to be

$$\begin{aligned}A_h^\mp((\boldsymbol{u},p),(\boldsymbol{v},q)) := \ & (\nu\nabla\boldsymbol{u},\nabla\boldsymbol{v})_\Omega + (\sigma\boldsymbol{u},\boldsymbol{v})_\Omega - (p,\nabla\cdot\boldsymbol{v})_\Omega + (\nabla\cdot\boldsymbol{u},q)_\Omega + \\ & + ((\boldsymbol{\beta}\cdot\nabla)\boldsymbol{u},\boldsymbol{v})_\Omega + \gamma_{div}(\nabla\cdot\boldsymbol{u},\nabla\cdot\boldsymbol{v})_\Omega + \\ & + \sum_K \delta_K(-\nu\triangle\boldsymbol{u} + (\boldsymbol{\beta}\cdot\nabla)\boldsymbol{u} + \sigma\boldsymbol{u} + \nabla p, (\boldsymbol{\beta}\cdot\nabla)\boldsymbol{v} + \nabla q)_{K\cap\Omega} + \\ & - \langle\nu\partial_n\boldsymbol{u},\boldsymbol{v}\rangle_{\Gamma_D} \mp \langle\nu\boldsymbol{u},\partial_n\boldsymbol{v}\rangle_{\Gamma_D} + \sum_{\Gamma_{D,K}} \gamma_D^\mp \frac{\nu}{h_K}\langle\boldsymbol{u},\boldsymbol{v}\rangle_{\Gamma_{D,K}} + \\ & + \langle p,\boldsymbol{n}\cdot\boldsymbol{v}\rangle_{\Gamma_D} - \langle\boldsymbol{n}\cdot\boldsymbol{u},q\rangle_{\Gamma_D} + \sum_{\Gamma_{D,K}} \frac{\gamma_1^\mp}{h_K}\langle\boldsymbol{n}\cdot\boldsymbol{u},\boldsymbol{n}\cdot\boldsymbol{v}\rangle_{\Gamma_{D,K}} + \\ & - \langle(\boldsymbol{n}\cdot\boldsymbol{\beta})^-\boldsymbol{u},\boldsymbol{v})\rangle_{\Gamma_D},\end{aligned}$$

$$\begin{aligned}L_h^\mp(\boldsymbol{v},q) := \ & (\boldsymbol{f},\boldsymbol{v})_\Omega + \sum_K \delta_K(\boldsymbol{f},(\boldsymbol{\beta}\cdot\nabla)\boldsymbol{v} + \nabla q)_{K\cap\Omega} + \\ & \mp\langle\nu\boldsymbol{g}_D,\partial_n\boldsymbol{v}\rangle_{\Gamma_D} + \sum_{\Gamma_{D,K}} \frac{\nu\gamma_D^\mp}{h_K}\langle\boldsymbol{g}_D,\boldsymbol{v}\rangle_{\Gamma_{D,K}} + \\ & - \langle\boldsymbol{n}\cdot\boldsymbol{g}_D,q\rangle_{\Gamma_D} + \sum_{\Gamma_{D,K}} \frac{\gamma_1^\mp}{h_K}\langle\boldsymbol{n}\cdot\boldsymbol{g}_D,\boldsymbol{n}\cdot\boldsymbol{v}\rangle_{\Gamma_{D,K}} + \\ & - \langle(\boldsymbol{n}\cdot\boldsymbol{\beta})^-\boldsymbol{g}_D,\boldsymbol{v})\rangle_{\Gamma_D},\end{aligned}$$

$$B((\boldsymbol{u},p),(\boldsymbol{v},q)) := (\boldsymbol{u},\boldsymbol{v})_{1,\tilde{\Omega}} + (p,q)_{1,\tilde{\Omega}}.$$

In this formulation the parameters $\gamma_D^\mp > 0$ and $\gamma_1^\mp \geq 0$ are penalty parameters

analogous to the scalar case. As it turns, out $\gamma_1^{\mp}$ can be set to zero; but $\gamma_1^{\mp} > 0$ obviously has an additional stabilizing effect in case of higher Reynolds numbers $Re \sim \nu^{-1}$ as well as in case of an unfitted mesh.
The resulting methods do have similar properties regarding accuracy and stability as in the scalar case. We refer to the resulting weak formulations as $(3.28)^-$ and $(3.28)^+$.

On the discrete space $\mathbf{W}_h = \mathbf{V}_h \times Q_h \subset (H_0^1(\tilde{\Omega}))^{d+1}$ we define the following expression:

$$\begin{aligned}\|(\boldsymbol{v}, q)\|_{\rho,h}^2 := \quad & \rho\Big[\|\boldsymbol{v}\|_{1,\tilde{\Omega}}^2 + \|q\|_{1,\tilde{\Omega}}^2\Big] + \nu|\boldsymbol{v}|_{1,\Omega}^2 + \sigma_0\|\boldsymbol{v}\|_{0,\Omega}^2 + \nu\|q\|_{0,\Omega}^2 + \\ & + \gamma_{div}\|\nabla\cdot\boldsymbol{v}\|_{0,\Omega}^2 + \sum_K \delta_K\|(\boldsymbol{\beta}\cdot\nabla)\boldsymbol{v} + \nabla q\|_{0,K\cap\Omega}^2 + \\ & + \sum_{\Gamma_{D,K}} \frac{\nu}{h_K}\|\boldsymbol{v}\|_{0,\Gamma_{D,K}}^2 + \||\boldsymbol{\beta}\cdot\boldsymbol{n}|^{\frac{1}{2}}\boldsymbol{v}\|_{0,\Gamma_D}^2 + \sum_{\Gamma_{D,K}} \gamma_1^{\mp} h_K^{-1}\|\boldsymbol{n}\cdot\boldsymbol{v}\|_{0,\Gamma_{D,K}}^2,\end{aligned}$$

its square root being a norm on the discrete space in case $\rho \geq \rho_0 > 0$ and Assumption A3 holds.

Note that due to the standard arguments already presented, there holds with $(\boldsymbol{u}, p)$ being the solution of the model problem (2.55)-(2.57) and $(\boldsymbol{u}_h^\rho, p_h^\rho) \in \mathbf{W}_h$ being the solution of the regularized problem (3.28) with regularization parameter $\rho > 0$, for all $(\boldsymbol{v}_h, q_h) \in \mathbf{W}_h$:

$$A_h^{\mp}((\mathbf{E}_2\boldsymbol{u} - \boldsymbol{u}_h^\rho, E_1 p - p_h^\rho), (\boldsymbol{v}_h, q_h)) = \rho B((\boldsymbol{u}_h^\rho, p_h^\rho), (\boldsymbol{v}_h, q_h)). \tag{3.29}$$

The vector-valued operator $\mathbf{E}_2 : (H^2(\Omega))^d \to (H^2(\tilde{\Omega}))^d$ is defined to be based on the standard extension operator $E_2 : H^2(\Omega) \to H^2(\tilde{\Omega})$, but acting on each component of the function. The operator $E_1 : H^1(\Omega) \to H^1(\tilde{\Omega})$ is the standard extension operator in the scalar case.

Let for simplicity ν be a constant value. We restrict ourself on the special case $0 < \nu \leq 1$ which is harder to handle. The case $\nu > 1$ is the easier one in general, but the proof of a theorem handling this is similar to the one given below, as ν is bounded away from zero. In that case, in the expression $\|(\cdot,\cdot)\|_{\rho,h}$ the factor ν of the $H^1(\Omega)$-semi-norm of the velocity and the $L^2(\Omega)$-norm of the pressure has to be replaced by 1.

We can now state the next theorem in order to show stability, assuring well-posedness

of the discrete problem in the sense of Babuška and Aziz. Note that compared to the scalar case streamline diffusion type Galerkin least squares stabilization terms are included right at the beginning. This is done in order to handle the instabilities possibly appearing in the considered case. Those due to the violation of a discrete inf-sup condition, as the FE spaces employed for the discretization are not compatible in the sense of Babuška. Moreover, those instabilities caused by a probably dominant convection term can be handled as well.

Theorem 3.2. *Let Assumptions A1-A3 be true and $\tilde{\Omega} \setminus \Omega$ be sufficiently smooth, $0 < \nu \leq 1, \gamma_{div} \geq 0, \gamma_D^{\mp} \geq \gamma_0 > 0, \gamma_1^{\mp} > 0$. Let there be constants δ_0, δ_1 and an elementwise constant function δ_K with*

$$0 < \delta_0 h_K^2 \leq \delta_K \leq \delta_1, \quad 0 \leq \sigma_K^2 \delta_K \leq \frac{\sigma_0}{2}, \text{ where } \sigma_K := \max_{x \in K} |\sigma(x)|.$$

Then there exists a $\beta_s > 0$ not depending on ν, h and ρ, such that for all $(\boldsymbol{u}_h, p_h) \in \boldsymbol{W}_h$:

$$\sup_{(\boldsymbol{v}_h, q_h) \in \boldsymbol{W}_h} \frac{(\rho B + A_h^{\mp})((\boldsymbol{u}_h, p_h), (\boldsymbol{v}_h, q_h))}{\|(\boldsymbol{v}_h, q_h)\|_{\rho,h}} \geq \beta_s \ \|(\boldsymbol{u}_h, p_h)\|_{\rho,h}. \tag{3.30}$$

Proof. We proceed as it is done in the case of "standard"-grids (see e.g. [RST08]). Set for abbreviation

$$\begin{aligned}
X_1^2 &:= \gamma_{div} \|\nabla \cdot \boldsymbol{v}\|_{0,\Omega}^2, & X_2^2 &:= \sum_K \delta_K \|(\boldsymbol{\beta} \cdot \nabla)\boldsymbol{v} + \nabla q\|_{0,K\cap\Omega}^2, \\
X_3^2 &:= \sum_{\Gamma_{D,K}} h_K^{-1} \|\boldsymbol{v}\|_{0,\Gamma_{D,K}}^2, & X_4^2 &:= \||\boldsymbol{\beta} \cdot \boldsymbol{n}|^{\frac{1}{2}} \boldsymbol{v}\|_{0,\Gamma_D}^2, \\
X_5^2 &:= \sum_{\Gamma_{D,K}} \gamma_1^{\mp} h_K^{-1} \|\boldsymbol{n} \cdot \boldsymbol{v}\|_{0,\Gamma_{D,K}}^2.
\end{aligned}$$

Now, first by diagonal testing, it is shown that the bilinear form $(\rho B + A_h^{\mp})(\cdot, \cdot)$ is coercive with respect to the natural norm defined by the square root of the sum below. As this part is very similar to the scalar one we skip the details here:

$$\begin{aligned}
(\rho B + A_h^{\mp})((\boldsymbol{v}_h, q_h), (\boldsymbol{v}_h, q_h)) \ \geq \ & \frac{1}{2}\Big\{\rho\Big[\|\boldsymbol{v}_h\|_{1,\tilde{\Omega}}^2 + \|q_h\|_{1,\tilde{\Omega}}^2\Big] + \\
& + \nu |\boldsymbol{v}_h|_{1,\Omega}^2 + \sigma_0 \|\boldsymbol{v}_h\|_{0,\Omega}^2 + \sum_{i=1}^{5} X_i^2\Big\}.
\end{aligned} \tag{3.31}$$

The inequality shows coercivity of the bilinear form on the discrete space, but still we lack control of the $L^2(\Omega)-$norm of the pressure.

In order to get into a position for giving an appropriate error analysis later on, and show the statement of the theorem to be true as well, the key is to bring Lemma 3.8 into play: As $q_h \in H^1(\tilde{\Omega})$, it exists a unique real constant c_0 with $q_h|_\Omega = q_{0,h} + c_0,\ q_{0,h} \in L^2_0(\Omega)$. From Lemma 3.8 it follows the existence of $\boldsymbol{w} \in (H^1_0(\tilde{\Omega}))^d$ with $\boldsymbol{w}|_{\Gamma_D} = 0$, and constants $C_\Omega, C_{\tilde{\Omega}} > 0$, such that $\|\boldsymbol{w}\|_{1,\tilde{\Omega}} \leq C_{\tilde{\Omega}}\|q_h\|_{0,\tilde{\Omega}}$, $\|\boldsymbol{w}\|_{1,\Omega} \leq C_\Omega\|q_h\|_{0,\Omega}$ and $-(\nabla\cdot\boldsymbol{w}, q_h)_\Omega = \|q_h\|^2_{0,\Omega}$. Let now $\boldsymbol{w}_h := \Pi_h\boldsymbol{w} \in \mathbf{V}_h$, Π_h be a Zhang-Scott like interpolation operator, see [SZ90], fulfilling the standard interpolation properties. Then there clearly exist positive constants $C'_\Omega, C'_{\tilde{\Omega}}$ with $\|\boldsymbol{w}_h\|_{1,\tilde{\Omega}} \leq C'_{\tilde{\Omega}}\|q_h\|_{0,\tilde{\Omega}}$ and $\|\boldsymbol{w}_h\|_{1,\Omega} \leq C'_\Omega\|q_h\|_{0,\Omega}$. For brevity we define

$$\sigma_{\max} := \|\sigma\|_{\infty,\Omega}.$$

Testing now with $(\boldsymbol{w}_h, 0)$ in the second argument, we get

$$\begin{aligned}
(\rho B + A_h^{\mp}) \quad ((\boldsymbol{v}_h, q_h), (\boldsymbol{w}_h, 0)) &= \rho\big[(\nabla\boldsymbol{v}_h, \nabla\boldsymbol{w}_h)_{\tilde{\Omega}} + (\boldsymbol{v}_h, \boldsymbol{w}_h)_{\tilde{\Omega}}\big] + \\
&+\nu(\nabla\boldsymbol{v}_h, \nabla\boldsymbol{w}_h)_\Omega + (\sigma\boldsymbol{v}_h, \boldsymbol{w}_h)_\Omega + ((\boldsymbol{\beta}\cdot\nabla)\boldsymbol{v}_h, \boldsymbol{w}_h)_\Omega + \\
&+\gamma_{div}(\nabla\cdot\boldsymbol{v}_h, \nabla\cdot\boldsymbol{w}_h)_\Omega - (q_h, \nabla\cdot(\boldsymbol{w}_h - \boldsymbol{w}))_\Omega + \|q_h\|^2_{0,\Omega} + \\
&+\sum_{\Gamma_{D,K}} \nu\gamma_D h_K^{-1}\langle\boldsymbol{v}_h, \boldsymbol{w}_h - \boldsymbol{w}\rangle_{\Gamma_{D,K}} - \langle(\boldsymbol{\beta}\cdot n)^-\boldsymbol{v}_h, \boldsymbol{w}_h - \boldsymbol{w}\rangle_{\Gamma_D} + \quad (3.32) \\
&+\sum_K \delta_K(-\nu\triangle\boldsymbol{v}_h + (\boldsymbol{\beta}\cdot\nabla)\boldsymbol{v}_h + \sigma\boldsymbol{v}_h + \nabla q_h, (\boldsymbol{\beta}\cdot\nabla)\boldsymbol{w}_h)_{K\cap\Omega} + \\
&-\langle\nu\partial_n\boldsymbol{v}_h, \boldsymbol{w}_h - \boldsymbol{w}\rangle_{\Gamma_D} \mp \langle\nu\boldsymbol{v}_h, \partial_n\boldsymbol{w}_h\rangle_{\Gamma_D} + \langle q_h, \boldsymbol{n}\cdot(\boldsymbol{w}_h - \boldsymbol{w})\rangle_{\Gamma_D} + \\
&+\sum_{\Gamma_{D,K}} \frac{\gamma_1^{\mp}}{h_K}\langle\boldsymbol{n}\cdot\boldsymbol{v}_h, \boldsymbol{n}\cdot(\boldsymbol{w}_h - \boldsymbol{w})\rangle_{\Gamma_{D,K}}.
\end{aligned}$$

The single terms appearing in relation (3.32) are bounded by standard arguments using the Cauchy-Schwarz and Young inequality, for the latter let $\varepsilon_1 > 0$ be a generic parameter. We only deal in detail with the more complicated terms:

$$\begin{aligned}
&\langle q_h, \boldsymbol{n}\cdot(\boldsymbol{w}_h - \boldsymbol{w})\rangle_{\Gamma_D} - (q_h, \nabla\cdot(\boldsymbol{w}_h - \boldsymbol{w}))_\Omega = \sum_K (\nabla q_h, \boldsymbol{w}_h - \boldsymbol{w})_{K\cap\Omega} \\
= \quad &\sum_K ((\boldsymbol{\beta}\cdot\nabla)\boldsymbol{v}_h + \nabla q_h, \boldsymbol{w}_h - \boldsymbol{w})_{K\cap\Omega} - \sum_K ((\boldsymbol{\beta}\cdot\nabla)\boldsymbol{v}_h, \boldsymbol{w}_h - \boldsymbol{w})_{K\cap\Omega}
\end{aligned}$$

$$
\begin{aligned}
&\leq \sum_K \delta_K^{\frac{1}{2}} \delta_K^{-\frac{1}{2}} \|(\boldsymbol{\beta}\cdot\nabla)\boldsymbol{v}_h + \nabla q_h\|_{0,k\cap\Omega} C_K h_K \|\boldsymbol{w}\|_{1,K\cap\Omega} + \\
&+ \sum_K \|(\boldsymbol{\beta}\cdot\nabla)\boldsymbol{v}_h\|_{K\cap\Omega} C_K h_K \|\boldsymbol{w}\|_{1,K\cap\Omega} \\
&\leq CX_2 \left(\sum_K \underbrace{h_K^2 \delta_K^{-1}}_{\leq \delta_0^{-1}} \|\boldsymbol{w}\|_{1,K\cap\Omega}^2 \right)^{\frac{1}{2}} + CC_\Omega h \|\boldsymbol{\beta}\|_{\infty,\Omega} |\boldsymbol{v}_h|_{1,\Omega} \|q_h\|_{0,\Omega} \\
&\leq C_1(\|\boldsymbol{\beta}\|_{\infty,\Omega}, \delta_0, \Omega)\Big[\frac{1}{2\varepsilon_1}|\boldsymbol{v}_h|_{1,\Omega}^2 + \frac{1}{2\varepsilon_1}X_2^2\Big] + \varepsilon_1 \|q_h\|_{0,\Omega}^2.
\end{aligned}
$$

Now we take a look at the terms resulting from least squares stabilization:

$$
\begin{aligned}
&\sum_K \delta_K(-\nu \underbrace{\triangle \boldsymbol{v}_h}_{=0} + (\boldsymbol{\beta}\cdot\nabla)\boldsymbol{v}_h + \sigma \boldsymbol{v}_h + \nabla q_h, (\boldsymbol{\beta}\cdot\nabla)\boldsymbol{w}_h)_{K\cap\Omega} \\
= &\sum_K (\delta_K((\boldsymbol{\beta}\cdot\nabla)\boldsymbol{v}_h + \nabla q_h), (\boldsymbol{\beta}\cdot\nabla)\boldsymbol{w}_h)_{K\cap\Omega} + \sum_K \delta_K(\sigma \boldsymbol{v}_h, (\boldsymbol{\beta}\cdot\nabla)\boldsymbol{w}_h)_{K\cap\Omega} \\
\leq &\sum_K \delta_K \|(\boldsymbol{\beta}\cdot\nabla)\boldsymbol{v}_h + \nabla q_h\|_{0,K\cap\Omega} \|\boldsymbol{\beta}\|_{\infty,K\cap\Omega} |\boldsymbol{w}_h|_{1,K\cap\Omega} + \\
+ &\sum_K \delta_K \sigma_K \|\boldsymbol{\beta}\|_{\infty,K\cap\Omega} \|\boldsymbol{v}_h\|_{0,K\cap\Omega} |\boldsymbol{w}_h|_{1,K\cap\Omega} \\
\leq &\ \delta_1^{\frac{1}{2}} X_2 \|\boldsymbol{\beta}\|_{\infty,\Omega} |\boldsymbol{w}_h|_{1,\Omega} + \delta_1 \sigma_{\max} \|\boldsymbol{\beta}\|_\infty \|v_h\|_{0,\Omega} |\boldsymbol{w}_h|_{1,\Omega} \\
\leq &\ C_2(\|\boldsymbol{\beta}\|_{\infty,\Omega}, \sigma_{\max}, \sigma_{\max}/\sigma_0, \delta_1, \Omega)\Big[\frac{1}{2\varepsilon_1}X_2^2 + \frac{\sigma_0}{2\varepsilon_1}\|v_h\|_{0,\Omega}^2\Big] + \varepsilon_1 \|q_h\|_{0,\Omega}^2.
\end{aligned}
$$

Finally we focus on the boundary terms:

$$
\begin{aligned}
\frac{1}{h_K}\gamma_D \langle \boldsymbol{v}_h, \boldsymbol{w}_h - \boldsymbol{w}\rangle_{\Gamma_{D,K}} &\leq \gamma_D h_K^{-\frac{1}{2}} \|\boldsymbol{v}_h\|_{0,\Gamma_{D,K}} h_K^{-\frac{1}{2}} \|\boldsymbol{w}_h - \boldsymbol{w}\|_{\Gamma_{D,K}} \\
\Longrightarrow \sum_{\Gamma_{D,K}} \nu\gamma_D h_K^{-1} \langle \boldsymbol{v}_h, \boldsymbol{w}_h - \boldsymbol{w}\rangle_{\Gamma_{D,K}} &\leq C_3(\gamma_D, \Omega)\frac{1}{2\varepsilon_1}X_3^2 + \frac{\varepsilon_1}{2}\|q_h\|_{0,\Omega}^2,
\end{aligned}
$$

$$\begin{aligned}
\langle(\boldsymbol{\beta}\cdot\boldsymbol{n})^{-}\boldsymbol{v}_h,\boldsymbol{w}_h-\boldsymbol{w}\rangle_{\Gamma_{D,K}} &\leq \||\boldsymbol{\beta}\cdot\boldsymbol{n}|\boldsymbol{v}_h\|_{0,\Gamma_{D,K}}h_K^{\frac{1}{2}}h_K^{-\frac{1}{2}}\|\boldsymbol{w}_h-\boldsymbol{w}\|_{0,\Gamma_{D,K}}\\
&\leq \||\boldsymbol{\beta}\cdot\boldsymbol{n}|\boldsymbol{v}_h\|_{0,\Gamma_{D,K}}C_K\|\boldsymbol{w}\|_{0,K\cap\Omega}\\
\Longrightarrow\langle(\boldsymbol{\beta}\cdot\boldsymbol{n})^{-}\boldsymbol{v}_h,\boldsymbol{w}_h-\boldsymbol{w}\rangle_{\Gamma_D} &\leq C_4(\Omega)\frac{1}{2\varepsilon_1}X_4^2+\frac{\varepsilon_1}{2}\|q_h\|_{0,\Omega}^2,\\
\langle\nu\partial_n\boldsymbol{v}_h,\boldsymbol{w}_h-\boldsymbol{w}\rangle_{\Gamma_{D,K}} &\leq \nu h_K^{\frac{1}{2}}\|\partial_n\boldsymbol{v}_h\|_{0,\Gamma_{D,K}}h_K^{-\frac{1}{2}}\|\boldsymbol{w}_h-\boldsymbol{w}\|_{0,\Gamma_{D,K}}\\
\Longrightarrow\langle\nu\partial_n\boldsymbol{v}_h,\boldsymbol{w}_h-\boldsymbol{w}\rangle_{\Gamma_D} &\leq C_5(\Omega)\frac{1}{2\varepsilon_1}X_3^2+\frac{\varepsilon_1}{2}\|q_h\|_{0,\Omega}^2,\\
\\
\langle\nu\boldsymbol{v}_h,\partial_n\boldsymbol{w}_h\rangle_{\Gamma_{D,K}} &\leq \mu h_K^{-\frac{1}{2}}\|\boldsymbol{v}_h\|_{0,\Gamma_{D,K}}h_K^{\frac{1}{2}}\|\partial_n\boldsymbol{w}_h\|_{0,\Gamma_{D,K}}\\
\Longrightarrow\langle\nu\boldsymbol{v}_h,\partial_n\boldsymbol{w}_h\rangle_{\Gamma_D} &\leq C_6(\Omega)\frac{1}{2\varepsilon_1}X_3^2+\frac{\varepsilon_1}{2}\|q_h\|_{0,\Omega}^2,\\
\\
\frac{\gamma_1^{\mp}}{h_K}\langle\boldsymbol{n}\cdot\boldsymbol{v}_h,\boldsymbol{n}\cdot(\boldsymbol{w}_h-\boldsymbol{w})\rangle_{\Gamma_{D,K}} &\leq \gamma_1^{\mp}h_K^{-\frac{1}{2}}\|\boldsymbol{n}\cdot\boldsymbol{v}_h\|_{0,\Gamma_{D,K}}h_K^{-\frac{1}{2}}\|\boldsymbol{n}\cdot(\boldsymbol{w}_h-\boldsymbol{w})\|_{0,\Gamma_{D,K}}\\
\Longrightarrow\sum_{\Gamma_{D,K}}\frac{\gamma_1^{\mp}}{h_K}\langle\boldsymbol{n}\cdot\boldsymbol{v}_h,\boldsymbol{n}\cdot(\boldsymbol{w}_h-\boldsymbol{w})\rangle_{\Gamma_{D,K}} &\leq C_7(\gamma_1^{\mp},\Omega)\frac{1}{2\varepsilon_1}X_5^2+\frac{\varepsilon_1}{2}\|q_h\|_0^2.
\end{aligned}$$

This yields the following inequality:

$$\begin{aligned}
&(\rho B+A_h^{\mp})((\boldsymbol{v}_h,q_h),(\boldsymbol{w}_h,0))\geq\rho\Big[-\frac{1}{2}\|\boldsymbol{v}_h\|_{1,\tilde{\Omega}}^2-\frac{C'_{\tilde{\Omega}}}{2}\|q_h\|_{0,\tilde{\Omega}}^2\Big]-\frac{C'_{\Omega}}{2\varepsilon_1}|\boldsymbol{v}_h|_{1,\Omega}^2+\\
&-C_8(\sigma_{\max},\sigma_{\max}/\sigma_0,\Omega)\frac{\sigma_0}{2\varepsilon_1}\|\boldsymbol{v}_h\|_{0,\Omega}^2-C_9(|\boldsymbol{\beta}|_{1,\Omega},\Omega)\frac{1}{2\varepsilon_1}|\boldsymbol{v}_h|_{1,\Omega}^2+\\
&-C_{10}(\gamma_{div},\Omega)\frac{1}{2\varepsilon_1}X_1^2+(1-8\varepsilon_1)\|q_h\|_{0,\Omega}^2-C_1\Big[\frac{1}{2\varepsilon_1}|\boldsymbol{v}_h|_{1,\Omega}^2+\frac{1}{2\varepsilon_1}X_2^2\Big]+\\
&-C_2\Big[\frac{1}{2\varepsilon_1}X_2^2+\frac{1}{2\varepsilon_1}\|\boldsymbol{v}_h\|_{1,\Omega}^2\Big]-\frac{C_3}{2\varepsilon_1}X_3^2-\frac{C_4}{2\varepsilon_1}X_4^2-\frac{C_{11}}{2\varepsilon_1}X_5^2.
\end{aligned}$$

Choosing now $\varepsilon_1=1/16$ gives

$$\begin{aligned}
(\rho B+A_h^{\mp})((\boldsymbol{v}_h,q_h),(\boldsymbol{w}_h,0))\geq\rho\Big[-\frac{1}{2}\|\boldsymbol{v}_h\|_{1,\tilde{\Omega}}^2-\frac{C'_{\tilde{\Omega}}}{2}\|q_h\|_{0,\tilde{\Omega}}^2\Big]+\\
-\frac{C_{12}}{2}\Big[|\boldsymbol{v}_h|_{1,\Omega}^2+\sigma_0\|\boldsymbol{v}_h\|_{0,\Omega}^2+\sum_{i=1}^{5}X_i^2\Big]+\frac{1}{2}\|q_h\|_{0,\Omega}^2,
\end{aligned}\tag{3.33}$$

with an appropriate constant $C_{12}(\|\boldsymbol{\beta}\|_{\infty,\Omega,},|\boldsymbol{\beta}|_{1,\Omega},\sigma_{\max},\delta_0,\delta_1,\gamma_D^{\mp},\gamma_1^{\mp},\gamma_{div},\Omega)>0$.

Now we combine (3.31) and (3.33) via testing by $(\alpha \boldsymbol{v}_h + \nu \boldsymbol{w}_h, \alpha q_h)$ in the second argument, where $\alpha \geq 0$ is a parameter:

$$(\rho B + A_h^{\mp})((\boldsymbol{v}_h, q_h), (\alpha \boldsymbol{v}_h + \nu \boldsymbol{w}_h, \alpha q_h)) \geq \rho \left[\frac{\alpha - 1}{2} \|\boldsymbol{v}_h\|_{1,\tilde{\Omega}}^2 + \frac{\alpha - C'_{\tilde{\Omega}}}{2} \|q_h\|_{0,\tilde{\Omega}}^2 \right] + \\ + \frac{\alpha - C_{12}}{2} \left[\nu |\boldsymbol{v}_h|_{1,\Omega}^2 + \sigma_0 \|\boldsymbol{v}_h\|_{0,\Omega}^2 + \sum_{i=1}^{5} X_i^2 \right] + \frac{\nu}{2} \|q_h\|_{0,\Omega}^2.$$

Fixing the parameter α by $\alpha := \max\left\{2, 1 + C'_{\tilde{\Omega}}, 1 + C_{12}\right\}$ yields

$$(\rho B + A_h^{\mp})((\boldsymbol{v}_h, q_h), (\alpha \boldsymbol{v}_h + \nu \boldsymbol{w}_h, \alpha q_h)) \geq \frac{1}{2} \|(\boldsymbol{v}_h, q_h)\|_{\rho,h}^2.$$

One clearly has that for an arbitrary $q_h \in Q_h$ there holds

$$\begin{aligned} \|(\nu \boldsymbol{w}_h, 0)\|_{\rho,h} &\leq \left[C'_{\tilde{\Omega}} + \tilde{C}(\sigma_{\max}, \gamma_{div}, \gamma_D, \delta_1, \|\boldsymbol{\beta}\|_{\infty,\Omega}, \Omega) C'_{\Omega} \right] \left(\rho \|q_h\|_{0,\tilde{\Omega}}^2 + \nu \|q_h\|_{0,\Omega}^2 \right)^{\frac{1}{2}} \\ &\leq \left[C'_{\tilde{\Omega}} + \tilde{C}(\sigma_{\max}, \gamma_{div}, \gamma_D, \delta_1, \|\boldsymbol{\beta}\|_{\infty,\Omega}, \Omega) C'_{\Omega} \right] \|(\boldsymbol{v}_h, q_h)\|_{\rho,h} \end{aligned}$$

due to the properties of $\boldsymbol{w}_h$ and the definition of $\|(\cdot,\cdot)\|_{\rho,h}$.
This finally yields, by setting

$$\beta_s := \frac{1}{2} \Big(\alpha + (C'_{\tilde{\Omega}} + \tilde{C} C'_{\Omega}) \Big)^{-1},$$

the desired inf-sup condition. □

Remark 3.2. Note that it would not be hard to adapt the last statement and related proof to cases, where at least parts of the fictitious domain boundary $\partial\tilde{\Omega}$ and $\Gamma = \partial\Omega$ coincide. A situation appearing while describing flow around a pinned or even moving rigid body for example, see e.g. Sections 5.1 and 5.2. So after adjusting the underlying function spaces, it is possible to deal with such situations as well.

3.3.2 A priori error in the symmetric case

Different to the scalar case, the error analysis will be carried out only for the symmetric problem, as the essential ideas of an analysis are shown already in the symmetrical case, while additional terms can be handled similar to the scalar asymmetrical one, and thus will bring not much additional enrichment to the work at hand.

As always let $\rho > 0$ be a fixed penalty parameter. In order to give an a priori analysis of the error we define similar to the scalar case:

$$\begin{aligned} \boldsymbol{e}^\rho := (\boldsymbol{e}_u^\rho, e_p^\rho) &:= (\mathbf{E}_2\boldsymbol{u} - \boldsymbol{u}_h^\rho, E_1 p - p_h^\rho) \\ &= (\mathbf{E}_2\boldsymbol{u} - \mathbf{I}^*\boldsymbol{u}, E_1 p - J^* p) + (\mathbf{I}^*\boldsymbol{u} - \boldsymbol{u}_h^\rho, J^* p - p_h^\rho). \end{aligned}$$

As usual let $(\boldsymbol{u}, p) \in \big(\mathbf{V}_{\Gamma_D}(\Omega) \times L^2(\Omega)\big) \cap \big((H^2(\Omega))^d \times H^1(\Omega)\big)$ be the weak solution of the original problem (2.55)-(2.57). Assume the FE function $(\boldsymbol{u}_h^\rho, p_h^\rho) \in \mathbf{W}_h$ to be the solution of the discrete regularized problem (3.28).
The vector valued operator $\mathbf{I}^*$ is defined to be $\mathbf{I}^* := \mathbf{I}_h\mathbf{E}_2$ with $\mathbf{I}_h$ being the standard nodal interpolation. For the pressure component we set $J^* := JE_1$, where J is the Zhang-Scott interpolation operator.

As we want to deal with the symmetric case, being an important specialization often needed in applications, we set $\boldsymbol{\beta} = \mathbf{0}$. Moreover, to keep things straight, we eliminate the dependencies regarding the constant parameters $\nu > 0, \sigma_0 > 0$ by simply setting $\nu = 1$ and $\sigma = 1$. We define the expression

$$\begin{aligned} \|(\boldsymbol{v}, q)\|^2_{\rho,h,sym} := \; & \rho\Big[\|\boldsymbol{v}\|^2_{1,\tilde{\Omega}} + \|q\|^2_{1,\tilde{\Omega}}\Big] + |\boldsymbol{v}|^2_{1,\Omega} + \|\boldsymbol{v}\|^2_{0,\Omega} + \|q\|^2_{0,\Omega} + \\ & + \gamma_{div}\|\nabla\cdot\boldsymbol{v}\|^2_{0,\Omega} + \sum_K \delta_K \|\nabla q\|^2_{0,K\cap\Omega} + \\ & + \sum_{\Gamma_{D,K}} h_K^{-1}\|\boldsymbol{v}\|^2_{0,\Gamma_{D,K}} + \sum_{\Gamma_{D,K}} \gamma_1^{\mp} h_K^{-1}\|\boldsymbol{n}\cdot\boldsymbol{v}\|^2_{0,\Gamma_{D,K}}, \end{aligned}$$

stemming from the original expression $\|(\cdot,\cdot)\|_{\rho,h}$. The next lemma gives information about the approximation properties of the discrete space $\mathbf{W}_h$ with respect to $\|(\cdot,\cdot)\|_{\rho,h,sym}$.

Lemma 3.9. *Let the assumptions of Theorem 3.2 be true. Let* $(\mathbf{z}_1, z_2)$ *be an element of* $(H^2(\Omega))^d \times H^1(\Omega)$*. Then there exists a constant* $C_{sym} > 0$ *not depending on* h*, such that*

$$\begin{aligned} \|(\mathbf{E}_2\boldsymbol{z}_1 - \mathbf{I}^*\boldsymbol{z}_1, E_1 z_2 - J^* z_2)\|_{\rho,h,sym} \quad &\leq \\ C_{sym} h \left(\sum_K \left(\rho + 1 + (\rho + \delta_K) h_K^{-2}\right) \left(\|\boldsymbol{z}_1\|^2_{2,\Omega\cap K} + \|z_2\|^2_{1,\Omega\cap K} \right) \right)^{\frac{1}{2}}&. \end{aligned} \tag{3.34}$$

Proof. As similar results have already been shown in case of the scalar model problem, things are kept short in this proof. Again the standard interpolation properties with respect to the underlying (non-fitted) discrete space come into play by using the extension and interpolation operators given above. From this, not going much into detail, we get:

$$\begin{aligned} &\|(\mathbf{E}_2\boldsymbol{z}_1 - \mathbf{I}^*\boldsymbol{z}_1, E_1 z_2 - J^* z_2)\|^2_{\rho,h,sym} = \rho\|\mathbf{E}_2\boldsymbol{z}_1 - \mathbf{I}^*\boldsymbol{z}_1\|^2_{1,\tilde{\Omega}} + \\ &\quad +\rho\|E_1 z_2 - J^* z_2\|^2_{1,\tilde{\Omega}} + \|\mathbf{E}_2\boldsymbol{z}_1 - \mathbf{I}^*\boldsymbol{z}_1\|^2_{1,\Omega} + \|E_1 z_2 - J^* z_2\|^2_{0,\Omega} + \\ &\quad +\gamma_{div}\|\nabla\cdot(\mathbf{E}_2\boldsymbol{z}_1 - \mathbf{I}^*\boldsymbol{z}_1)\|^2_{0,\Omega} + \sum_K \delta_K |E_1 z_2 - J^* z_2|^2_{1,K\cap\Omega} + \\ &\quad + \sum_{\Gamma_{D,K}} h_K^{-1}\|\mathbf{E}_2\boldsymbol{z}_1 - \mathbf{I}^*\boldsymbol{z}_1\|^2_{0,\Gamma_{D,K}} + \sum_{\Gamma_{D,K}} h_K^{-1}\|\boldsymbol{n}\cdot(\mathbf{E}_2\boldsymbol{z}_1 - \mathbf{I}^*\boldsymbol{z}_1)\|^2_{0,\Gamma_{D,K}} \\ \leq\ & C(\gamma_{div}, \tilde{\Omega}, \Omega) \sum_K \Big[\rho h_K^2 \|\boldsymbol{z}_1\|^2_{2,K\cap\Omega} + \rho\|z_2\|^2_{1,K\cap\Omega} + h_K^2\|\boldsymbol{z}_1\|^2_{2,K\cap\Omega} + \\ &\quad + h_K^2\|z_2\|^2_{1,K\cap\Omega} + \delta_K\|z_2\|^2_{1,K\cap\Omega}\Big] \\ \leq\ & C\sum_K \Big[(\rho+1) h_K^2 \|\boldsymbol{z}_1\|^2_{2,K\cap\Omega} + (h_K^2 + \rho + \delta_K)\|z_2\|^2_{1,K\cap\Omega}\Big]. \end{aligned}$$

Using this, the given estimate follows directly. □

Now we give the a priori error estimate with respect to $\|(\cdot,\cdot)\|_{\rho,h,sym}$, which controls both the quantities $\|\boldsymbol{e}_u^\rho\|_{1,\Omega}$ and $\|e_p^\rho\|_{0,\Omega}$.

Lemma 3.10. *Let* $\nu = \sigma = 1$, $\boldsymbol{\beta} = 0$ *and the assumptions of Theorem* (3.2) *be true. Then for the solution of the discrete regularized problem* (3.28) *it holds the a priori error bound*

$$\|\boldsymbol{e}^\rho\|_{\rho,h,sym} \leq Ch\Big[\sum_K (\rho + 1 + (\delta_K + \rho)h_K^{-2})(\|\boldsymbol{E}_2\boldsymbol{u}_h\|^2_{2,K} + \|E_1 p_h\|^2_{1,K})\Big]^{\frac{1}{2}}, \tag{3.35}$$

with a constant $C > 0$ *not depending on* h *and* ρ*.*

Proof. Employing Theorem 3.2, which clearly covers the case under consideration as well, yields:

$$\begin{aligned} & \|((\boldsymbol{u}_h^\rho - \mathbf{I}^*\boldsymbol{u}, p_h^\rho - J^*p))\|_{\rho,h,sym} \\ \leq\ & \beta_s^{-1} \sup_{(\boldsymbol{v}_h,q_h)\in\mathbf{W}_h} \frac{(\rho B + A_h^\mp)((\boldsymbol{u}_h^\rho - \mathbf{I}^*\boldsymbol{u}, p_h^\rho - J^*p),(\boldsymbol{v}_h,q_h))}{\|(\boldsymbol{v}_h,q_h)\|_{\rho,h,sym}}. \end{aligned} \tag{3.36}$$

As we deal with a regularized method, we lack the Galerkin orthogonality with respect to the discrete spaces used for the purpose. Using relation (3.29) instead, we are able to work around this problem, similar to the scalar case. Thus, in order to derive an upper bound of the term on the right hand side of the latest equation:

$$\begin{aligned} & (\rho B + A_h^\mp)((\boldsymbol{u}_h^\rho - \mathbf{I}^*\boldsymbol{u}, p_h^\rho - J^*p),(\boldsymbol{v}_h,q_h)) \\ =\ & (\rho B + A_h^\mp)((\mathbf{E}_2\boldsymbol{u} - \mathbf{I}^*\boldsymbol{u}, E_1p - J^*p),(\boldsymbol{v}_h,q_h)) - \rho B((\mathbf{E}_2\boldsymbol{u}, E_1p),(\boldsymbol{v}_h,q_h)) \\ =\ & \sum_K \Big\{ \rho\Big[(\mathbf{E}_2\boldsymbol{u} - \mathbf{I}^*\boldsymbol{u}, \boldsymbol{v}_h)_{1,K} + (E_1p - J^*p, q_h)_{1,K}\Big] + (\mathbf{E}_2\boldsymbol{u} - \mathbf{I}^*\boldsymbol{u}, \boldsymbol{v}_h)_{1,K\cap\Omega} + \\ & -(E_1p - J^*p, \nabla\cdot\boldsymbol{v}_h)_{K\cap\Omega} + (\nabla\cdot(\mathbf{E}_2\boldsymbol{u} - \mathbf{I}^*\boldsymbol{u}), q_h)_{K\cap\Omega} + \\ & +\gamma_{div}(\nabla\cdot(\mathbf{E}_2\boldsymbol{u} - \mathbf{I}^*\boldsymbol{u}), \nabla\cdot\boldsymbol{v}_h)_{0,K\cap\Omega} + \\ & +\delta_K(-\triangle(\mathbf{E}_2\boldsymbol{u} - \mathbf{I}^*\boldsymbol{u}) + (\mathbf{E}_2\boldsymbol{u} - \mathbf{I}^*\boldsymbol{u}), \nabla q_h)_{K\cap\Omega} + \\ & +\delta_K(\nabla(E_1p - J^*p), \nabla q_h)_{K\cap\Omega} - \langle\nu\partial_n(\mathbf{E}_2\boldsymbol{u} - \boldsymbol{I}^*u), \boldsymbol{v}_h\rangle_{\Gamma_{D,K}} + \\ & \mp\langle\nu(\mathbf{E}_2\boldsymbol{u} - \boldsymbol{I}^*u), \partial_n\boldsymbol{v}_h\rangle_{\Gamma_{D,K}} + \nu\gamma_D^\mp h_K^{-1}\langle\mathbf{E}_2\boldsymbol{u} - \mathbf{I}^*\boldsymbol{u}, \boldsymbol{v}_h\rangle_{\Gamma_{D,K}} + \\ & +\langle E_1p - J^*p, \boldsymbol{n}\cdot\boldsymbol{v}_h\rangle_{\Gamma_{D,K}} - \langle\boldsymbol{n}\cdot(\mathbf{E}_2\boldsymbol{u} - \mathbf{I}^*\boldsymbol{u}), q_h\rangle_{\Gamma_{D,K}} + \\ & +h_K^{-1}\gamma_1^\mp\langle\boldsymbol{n}\cdot(\mathbf{E}_2\boldsymbol{u} - \mathbf{I}^*\boldsymbol{u}), \boldsymbol{v}_h\rangle_{\Gamma_{D,K}} - \rho\Big[(\mathbf{E}_2\boldsymbol{u}, \boldsymbol{v}_h)_{1,K} + (E_1p_h, q_h)_K\Big]\Big\} \\ \leq\ & C\Big[\sum_K(\rho h_K^2 + h_K^2 + \delta_K)\|\mathbf{E}_2\boldsymbol{u}\|_{2,K\cap\Omega}^2 + \\ & +(\rho + h_K^2 + \delta_K)\|E_1p\|_{1,K}^2 + \rho\Big\{\|\mathbf{E}_2\boldsymbol{u}\|_{2,K}^2 + \|E_1p\|_{1,K}^2\Big\}\Big]^{\frac{1}{2}}\|(\boldsymbol{v}_h,q_h)\|_{\rho,h,sym} \\ \leq\ & Ch\Big\{\sum_K(\rho + 1 + (\rho+\delta_K)h_K^{-2})(\|\mathbf{E}_2\boldsymbol{u}\|_{2,K}^2 + \|E_1p\|_{1,K}^2)\Big\}^{\frac{1}{2}}\|(\boldsymbol{v}_h,q_h)\|_{\rho,h,sym}. \end{aligned}$$

Using this bound together with relation (3.36), the claim follows now by splitting $\boldsymbol{e}^\rho$ into approximation and method error, Lemma 3.9 and a simple triangle inequality. □

3.4 Time discretization

In order to handle non-stationary problems we will focus on Rothe's method. This means first a semi-discretization in time is carried out, using suitable finite difference approximations for the time derivative. After that, we treat the spacial behaviour by the finite element method. As we want to handle time-dependent domains and local refinement, Rothe's method is better suited compared to the classical method of lines, where the spacial discretization by the FEM is carried out first. A review on handling time-dependent problems by the finite element method can be found e.g. in [Ran06, QV94, GR94, Glo03].

To fix the idea, let F be a non-linear differential operator in space, e.g. resulting from the RDC subproblems given in the first chapter, and acting on an appropriate function u, which may be time-dependent as well. Following Rothe's method the initial value problem

$$\partial_t u + F(u) = 0, \quad t \in (0,T), \quad u(0) = u_0, \tag{3.37}$$

will be discretized in time first, with u being an element of a suitable Hilbert space.

Let $0 = t_0 < t_1 < \cdots < t_N = T$ be a partition of the time interval $[0,T]$. One family of schemes for the semi-discretization in time is the so called one-step θ scheme. On an appropriate function space V, with $u^0 = u(\cdot,0) \in V$ given, it can be written as:

For each time step $n \in \{1,\dots,N\}$ solve the problem

$$u^n \in V: \ \left(\frac{u^n - u^{n-1}}{\tau_n}, v\right)_\Omega + \mathcal{A}(\theta u^n + (1-\theta)u^{n-1}; v) = 0 \quad \forall v \in V, \tag{3.38}$$

where $\mathcal{A}$ is the semi-linear form resulting from passing over to the weak formulation, $\tau_n := t_n - t_{n-1}$ is the discrete nth time step size, $u^n := u(\cdot,t_n) \in V$ and $\theta \in [0,1]$ is a continuous parameter.

By choosing $\theta = 1$ respectively $\theta = 0$, the implicit and explicit Euler schemes can be obtained. The implicit Euler scheme is very stable and has good smoothing properties in case of convection dominated problems, but is only of first order time accuracy; moreover it is very dissipative, leading to unwanted damping effects for example in flow problems. The explicit Euler scheme is also limited to first order accuracy, and additionally to very small time steps necessary to ensure the stability

of the resulting scheme. For this reasons the case $\theta = 0$ is avoided in this work. The choice $\theta = \frac{1}{2}$ gives a variant of the second order accurate Crank-Nicolson scheme, which is semi-implicit and less dissipative than the implicit Euler scheme.

As an alternative, the A-stable backward differencing scheme of order two (BDF2) is given: Instead of approximating the time derivative by the standard difference quotient, the one sided difference quotient

$$\partial_t u \approx \frac{\frac{3}{2}u^n - 2u^{n-1} + \frac{1}{2}u^{n-2}}{\tau_n}$$

is used for approximation.

Following that, and again after (uniform) partition of the time-interval in each time step $n \in \{2, \dots, N\}$, with $u^{n-1}, u^{n-2} \in V$ given, solve

$$u^n \in V : \left(\frac{\frac{3}{2}u^n - 2u^{n-1} + \frac{1}{2}u^{n-2}}{\tau_n}, v \right)_\Omega + \mathcal{A}(u^n; v) = 0 \quad \forall\, v \in V. \tag{3.39}$$

The semi-linear form $\mathcal{A}$ again originates from the resulting weak formulation. This scheme is little dissipative due to its A-stability. The one-step θ scheme given above can be used in order to get an adequate second starting value, as noted in [Glo03]. Moreover, the time step size is assumed to be constant during the whole computation, but there are variants of the BDF2 scheme being able to handle varying time steps as well.

With that in mind, for each time step an equation being discretized in time results, which can now be handled by the finite element method after passing over to a finite dimensional subspace and linearization (see Subsection 4.3) of the resulting discrete weak formulation. The resulting equations, when stemming from flow or RDC problems, in all cases will have the form discussed in the former sections of this chapter.

4 Numerical treatment

This chapter deals with the technical details in order to handle the numerical procedures necessary for implementation of the techniques introduced in the former parts of this work. The C++ program library deal.II (see [BHK07]) is used as a central basis for this attempt. First one has to think about the way of getting a suitable and accurate approximation of the original domain Ω under consideration. As we have to deal with unfitted grids with respect to the boundary $\Gamma = \partial\Omega$, suitable quadrature rules have to be provided about to assemble the matrix and right hand side entries of the linear equation systems resulting from the introduced methods. Another aspect is the linearization of the underlying non-linear problems in a suitable way. At the end, various numerical tests of the methods proposed are presented in order to confirm the theory and implementational methods.

4.1 Approximation of the domain Ω and local integration

Providing Assumptions A1-A3 of Chapter 3 hold true, it is possible to approximate the boundary zone, that is the set of local elements $\Omega \cap K$, with $\Omega \cap \Gamma \neq \emptyset$, where K is an element of the underlying triangulation of the hold all domain $\tilde{\Omega}$, by shape regular polyhedra. With that in mind, it is obvious to approximate the boundary $\Gamma = \partial\Omega$ by a set of piecewise polygons

$$\Gamma_h := \left\{(x,y) \in \mathbb{R}^2 : \ \phi_h(x,y) = 0\right\}, \quad \phi_h = I_h\phi,$$

in case of using the piecewise bilinear FE interpolant ϕ_h of the level set function ϕ, describing the boundary with respect to the triangulation, see Figure 4.1.

In order to get an accurate approximation, preserving the asymptotic behaviour of the overall method, first the intersection points of Γ_h with the underlying grid

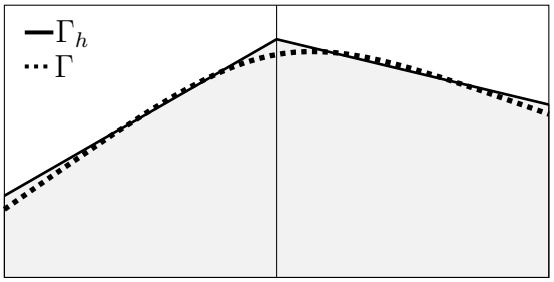

Figure 4.1: Example of a smooth domain Ω bordered by Γ and approximated piecewise polygonal domain Ω_h bordered by Γ_h on two local neighbouring elements in the boundary zone. The local domain Ω_h is shaded grey.

have to be estimated. This is done element by element using the piecewise bilinear approximation of the level set function ϕ, describing the boundary implicitly. A suitable approximation of the original domain Ω then is given by the polygonal set

$$\Omega_h := \{(x, y) \in \mathbb{R}^2 : \ \phi_h(x, y) < 0\}.$$

Each element K of the covering triangulation is marked whether it is part of Ω, being part of the boundary zone ($K \cap \Gamma \neq \emptyset$), or lying completely outside the domain of interest, see Figure 4.2. According to that, there are three different cases to treat with respect to numerical quadrature. The criterion is simply according to the signs of the level set function, being evaluated at the vertices of an element. This can in principle be generalized to the full three dimensional case, again by using for example a nodewise interpolant of the original level set function, see [LN11]. However, the local contributions to the stiffness matrix and right hand side are obtained regarding the three possible cases.

Case 1:
The numerical integrations on the elements completely within Ω is handled the standard way, using the deal.II routines for such tasks. The deal.II library provides a whole zoo of quadrature rules. In particular we utilize Gaussian quadrature within the implementations.

Case 2:
In the case of an element being part of the boundary zone, only the part lying within the approximated domain, using the approximate polygonal boundary description locally, is considered for integration regarding the weak formulation of the original problem to be solved on Ω, see (3.2) and (3.28).

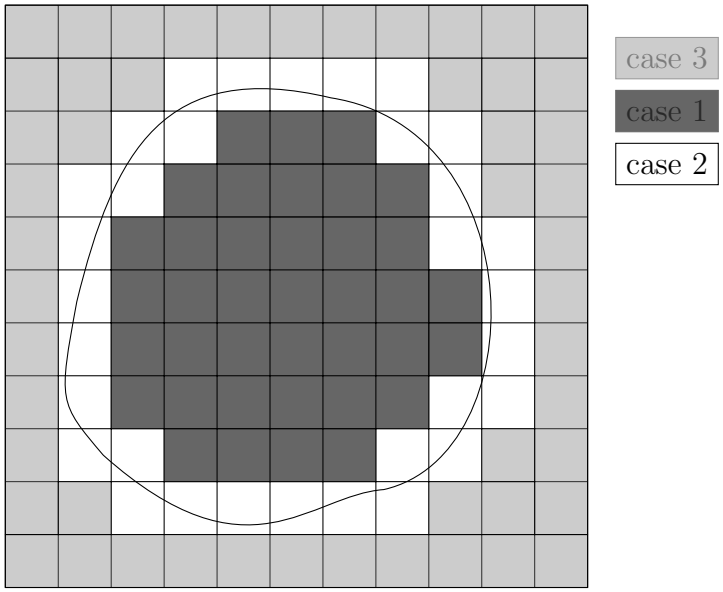

Figure 4.2: Example of a grid partitioned into those cells lying inside Ω (case 1, dark shaded), those in the boundary zone (case 2, white) and those cells outside Ω (case 3, bright shaded). $\overline{\Omega}_h^* \subset \tilde{\Omega}$ from (4.1) below is the union of white and dark shaded elements.

A C++ class LocalIntegrationData, developed for handling this case, provides the infrastructure for giving the elementwise information regarding local intersections with the boundary, splitting the local geometry into elementary units, being quadrilaterals, and giving the quadrature data (quadrature points and weights) in order to generate a suitable quadrature rule needed for integration. Examples for this kind of splitting are given in Figure 4.3.
In older implementations the splitting into elementary units has been into quadrilaterals and triangles, the quadrature formulas being generated according to [Str71]: Starting with a simple trapezoidal rule up to nine-point Gaussian quadrature rule for a local rectangle.
The final implementation introduces a splitting into quadrilaterals only. This has the advantage of bringing the whole lot of two dimensional quadrature rules provided by the deal.II library into play directly (deal.II by itself is only able to handle quadrilateral and hexahedral geometries). The analogous things are provided by the member functions of the LocalIntegrationData class in the case of contributions from local boundary integrals on Γ_h.

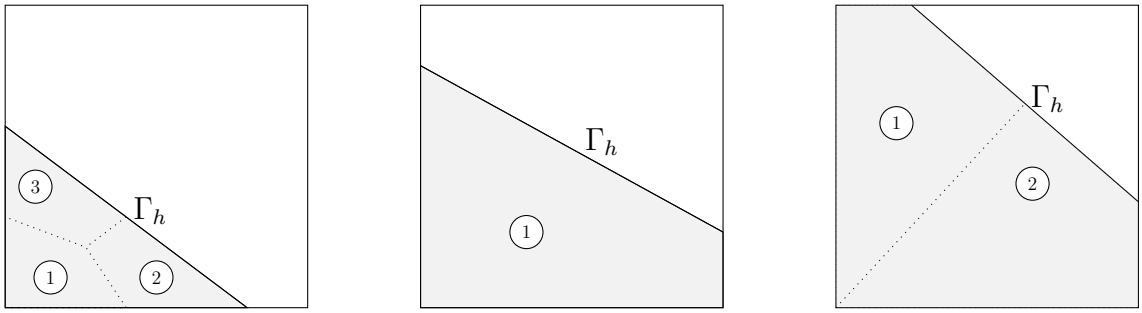

Figure 4.3: Examples for splitting the local approximations $K \cap \Omega_h$ in the boundary zone (marked in grey colour) into quadrilaterals for ease of elementwise cut-integration, required by the FD methods at hand. Left splitting results in three, the right one into two quadrilaterals, while the one in the middle can be treated directly.

Case 3:

The last situation, that is an element K lying completely outside the domain Ω, can be handled in two ways. One is that integrations in order to fill the system matrix are simply carried out for the bilinear form from regularization on that cell, which is the standard way described in the former chapter. The other is handled not exactly as in the original regularized method stated above. Instead of employing the bilinear form $b(\cdot,\cdot)$ from (3.2), when dealing with an RDC system, or $B(\cdot,\cdot)$ for an Oseen problem from Section 3.3, both "living" on the whole grid, the forms

$$b_h(u_h, v_h) := (\nabla u_h, \nabla v_h)_{\Omega_h^*} \quad \text{or} \quad B_h(\boldsymbol{u}_h, \boldsymbol{v}_h) := (\nabla \boldsymbol{u}_h, \nabla \boldsymbol{v}_h)_{\Omega_h^*}$$

are used for regularization along with the standard deal.II routines for integration.

The set Ω_h^* is defined as

$$\Omega_h^* := \{K \in T_h : \ \overline{K} \subset \overline{\Omega}\} \cup \{K \in T_h : \ \Gamma \cap K \neq \emptyset\}, \tag{4.1}$$

see Figure 4.2. The obvious alternative choice $\tilde{\Omega} = \Omega_h^*$ for the fictitious domain is discussed and employed e.g. in [BH10a, BH10b].

Doing so, those degrees of freedom sharing no support with those lying in $\overline{\Omega}_h^*$, are constraint to zero. Note that this could be interpreted as an artificial jump of the coefficients, but the convergence properties of the overall scheme is preserved, as on the one hand we are only interested in the restriction of the solution to the domain Ω and on the other hand the triangulation covers the interface describing the jump exactly, see [Hac86]. However, we could have constrained the discrete solution of

problem (3.2)/(3.28) to another value in the case of not directly involved degrees of freedom, as the discrete solution (as well as the underlying continuous one) has no physical significance in this part of the fictitious domain.

4.2 A geometrical regularization method

In order to ensure the stability of the discrete problems resulting form the regularized ones, and to get a suitable error analysis, Assumptions A1-A3 have been made in Chapter 3. In practice Assumption A2 and A3 are not fulfilled on an arbitrary shape regular mesh in general, at least not locally. Especially the violation of Assumption A3 results in local instabilities in the numerical solution, to be observed as needle-like peak singularities lying slightly outside the domain Ω. This is due to arbitrary small entries in the system matrix, stemming from cut-integration on elements in the boundary zone. One possibility to handle this problem would be to vary the shape of an element: If necessary, slightly shift the vertices of an element in the interface zone, taking into account the position of the intersection points, in order to get a local inequality (3.6) fulfilled.
While this is a good choice in case of a stationary domain Ω, this could lead to problems in the case of $\Omega = \Omega(t)$. Another possibility of handling the drawback of Assumption A3 is not fulfilled would be to slightly shift the intersection points of the discrete zero level set and underlying grid instead of the vertices (if necessary), in order to preserve the mesh, which is a central desire of our methods at hand. Clearly, these shifts have to be made in such a way that the asymptotic behaviour of the overall numerical method is preserved.

The strategy realized in the implementation, if an additional geometrical regularization is desired, in case of an element K with $K \cap \Gamma \neq \emptyset$, is the following. It clearly orients itself on the definition of $h_{\Gamma_{D,K}}$, see (3.3) and Figure 4.4 for an example:

- First compute the two intersection points of approximated boundary Γ_h and ∂K,
- estimate the distances d_1, d_2 of the in each case closest grid-nodes within Ω to the intersections,
- given a number $l \in (0, 1)$: If $\min\{d_1, d_2\} < lh_K$, find this minimum and move the affected intersection point(s), such that both points have a distance not less then lh_K to the closest inner node.

The choice of the parameter l ideally should recover the $\mathcal{O}(h^2)$-error of the overall geometrical approximation. Regularization methods in the same spirit have been realized in [CB09, DBDV10].

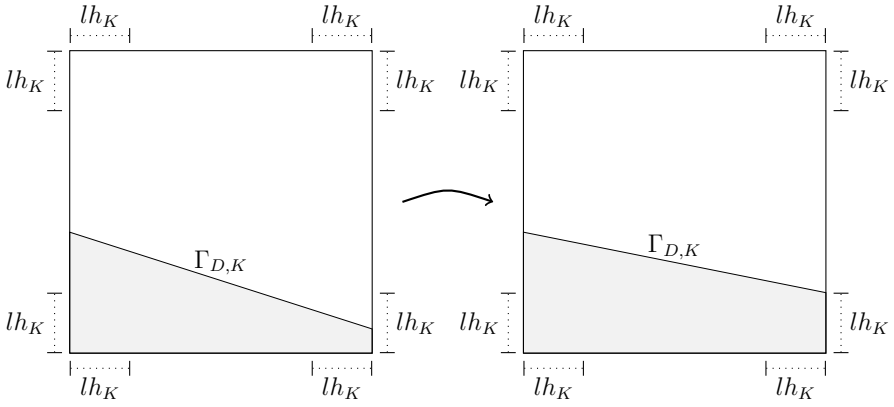

Figure 4.4: Example of the local geometrical regularization. The right intersection point of approximate boundary and grid is slightly moved in order to get a sufficiently shape regular artificial element $K \cap \Omega_h$ in terms of Assumption A3, while the overall order of convergence is preserved.

4.3 Non-linear defect correction

In the stationary non-linear case, the resulting equation system will be solved using fixed point defect correction iteration based on a Newton or Quasi-Newton method. In particular the method is interpreted as a defect correction iteration based on the standard Newton method. The Jacobian of the underlying non-linear residual R, resulting from the non-linear regularized/penalized formulations, is substituted by an adequate approximation $D\tilde{R}$ if necessary.

The original residual can be written out as follows:

$$R(\mathbf{u}; \mathbf{v}) = \sum_{i=1}^{N} R^i(\mathbf{u}; \mathbf{v}), \tag{4.2}$$

with $R^i = R^i_{\tilde{\Omega}} + R^i_{\Omega} + R^i_{\Gamma} + R^i_{stab}$ and N being the number of component functions of the solution $\mathbf{u}$. The different terms of R^i, in order of appearance in the summation, are the residual contributions in the weak formulation resulting from regularization, the original problem on the domain Ω, the ones from weakly imposing the boundary

condition and ensuring stability in case $\boldsymbol{\beta} \neq \mathbf{0}$ and/or violation of the discrete inf-sup condition by Galerkin least squares stabilization.

There are different kinds of pre-linearization in order to get efficient schemes for different kinds of non-linear problems, taking the special behaviour of the underlying problem into account. In all cases these methods have to lead to an approximate Jacobian that is close enough to the original one in order to get an accurate scheme. As such techniques are dependent on the special character of the problem, this will be discussed in the application parts. Only a general procedure is described within this section. Let i be an iteration index. The resulting fixed-point iteration then writes:

1. Start with a predictor u^0,
2. Find $\delta\mathbf{u}^i$ such that:

$$\begin{aligned} D\tilde{R}(\mathbf{u}^i;\mathbf{v})(\delta\mathbf{u}^i) &= -R(\mathbf{u}^i;\mathbf{v}) \quad \forall \mathbf{v} \in \mathbf{V}, \\ \mathbf{u}^{i+1} &:= \mathbf{u}^i + \alpha\delta\mathbf{u}^i, \end{aligned}$$

   while $\|R(\mathbf{u}^i)\| < tol$.

In this procedure tol is a very small number, e.g. of order $\mathcal{O}(h^2)$ at min while using globally refined meshes, such that the error of the non-linear scheme is reduced down to the approximation error, as bilinear FE are used for spatial discretization. The parameter α is set to $\alpha := 2^{-k}$, with k being the smallest non-negative integer such that $\|R(\mathbf{u}^i + 2^{-k}\delta\mathbf{u}^i)\| < \|R(\mathbf{u}^i)\|$, in order to ensure the monotonicity of the iteration scheme. In each iteration step the linear system for the next solution update is solved via a CG solver in the symmetric, or a GMRES solver in the non-symmetric case, in both cases preconditioned by a sparse LU or ILU decomposition of the system matrix. The deal.II intern linear algebra module is utilized for that. Moreover, the sparse direct solver UMFPACK, see [Dav04], can be used for solving the resulting system or providing the LU decomposition.

4.4 Numerical accuracy

Several numerical examples with $\Omega = \mathbb{B}_1(0)$ are presented in order to demonstrate the methods introduced during the former parts of this work with respect to the model equations. We will concentrate on the case of pure Dirichlet problems, as these essential boundary conditions are much harder to impose in a weak sense then the natural Neumann conditions. Besides that and at first, we will test the LocalQuadratureData class.

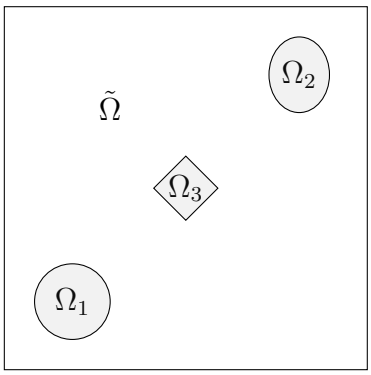

Figure 4.5: The rectangular hold all domain $\tilde{\Omega} = (-1.2, 1.2)^2$ for test case 0 with given circle, ellipse and rectangle embedded for testing the local integrator. The area $meas\big(\tilde{\Omega} \setminus (\Omega_1 \cup \Omega_2 \cup \Omega_3)\big)$ along with $meas\big(\partial\,(\Omega_1 \cup \Omega_2 \cup \Omega_3)\big)$ have to be estimated by numerical integrations using the LocalQuadratureData class member functions.

Test case 0

First, a non-trivial numerical test regarding the LocalQuadratureData class, used for carrying out the cut-integrations in our FD method, is presented. The problem at hand is: Estimate, by numerical integration, the area of $\Omega := \tilde{\Omega} \setminus (\Omega_1 \cup \Omega_2 \cup \Omega_3)$, with $\tilde{\Omega}$ being the rectangle $(-1.2, 1.2)^2$ and

$$\begin{aligned}
\Omega_1 &:= \mathbb{B}_{0.25}(-0.75, -0.75), \\
\Omega_2 &:= \left\{ (x,y) \in \mathbb{R}^2 : \left(\frac{x-0.75}{0.2}\right)^2 + \left(\frac{y-0.75}{0.25}\right)^2 < 1 \right\}, \\
\Omega_3 &:= \left\{ (x,y) \in \mathbb{R}^2 : |x| + |y| < 0.3/\sqrt{2} \right\},
\end{aligned}$$

see picture 4.5. Moreover, the length of $\Gamma := \partial\,(\Omega_1 \cup \Omega_2 \cup \Omega_3)$ has to be estimated. The tests are carried out starting with a four times up to ten times globally refined

mesh covering $\tilde{\Omega} = (-1.2, 1.2)^2$. In this globally refined case the order of convergence is expected to be $\mathcal{O}(h^2)$, which is reached as the results shown in Table 4.1 indicate.

Cycle	h	Error $meas(\Omega)$	Rate	Error $meas(\Gamma)$	Rate
4	0.2121	2.77e-02	-	6.32e-02	-
5	0.1061	6.86e-03	2.01	1.65e-02	1.94
6	0.0530	1.69e-03	2.02	4.04e-03	2.02
7	0.0265	4.43e-04	1.93	1.03e-03	1.98
8	0.0133	1.09e-04	2.03	2.54e-04	2.01
9	0.0066	2.73e-05	2.00	6.43e-05	1.98
10	0.0033	6.75e-06	2.01	1.59e-05	2.02

Table 4.1: Absolute errors for $meas(\Omega)$ and $meas(\Gamma)$, with $\Omega := \tilde{\Omega} \setminus (\Omega_1 \cup \Omega_2 \cup \Omega_3)$ and $\Gamma := \partial(\Omega_1 \cup \Omega_2 \cup \Omega_3)$, resulting from the approximate integration, using member functions of the LocalIntegrationData class for test case 0. The results show almost optimal order of convergence.

Test case 1

Test case 1 deals with a non-linear reaction-diffusion problem on $\Omega = \mathbb{B}_1(0)$ of the form

$$\boldsymbol{u} = (u_1, u_2) \in (C^2(\Omega) \cap C^0(\overline{\Omega}))^2 : \begin{cases} -\triangle u_1 = \sin(u_2) + f_1, \\ -\triangle u_2 = \sin(u_1) + f_2, \\ \boldsymbol{u}|_\Gamma = \boldsymbol{g}. \end{cases} \tag{4.3}$$

The equation data f_1, f_2 and $\boldsymbol{g}$ are defined, such that the analytical solution is $\boldsymbol{u} = (\exp(4x), x^3 - y^3)$. Formulations $(3.2)^-$ and $(3.2)^+$ have been employed in order to compute a numerical solution to the problem, without additional geometrical regularization, while the degrees of freedom without support in $\Omega \subset \tilde{\Omega}$ have been constrained to zero.

The relative H^1- and L^2- errors with respect to Ω_h are presented, the stabilization parameter γ_D^- is calibrated to a value of 300 and γ_D^+ to 50 - only the sixth part of γ_D^-, while $\rho = h^2$. Parameter γ_D^- has to be set to such a huge value due the unfitted grid, see also the discussion in Chapter 2. A four times globally refined Cartesian mesh has been used as a starting grid for the calculations. As can be seen from Table 4.2 the error-reduction rates are optimal in case of both variants of Nitsches method. The resulting graphical output is given in Picture 4.6. As linearization technique Newtons method has been used, while in each iteration step a preconditioned CG solver served as a linear solver. However, the Newton iteration converges to an absolute error of the non-linear residual of less than $tol = 10^{-12}$ in

h	#Dofs	$\|e_1^\rho\|_{0,\Omega_h}/\|u_1\|_{0,\Omega_h}$	Rate	$\|e_1^\rho\|_{1,\Omega_h}/\|u_1\|_{1,\Omega_h}$	Rate
symmetric Nitsche method					
0.2121	578	6.06e-02	-	1.57e-01	-
0.1061	2178	1.53e-02	1.98	8.21e-02	0.93
0.0530	8450	3.54e-03	2.11	4.12e-02	1.00
0.0265	33282	8.51e-04	2.06	2.09e-02	0.98
0.0133	132098	2.07e-04	2.04	1.05e-02	0.99
0.0066	526338	5.11e-05	2.02	5.29e-03	0.99
asymmetric Nitsche method					
0.2121	578	6.03e-02	-	1.59e-01	-
0.1061	2178	1.53e-02	1.98	8.31e-02	0.94
0.0530	8450	3.57e-03	2.10	4.12e-02	1.01
0.0265	33282	8.66e-04	2.04	2.12e-02	0.96
0.0133	132098	2.12e-04	2.03	1.06e-02	1.00
0.0066	526338	5.23e-05	2.02	5.35e-03	0.98

h	#Dofs	$\|e_2^\rho\|_{0,\Omega_h}/\|u_2\|_{0,\Omega_h}$	Rate	$\|e_2^\rho\|_{1,\Omega_h}/\|u_2\|_{2,\Omega_h}$	Rate
symmetric Nitsche method					
0.2121	578	5.35e-02	-	1.28e-01	-
0.1061	2178	1.00e-02	2.42	6.03e-02	1.08
0.0530	8450	2.53e-03	1.99	2.98e-02	1.02
0.0265	33282	6.02e-04	2.07	1.49e-02	1.00
0.0133	132098	1.47e-04	2.04	7.47e-03	1.00
0.0066	526338	3.58e-05	2.03	3.73e-03	1.00
asymmetric Nitsche method					
0.2121	578	5.25e-02	-	1.29e-01	-
0.1061	2178	9.89e-03	2.41	6.10e-02	1.08
0.0530	8450	2.52e-03	1.97	2.98e-02	1.03
0.0265	33282	6.06e-04	2.06	1.51e-02	0.98
0.0133	132098	1.48e-04	2.03	7.49e-03	1.01
0.0066	526338	3.63e-05	2.03	3.76e-03	0.99

Table 4.2: Relative $H^1(\Omega_h)$- and $L^2(\Omega_h)$-errors for test case 1, using both the symmetric and asymmetric Nitsche formulations $(3.2)^\mp$. Above: For solution component 1, below: For solution component 2 - in all cases showing optimal error-reduction rates.

at most four steps, showing the quadratic reduction rate expected for the method. As a pre-conditioner the LU decomposition of the Jacobian from the first iteration has been used for all iteration steps.

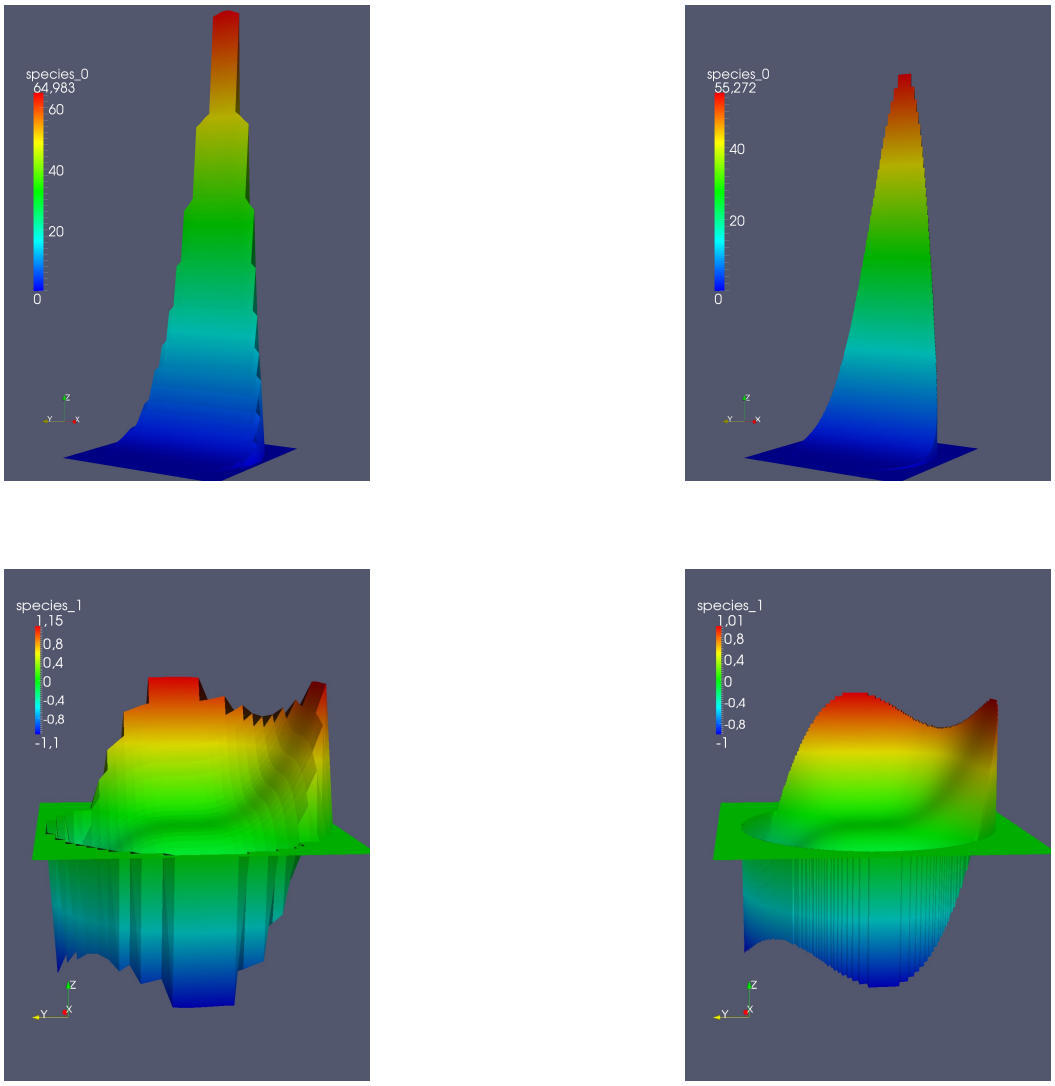

Figure 4.6: Finite element solution of test case 1, with $\tilde{\Omega} := (-1.2, 1.2)^2$. Left picture-row: Components of the finite element solution after five global refinements. Right picture-row: Finite element solutions after eight global refinements.

Test case 2

Now a first example treating a convection dominated problem is considered using the formulation $(3.9)^-$:

$$\begin{aligned} -\epsilon \triangle u + \boldsymbol{\beta} \cdot \nabla u &= f \text{ on } \mathbb{B}_1(0), \\ u &= 0 \text{ on } S^1, \end{aligned}$$

where $\epsilon = 10^{-5}$, $f = 1$ and $\boldsymbol{\beta} = (1, 0)$. The right picture in Figure 4.7 shows the solution resulting from the discrete regularized problem with additional SD enabled, while the left one is obtained using the (regularized) standard Galerkin method. In both cases it was $\gamma_D^- = 300$, $\rho = h^2$, the SD stabilization parameters chosen due to Chapter 3 with $\delta_0 = 1$. Both pictures show the discrete fictitious domain finite element solution on a six times globally refined mesh, the fictitious domain being $(-1, 1) \times (-1, 1)$. The right result is showing only small peaks next to the out-flow boundary, which is due to the choice of $\tilde{\Omega}$. The effect of the streamline diffusion is clearly observable. The left one on the same grid shows the typical over- and undershots applying in this situation, as no stabilization has been added.

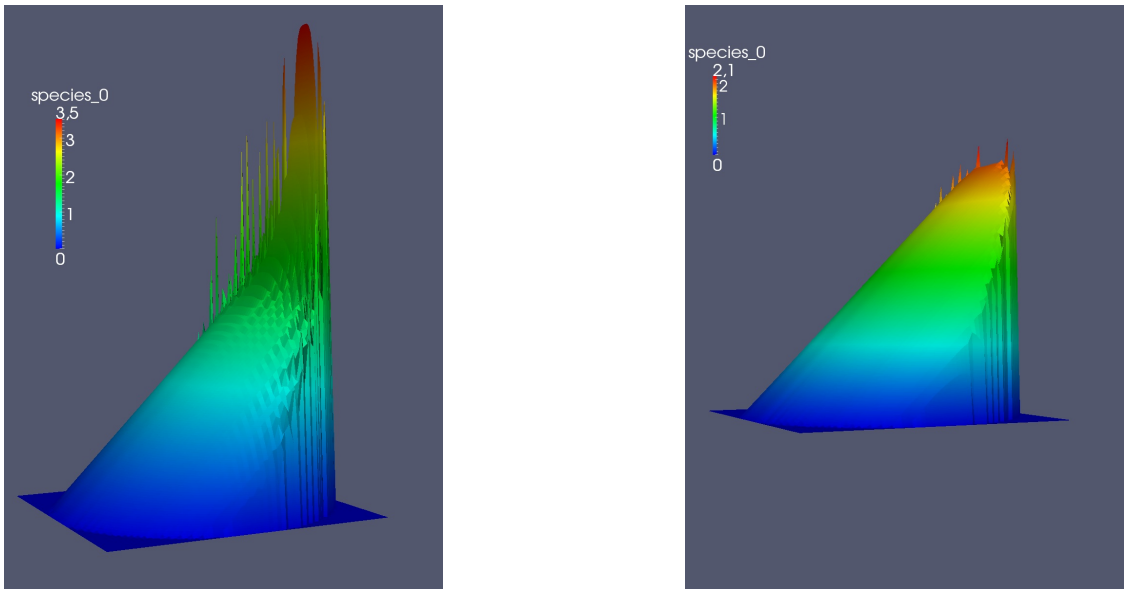

Figure 4.7: Right: Finite element solution of the convection dominated problem from test case 2, stabilised by SD - only small oscillations are observable. Left picture: Finite element solution of the same problem based on the standard Galerkin method, showing heavy over- and undershots.

Test case 3

In order to show the accuracy of the stabilized method, now a linear scalar test-case of a convection dominated RDC problem of the form

$$\begin{aligned} -\epsilon\triangle u + \boldsymbol{\beta}\cdot\nabla u + u &= f \text{ on } \mathbb{B}_1(0), \\ u &= g_D \text{ on } S^1, \end{aligned}$$

is presented, the stabilization parameters chosen as above. The data being defined such that

$$u(x,y) = \frac{1}{2}\left(1 - \tanh\left(\frac{x}{0.05}\right)\right),$$

which is a smoothed step-function and $\epsilon = 10^{-5}$. Again it is $\Omega = \mathbb{B}_1(0)$, while $\tilde{\Omega} := (-1.2, 1.2)^2$, $\gamma_D^- = 300$ and $\rho = h^2$, using formulation $(3.9)^-$.

As in case of the first test, a four times globally refined Cartesian mesh has been used as a starting grid. The results can be found in Figure 4.8 and Table 4.3, showing optimal order of convergence with respect to both the $H^1(\Omega_h)$- and $L^2(\Omega_h)$-norms. This is unless only $\mathcal{O}(h)$ can be granted a priori from (3.22), while in general $\mathcal{O}(h^{3/2})$ can be expected from the common estimations found in the literature. A higher order then expected is a circumstance often observed in case of the SD method, see [Zho97].

h	# Dofs	$\|e^\rho\|_{0,\Omega_h}/\|u\|_{0,\Omega_h}$	Rate	$\|e^\rho\|_{1,\Omega_h}/\|u\|_{1,\Omega_h}$	Rate
0.1945	289	1.81e-01	-	7.65e-01	-
0.0972	1089	3.55e-02	2.35	4.04e-01	0.92
0.0486	4225	8.76e-03	2.02	1.85e-01	1.12
0.0243	16641	2.04e-03	2.09	9.13e-02	1.02
0.0122	66049	4.79e-04	2.09	4.52e-02	1.01
0.0061	263169	1.15e-04	2.05	2.25e-02	1.00
0.0030	1050625	2.83e-05	2.03	1.12e-02	1.00

Table 4.3: Results for test case 3 using formulation $(3.9)^-$, showing optimal order of convergence measured in relative $H^1(\Omega_h)$- as well as relative $L^2(\Omega_h)$-norm.

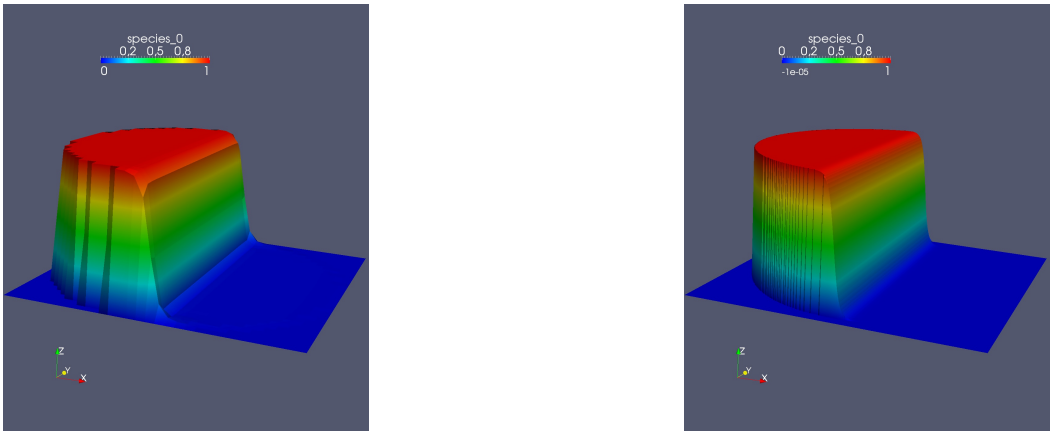

Figure 4.8: Resulting FE solution using $(3.9)^-$ for test case 3. Left: Solution on a five times globally refined grid. Right: Solution on an eight times globally refined grid.

Test case 4

At the end a numerical example treating the stationary Navier-Stokes problem is presented. It is $\Omega = \mathbb{B}_1(\mathbf{0})$ and:

$$(\boldsymbol{u}, p) : \begin{cases} -\triangle \boldsymbol{u} + (\boldsymbol{u} \cdot \nabla)\boldsymbol{u} + \boldsymbol{u} + \nabla p = \boldsymbol{f} & \text{in } \Omega, \\ \nabla \cdot \boldsymbol{u} = 0 & \text{in } \Omega, \\ \boldsymbol{u} = \boldsymbol{g} & \text{on } \Gamma. \end{cases} \tag{4.4}$$

The equation data are chosen such that

$$\begin{aligned} \boldsymbol{u} &= (\cos(x)\sinh(y), \sin(x)\cosh(y)), \\ p &= -\sin(x)\sinh(y) \end{aligned}$$

is the resulting analytical solution of the problem. The numerical tests have been accomplished using the FE formulations $(3.28)^-$ and $(3.28)^+$, while $\tilde{\Omega} = (-1.2, 1.2)^2$. A direct solver based on the UMFPACK library has been employed for solving the resulting system. A Quasi-Newton method based on an Oseen linearization has been used in order to linearize the problem. The iteration has been carried out until the non-linear residual was below $\frac{h^2}{100}$, which was reached in four steps at max. The regularization and penalty parameters, after fitting by hand, have been set to $\rho = \frac{h^2}{10}$,

while $\gamma_D^- = 300$ along with $\gamma_D^+ = 50$, $\gamma_1^- = 10$ and $\gamma_1^+ = 1$. The elementwise constant least squares stabilization parameters have been set to $\delta_K := h_K^2$ and $\gamma_{div} = h_K$, which coincides with the choice in [RST08] for the case $\nu = 1$.
Again starting point for the computations was a four times globally refined Cartesian grid. The results regarding the usual error analysis in case of the symmetric and asymmetric Nitsche method are shown in Table 4.4 and 4.5. A graphical output for both velocity $\boldsymbol{u}$ and pressure p is shown in Figure 4.9 and 4.10.

It can be seen that both methods match each other regarding accuracy, while the penalty parameter in case of the asymmetric Nitsche method can be chosen six times smaller then in the symmetric Nitsche method. The reason again is the unfitted grid along with the cut-integrations. The order of converge is almost optimal in case of the velocity variable regarding both the L^2- and H^1-norm with respect to Ω_h. The order of convergence in the $L^2(\Omega_h)$-norm for the pressure is suboptimal and about 1.7. As the a priori error bound in case of the linear symmetrical Stokes problem (3.35) grants only an order 1, this still is a good result.

h	# Dofs	$\|\boldsymbol{e}_u^\rho\|_{0,\Omega_h}/\|\boldsymbol{u}\|_{0,\Omega_h}$	rate	$\|\boldsymbol{e}_u^\rho\|_{1,\Omega_h}/\|\boldsymbol{u}\|_{1,\Omega_h}$	rate
symmetric Nitsche method					
0.2121	578	5.67e-03	-	3.64e-02	-
0.1061	2178	2.57e-03	1.16	1.51e-02	1.27
0.0530	8450	7.89e-04	1.70	7.12e-03	1.09
0.0265	33284	2.13e-04	1.89	3.46e-03	1.04
0.0133	132098	5.46e-05	1.96	1.69e-03	1.03
0.0066	526338	1.38e-05	1.99	8.44e-04	1.00
asymmetric Nitsche method					
0.2121	578	5.68e-03	-	3.53e-02	-
0.1061	2178	2.57e-03	1.15	1.50e-02	1.24
0.0530	8450	7.89e-04	1.70	7.08e-03	1.08
0.0265	33284	2.12e-04	1.89	3.45e-03	1.04
0.0133	132098	5.46e-05	1.96	1.69e-03	1.03
0.0066	526338	1.38e-05	1.99	8.43e-04	1.00

Table 4.4: Relative error-reduction rates for the velocity component for test case 4, measured in $(L^2(\Omega_h))^2$- and $(H^1(\Omega_h))^2$-norm. The results are showing almost optimal order of convergence in case of the symmetric and asymmetric Nitsche method, while using unfitted grids.

h	# Dofs	$\|e_p^\rho\|_{0,\Omega_h}/\|p\|_{0,\Omega_h}$	rate
symmetric Nitsche method			
0.2121	289	1.78e-01	-
0.1061	1089	6.93e-02	1.36
0.0530	4225	2.12e-02	1.71
0.0265	16639	6.34e-03	1.74
0.0133	66049	1.94e-03	1.71
0.0066	263169	6.19e-04	1.65
asymmetric Nitsche method			
0.2121	289	1.76e-01	-
0.1061	1089	6.87e-02	1.40
0.0530	4225	2.11e-02	1.70
0.0265	16639	6.31e-03	1.74
0.0133	66049	1.93e-03	1.71
0.0066	263169	6.16e-04	1.65

Table 4.5: Relative $L^2(\Omega_h)$-error-reduction rates for the pressure component for test case 4. The result shows an order of convergence of about 1.7 both for the symmetric and asymmetric Nitsche method. This is being less then optimal, but still good and of higher order.

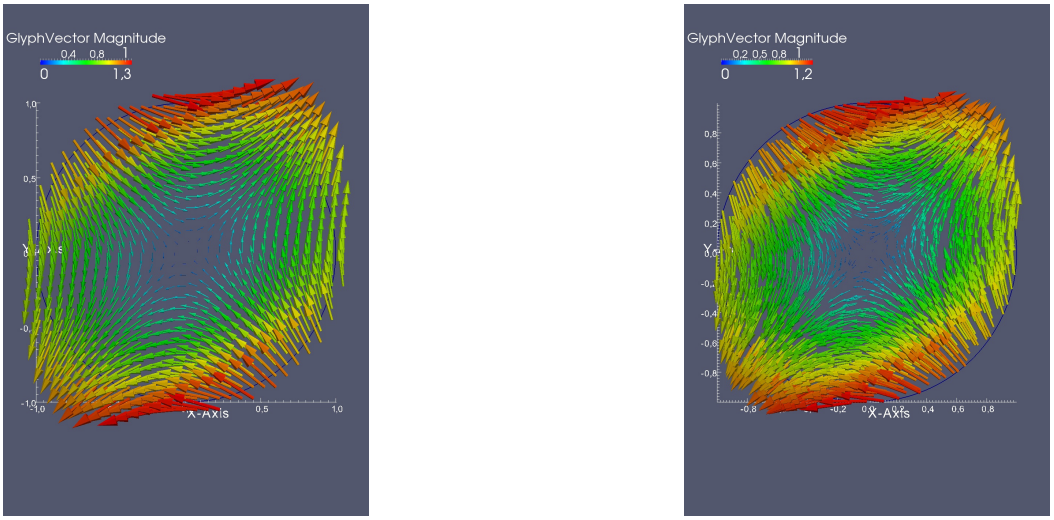

Figure 4.9: Numerical solution of the velocity variable for test case 4. Left: On a five times globally refined grid. Right: On an eight times globally refined grid. The degrees of freedom without support on Ω have been set to zero.

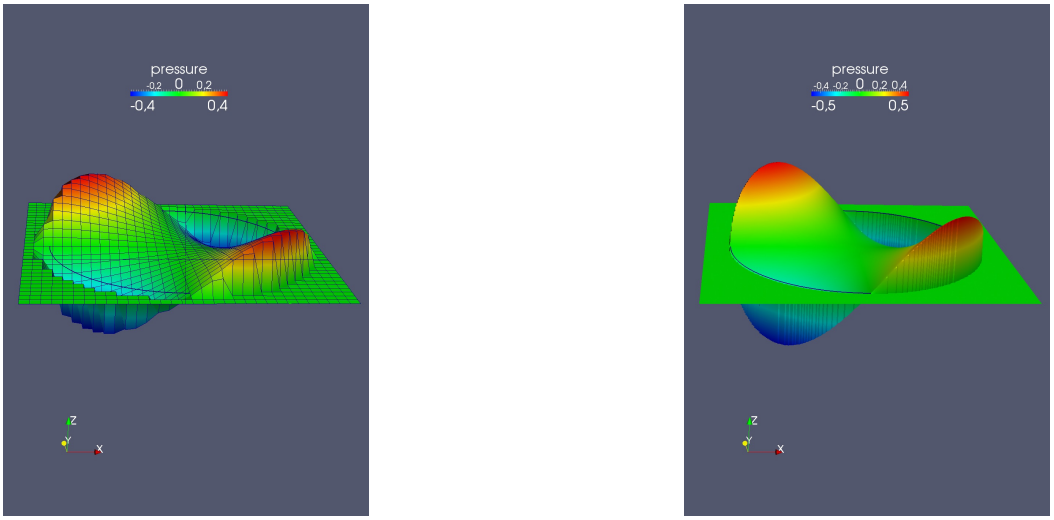

Figure 4.10: Numerical solution of the pressure variable for test case 4. Left: On a five times globally refined grid. Right: On an eight times globally refined grid. As in case of the velocity the degrees of freedom without support on Ω have been set to zero.

5 Applications

This chapter is addressed to various application in order to confirm, test and explore the possibilities of the new FD methods. The focus within the application chapter is solely on the asymmetric versions of Nitsches method, as stability is preferred over high accuracy in our case, while the accuracy tests from Chapter 4 suggest that in practice the difference in error-reduction is not very big. The outline is as follows: First, a benchmark example regarding steady laminar flow around a plain cylinder is presented, followed by a related unsteady flow problem using the same geometrical setting. Moreover, we treat Boussinesq equations on a series of differently shaped stationary domains. In the end a moving boundary value problem, again from the flow section, is presented.

5.1 Application I: Steady laminar flow around a plain cylinder

The flow around a plain cylinder at low Reynolds number is a widely used benchmark problem in fluid dynamics. This is for good reason, as it belongs to a class of standard problems in order to explore and test the flow around a rigid obstacle. The following test problem was originally launched by Turek et al. in [ST96] as test case 2D-1. Experimental data are available for comparison with plenty of existing numerical data, while the underlying geometry is relatively simple but complicated enough to provoke effects due to non-linearity as well as non-symmetry.

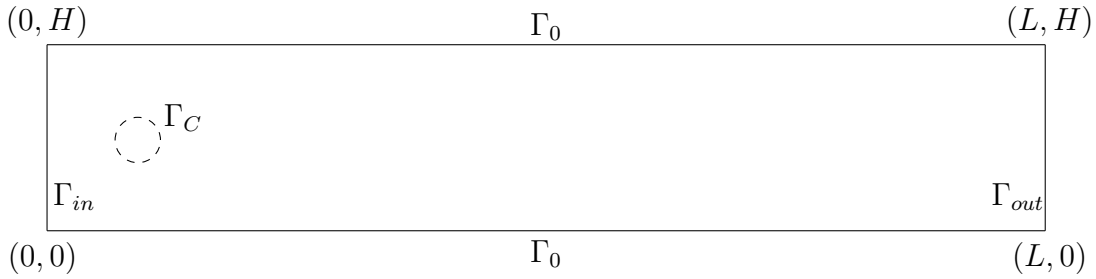

Figure 5.1: Geometry of the first application: Plain rectangular canal $\tilde{\Omega}$ with inflow boundary Γ_{in}, outflow boundary Γ_{out}, non-slip boundary Γ_0 and plain cylinder boundary Γ_C. Γ_C is described only implicitly by a characteristic zero level set.

5.1.1 Problem setting

The steady Navier-Stokes equations, in $\Omega := (0, L) \times (0, H) \setminus \mathbb{B}_R(P_m)$, in the form:

$$\begin{aligned} -\nu \triangle \boldsymbol{u} + (\boldsymbol{u} \cdot \nabla)\boldsymbol{u} + \nabla p &= \mathbf{0} \quad \text{in } \Omega, \\ \nabla \cdot \boldsymbol{u} &= 0 \quad \text{in } \Omega, \\ \boldsymbol{u} &= \mathbf{0} \quad \text{on } \Gamma_0 \cup \Gamma_C, \\ \boldsymbol{u} &= \boldsymbol{g} \quad \text{on } \Gamma_{in}, \\ \nu \partial_n \boldsymbol{u} - \mathbf{n} p &= \mathbf{0} \quad \text{on } \Gamma_{out}, \end{aligned} \tag{5.1}$$

$$H = 0.41,\ L = 2.2,\ R = 0.05,\ P_m = (0.2, 0.2),$$

$$U_m = 0.3,\ \boldsymbol{g} = (4U_m y(H - y)/H^2, 0),\ \nu = 10^{-3},$$

have to be solved. The benchmarking geometry is sketched in Figure 5.1.

5.1.2 Numerical details

The benchmarking geometry sketched in Figure 5.1 more exact shows the fictitious domain

$$\tilde{\Omega} := (0, L) \times (0, H)$$

for launching the FD method $(3.28)^+$ based on regularization and the asymmetric Nitsche method introduced in Section 3.3, but with the adjusted velocity and pressure spaces

$$\begin{aligned} \mathbf{V}_h &:= \left\{ \boldsymbol{v}_h \in \left(C^0(\overline{\tilde{\Omega}}) \right)^d : \ \boldsymbol{v}_h|_K \in \ (Q_1(K))^d \ \forall K \in T_h \right\} \cap \left(\boldsymbol{V}_0(\tilde{\Omega}) \right), \\ Q_h &:= \left\{ q_h \in C^0(\overline{\tilde{\Omega}}) : \ q_h|_K \in Q_1(K) \ \forall K \in T_h \right\}, \end{aligned}$$

with respect to a triangulation T_h of the nearly Cartesian mesh. The inhomogeneous inflow condition is enforced strongly in the first non-linear iteration step.
During the solution process, an Oseen linearization together with defect correction takes place, substituting in the non-linear convection term the current solution by the one from the last iteration step:

$$(\boldsymbol{u}_h^{i+1} \cdot \nabla)\boldsymbol{u}_h^{i+1} \longrightarrow (\boldsymbol{u}_h^{i} \cdot \nabla)\boldsymbol{u}_h^{i+1}.$$

For the numerical calculations we rely on the asymmetric Nitsche method $(3.28)^+$ for its better stability properties. No further geometrical regularization (see Section 4.2) takes place during the computations.

While in the original problem the cylinder, or a geometrically approximation of the latter, is cut out of the rectangular channel, the rigid obstacle is only represented by a characteristic level set function describing the closed circle. However, under normal circumstances, as the geometry is a relatively simple one, the usage of a boundary-fitted grid, covering the inner boundary in an adequate way, is to be preferred. But also it is a good test for a FD method.

The grids for numerical calculations stem from a standard rectangular triangulation of the whole channel (see Figure 5.2 picture above), which then is three times (see Figure 5.2 picture below), four and five times globally refined, while three local refinement steps take place next to the inner cylinder boundary. More exact: An

element is refined, if itself or its neighbour is cut by the boundary of the cylinder at some level during refinement. That is also what naturally happens in a boundary-fitted method, as the grid is much more refined next to the cylinder in order to give better a approximation of the curved cylinder boundary.

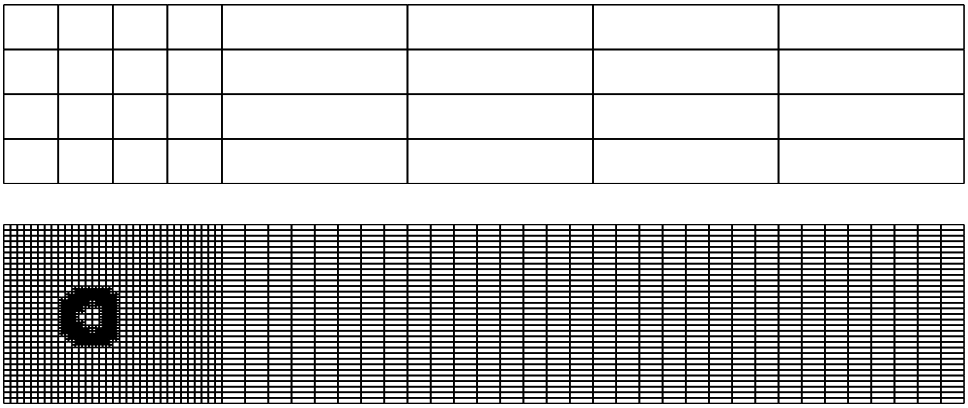

Figure 5.2: Above: Coarse pre-refined rectangular mesh for the fluid benchmark problem. Below: First computational mesh consisting of 4940 elements, originating from the one above by three times global followed by three times local refinement, in case an element or its neighbour is cut by the cylinder boundary at some level during refinement.

5.1.3 Benchmark quantities

Typical benchmark quantities are the following ones, being functionally dependent on the pressure p and the velocity $\boldsymbol{u}$:

$$J_{\triangle p}(p) := p(0.15, 0.2) - p(0.25, 0.2), \tag{5.2}$$

$$J_{drag}(\boldsymbol{u}, p) := \frac{2}{\overline{U}^2 D} \int_{\Gamma_C} \left(\left(2\nu(\nabla \boldsymbol{u} + \nabla \boldsymbol{u}^T) - p\boldsymbol{I} \right) \cdot \mathbf{n} \right) \cdot \boldsymbol{e}_x \, ds, \tag{5.3}$$

$$J_{lift}(\boldsymbol{u}, p) := \frac{2}{\overline{U}^2 D} \int_{\Gamma_C} \left(\left(2\nu(\nabla \boldsymbol{u} + \nabla \boldsymbol{u}^T) - p\boldsymbol{I} \right) \cdot \mathbf{n} \right) \cdot \boldsymbol{e}_y \, ds, \tag{5.4}$$

where $\overline{U} = 0.3$, yielding a Reynolds number $Re = \overline{U}D/\nu = 20$. It is $D = 2R$ and $\boldsymbol{e}_x,\ \boldsymbol{e}_y$ are the standard unit vectors in x- and y-direction. The drag coefficient J_{drag} defined by the boundary integral (5.3) physically gives a measure for the resistance of the body within the fluid environment, while the lift coefficient J_{lift} from (5.4) is related to the lift force regarding the flow around the cylinder.

It is possible to represent the drag and lift coefficients by area integrals, which is more robust and accurate compared to the boundary integral representation, see e.g. [BR06].
In order to do so, and to treat things on the numerical level, we first migrate to the discrete setting, i.e. Γ_C is substituted by the piecewise polynomial approximation $\Gamma_{C,h}$, characterised by the nodewise Finite Element interpolant of a signed distance function ϕ_{cyl}, describing Γ_C by its zero level set, see Subsection 4.1.
Then, in the resulting weak formulation of (5.1) the test function is set to be

$$\hat{\boldsymbol{v}}_{d,h}|_{\tilde{\Omega}} := (1+\phi_{cyl,h},0), \quad \hat{\boldsymbol{v}}_{d,h}|_{\partial\tilde{\Omega}} := \boldsymbol{0}, \tag{5.5}$$

$$\hat{\boldsymbol{v}}_{l,h}|_{\tilde{\Omega}} := (0,1+\phi_{cyl,h}), \quad \hat{\boldsymbol{v}}_{l,h}|_{\partial\tilde{\Omega}} := \boldsymbol{0}. \tag{5.6}$$

one after another.

Note that $\hat{\boldsymbol{v}}_{d,h}|_{\Gamma_{C,h}} = \boldsymbol{e}_x$, $\hat{\boldsymbol{v}}_{l,h}|_{\Gamma_{C,h}} = \boldsymbol{e}_y$ and these test functions are contained in $(H_0^1(\tilde{\Omega}))^2$. That along with backward partial integration, while utilizing consistency, including the divergence-free constraint, gives alternatively:

$$\begin{aligned} J_{drag,h}(\boldsymbol{u},p) &:= C\Big[\big(2\nu\boldsymbol{\epsilon}(\boldsymbol{u}),\boldsymbol{\epsilon}(\hat{\boldsymbol{v}}_{d,h})\big)_{\Omega_h} + \big((\boldsymbol{u}\cdot\nabla)\boldsymbol{u},\hat{\boldsymbol{v}}_{d,h}\big)_{\Omega_h} - \big(p,\nabla\cdot\hat{\boldsymbol{v}}_{d,h}\big)_{\Omega_h}\Big], \\ J_{lift,h}(\boldsymbol{u},p) &:= C\Big[\big(2\nu\boldsymbol{\epsilon}(\boldsymbol{u}),\boldsymbol{\epsilon}(\hat{\boldsymbol{v}}_{l,h})\big)_{\Omega_h} + \big((\boldsymbol{u}\cdot\nabla)\boldsymbol{u},\hat{\boldsymbol{v}}_{l,h}\big)_{\Omega_h} - \big(p,\nabla\cdot\hat{\boldsymbol{v}}_{l,h}\big)_{\Omega_h}\Big], \end{aligned}$$

where $C := \frac{2}{\overline{U}^2 D}$, $\boldsymbol{\epsilon}(\boldsymbol{v}) := \frac{1}{2}\big(\nabla\boldsymbol{v} + \nabla\boldsymbol{v}^T\big)$ and Ω_h is the polygonal implicitly given approximation of Ω, see again Section 4.1.
From this the drag and lift coefficients are computed on the discrete level in all the calculations.

5.1.4 Results and observations

The general behaviour of the fluid flow around the inner cylinder, along with the resulting pressure and pressure isolines, both on the fictitious domain given above, are shown in Figure 5.3. The pictures stem from numerical calculations on a mesh with 137,133 degrees of freedom. As expected, the velocity magnitude is highest on both sides of the inner boundary, while pressure maximum and minimum are to be found on nearly diametrical points regarding the cylinder geometry in downstream direction. A recirculation-zone is established downstream past the cylinder. Note that due to the slightly non-symmetric geometry the solution is also slightly non-

symmetric, while the solutions are smooth and the flow is laminar, as the Reynolds number is low.

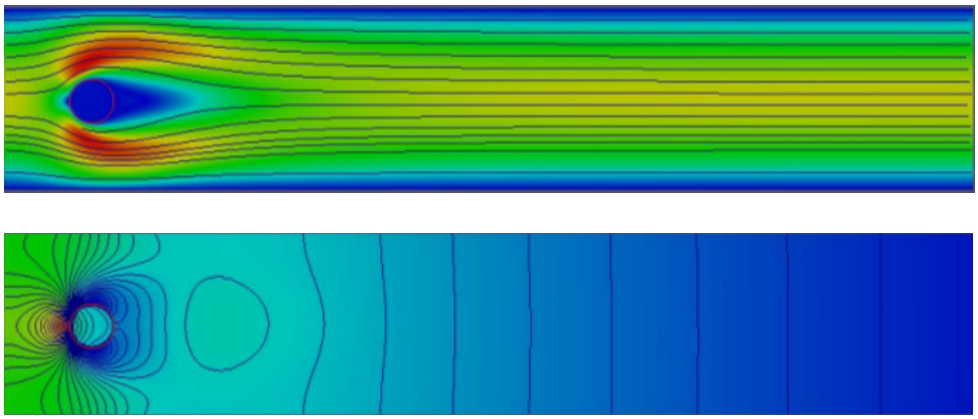

Figure 5.3: General behaviour of the solution from the fluid benchmark problem on the fictitious domain $(0, 2.2) \times (0, 0.41)$. Above: Velocity profile including streamlines; the resulting flow is laminar and slightly asymmetric due to the implicitly given geometry. Below: Resulting pressure profile along with pressure contours. Note that the velocity field as well as the pressure variable is defined on the whole mesh, as can be seen from the pictures. The cylinder is described by a characteristic level set function, with the zero level set contour shown in the pictures.

In order to minimize the number of parameters stemming from regularization, stabilization and penalization, first a lower bound for the parameter γ_D has to be identified. It turns out that setting $\gamma_D = 30$, along with $\gamma_1 = 1$, gives sufficiently good results, such that in all calculations within this section the Nitsche parameters are pinned to these values.
Next the choice $\delta_K := \delta_0 \min\{h_K, h_K^2/\nu\}$, $\gamma_{div} = \delta_K$ is made, which is a possible choice, with only one additional parameter δ_0 originating from stabilization. Within this configuration we first set $\rho := h_K^2/10$, a choice being ideal in case of the symmetric Stokes problem, see error estimate (3.35), and alternatively $\rho := h_K^3$. In order to find a good value for the parameter δ_0, several runs with $\delta_0 \in \{0.05, 0.1, 1\}$ are carried out.

As can be seen from Table 5.1, the results are in good agreement with the ones published in the original paper [ST96] regarding accuracy and the number of degrees of freedom to get a reliable result. Also the more recent results from [Win07] and

[SGW11] are matched. In [Win07] different FE pairings and continuous interior penalty stabilization have been used, while [SGW11] can be assigned to the fictitious domain context, using XFEM and domain decomposition.

The values of drag, lift and pressure difference coefficients are all together within the lower and upper bounds given in [ST96] after three refinement cycles, in case the parameters of the method are chosen well. While the choices $\rho = h_K^2/10$ and $\rho = h_K^3$ are sufficient along with $\delta_0 = 0.1$ or $\delta_0 = 0.05$, it can be seen from Table 5.1 that $\delta_0 = 1$ gives no results within the claimed accuracy. Furthermore, the functional values are quite sensitive especially regarding the choice of δ_0, which is not a big surprise.

$\gamma_D = 30, \gamma_1 = 1, \gamma_{div} = \delta_K = \delta_0 \min\{h_K, h_K^2/\nu\}$					
	$\#Dofs$	h_{min}	J_{drag}	J_{lift}	$J_{\triangle p}$
Lower bound			5.5700	0.0104	0.1172
Upper bound			5.5900	0.0110	0.1176
$\rho = h_K^2/10$ $\delta_0 = 1$	15693	0.00253	5.77830	0.01368	0.11375
	43554	0.00126	5.66564	0.00913	0.11515
	137133	0.00063	5.62323	0.01012	0.11657
	470925	0.00032	5.60420	0.00996	0.11724
$\rho = h_K^2/10$ $\delta_0 = 0.1$	15693	0.00253	5.65120	0.00969	0.11761
	43554	0.00126	5.60955	0.01244	0.11735
	137133	0.00063	**5.58971**	**0.01070**	**0.11738**
	470925	0.00032	**5.58307**	**0.01061**	**0.11742**
$\rho = h_K^2/10$ $\delta_0 = 0.05$	15693	0.00253	5.64743	0.00962	0.11803
	43554	0.00126	5.60776	0.01265	0.11751
	137133	0.00063	**5.58848**	**0.01075**	**0.11746**
	470925	0.00032	**5.58145**	**0.01052**	**0.11744**
$\rho = h_K^3$ $\delta_0 = 1$	15693	0.00253	5.69177	0.01186	0.11335
	43554	0.00126	5.64366	0.00859	0.11499
	137133	0.00063	5.61725	0.01004	0.11652
	470925	0.00032	5.60258	0.00993	0.11723
$\rho = h_K^3$ $\delta_0 = 0.1$	15693	0.00253	5.57879	0.00742	0.11722
	43554	0.00126	5.59040	0.01184	0.11719
	137133	0.00063	**5.58415**	**0.01064**	**0.11734**
	470925	0.00032	**5.58150**	**0.01058**	**0.11742**
$\rho = h_K^3$ $\delta_0 = 0.05$	15693	0.00253	5.57540	0.00733	0.117641
	43554	0.00126	5.58869	0.01205	0.11735
	137133	0.00063	**5.58293**	**0.01067**	**0.11743**
	470925	0.00032	**5.58067**	**0.01063**	**0.11744**

Table 5.1: Results for the benchmark quantities J_{drag}, J_{lift} and $J_{\triangle p}$ on four grids with increasing subtly; bounds taken from [ST96]. The Nitsche parameters have been fitted and pinned to $\gamma_D = 30$ and $\gamma_1 = 1$, while ρ, γ_{div} and δ_K are varied in order to find a reliable configuration of parameters. As can be seen, the choices $\gamma_{div} = \delta_K = \delta_0 \min\{h_K, h_K^2/\nu\}$ with $\delta_0 \in \{0.1, 0.05\}$ give accurate results in case $\rho \in \{h_K^2/10, h_K^3\}$. The number of degrees of freedom noteworthy to get results within the claimed accuracy is 137,133 using the grids described above. The minimal cell diameter of a triangulation T_h is $h_{min} := \min\{diam(h_K) : \ h_K \in T_h\}$.

5.2 Application II: Non-steady flow around a plain cylinder

Application II is addressed to non-steady flow around a plain cylinder. The general ability of the developed methods for simulating problems from this field shall be explored. In order to compare our results with reference solutions, known results to be found on the FEATFLOW homepage by Turek (cf. [Tur98]) are used, utilizing the same setting shown in Application I.

5.2.1 Problem setting

The non-steady Navier-Stokes equations, in $\Omega := \big((0,L)\times(0,H)\setminus\mathbb{B}_R(P_m)\big)\times I$, in the form:

$$\begin{aligned}
\partial_t \boldsymbol{u} - \nu\triangle\boldsymbol{u} + (\boldsymbol{u}\cdot\nabla)\boldsymbol{u} + \nabla p &= \mathbf{0} && \text{in } \Omega\times I,\\
\nabla\cdot\boldsymbol{u} &= 0 && \text{in } \Omega\times I,\\
\boldsymbol{u} &= \mathbf{0} && \text{on } \big(\Gamma_0\cup\Gamma_C\big)\times I,\\
\boldsymbol{u} &= \boldsymbol{g} && \text{on } \Gamma_{in}\times I,\\
\nu\partial_n\boldsymbol{u} - \mathbf{n}p &= \mathbf{0} && \text{on } \Gamma_{out}\times I,
\end{aligned} \tag{5.7}$$

have to be solved, with the same parameters L, H, R, P_m and ν already used in Application I, but setting $U_m = 3/2$. This finally yields a maximum Reynolds number $Re = 100$, which means leaving the laminar regime. The inflow condition is weighted by $\min\{1,t\}$ in order to provoke a distinct phase of oscillating flow. In addition we set $I := (0,5]$, as well as "starting from rest" initial conditions.

We will compare our results with the ones from [Tur98], where Turek shows how hard it is to get reliable solutions in case of flow problems even in case of such a relatively low Reynolds number. The drag and lift coefficients defined by (5.3) and (5.4) have to be computed in each time step.

5.2.2 Numerical details

The common Oseen linearisation is used to treat the resulting non-linear system, while utilizing the asymmetric Nitsche method $(3.28)^+$. As we have to deal with a time-dependent, non-linear problem, it is necessary to solve the resulting temporary linear systems hundreds of times. During the solution process, assembling the matrix and the LU-decomposition based pre-conditioner are the most time-consuming parts. So in addition the system matrix is assembled completely new only as long as the l_2-norm of the non-linear residual is bigger than 10^{-5}. This is a rather heuristic, but economical strategy, in order to shorten the computational times along with getting adequate solutions.

For time discretization the BDF2 scheme is used, with one implicit Euler step in the beginning for construction of a second starting value. As a fully implicit scheme is utilized, there are no too bad restrictions regarding the time step length. Nevertheless, the time step is chosen to be of about the same order of magnitude as the smallest cell-diameter resulting from space discretization.

The coarse grid, on which the final one for the computations is based on, is shown in Figure 5.4. The finer grids for the computations result from the coarse one by three and four times global, followed by three time local refinement, similar to Application I, while clearly the same definition for the discrete spaces is used in both cases. The first grid then has 5964 cells and 18861 degrees of freedom, while the second has 18,036 cells and 56034 degrees of freedom. The smallest cell-diameter appearing is $h_{min} \approx 0.00126$, such that the time step is set to $\triangle t = 0.001$.

The parameters for regularization, stabilization and penalization are set to $\rho = 0.1h_K^2$, $\gamma_{div} = \delta_K = 0.1h_K$, $\gamma_D = 50$ and $\gamma_1 = 5$, based on the observations of Application I. By choosing $\triangle t = \mathcal{O}(h_{min})$, this is a feasible choice in case of the stabilization parameter.

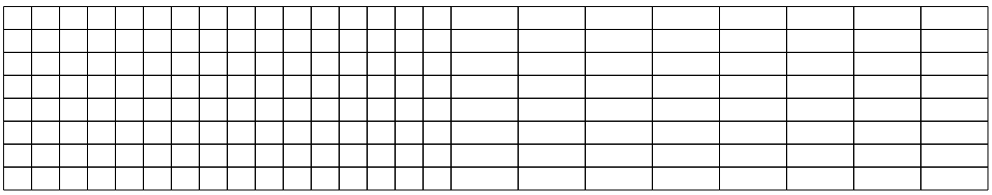

Figure 5.4: Pre-refined near Cartesian grid, used for testing the new methods.

5.2.3 Results and observations

First thing the results show is that an unsteady flow develops in time, including the effect of vortex shedding, see Figures 5.6 an 5.7.

We want to compare the solutions found by our FD based method on the grids described above to solutions by Turek.
Following Turek, a grid consisting of 130 cells, with 702 degrees of freedom, called the level-1 grid, while using non-conforming, non-parametric rotated bilinear FE, is used, see Figure 5.5. This initial-grid then is k times uniformly refined, the resulting mesh is called level-k grid. Turek used a fractional step theta scheme with adaptive-time stepping. He concludes that the first qualitative reliable result can be found by the level-4 solution, while higher level solutions roughly spoken yield more or less the same qualitative reliable result.

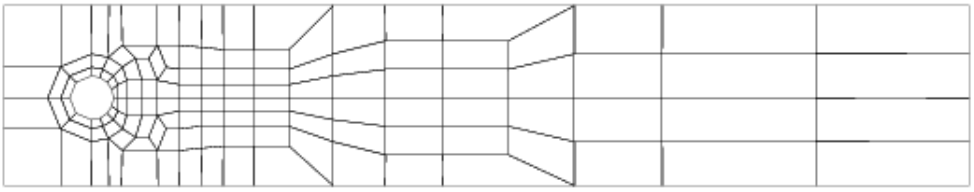

Figure 5.5: Boundary-fitted coarse a priori grid ("level-1") taken from [Tur98].

Picture 5.8 shows drag- and lift-coefficient over time plots, stemming from the own computations, along with those found by Turek on the level-4 (8,320 cells / 42,016 degrees of freedom) and the level-7 grid (532,480 cells / 2,665,728 degrees of freedom). The latter serving as the reference solution.

It has to be said that this two solutions have been selected, because the level-4 solution is the first one giving at least qualitatively reliable results compared to the reference solution, and at the same time being the one next to our own, taking into account the spacial resolution. Thus, it would be desirable if our solution would be at least in its range.

The results from our method slightly underestimate the drag compared to the reference solution, including a shift in the oscillation-frequency, see Figure 5.8. But

after the development of the unsteady state is reached, they are better then level-4 result by Turek, which for itself overestimates the drag in time. In case of the lift vs. time result, our results are between the level-4 and the reference solution after the oscillations are fully developed, but being closer to the reference solution. Moreover, the solution on the finer grid gives better results, which is not a big surprise.

In view of using a method from the fictitious domain context, where often mean values in case of drag and lift over time are taken for comparison after the fully developed oscillations phase is reached (see e.g. [YMUS99] and the literature therein), this is a very good result. In particular, it has been shown that the new methods are able to deal with unsteady flow problems in principle.

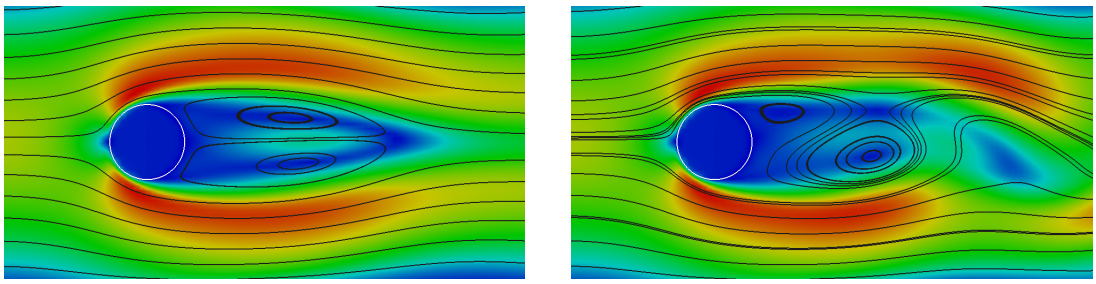

Figure 5.6: Velocity close-ups in the near wake of the inner cylinder. Left: Streamlines and velocity magnitude short-time after the flow is fully developed, showing a (nearly) laminar behaviour at first. Right: Instantaneous streamline and velocity-magnitude plot; vortex shedding appears.

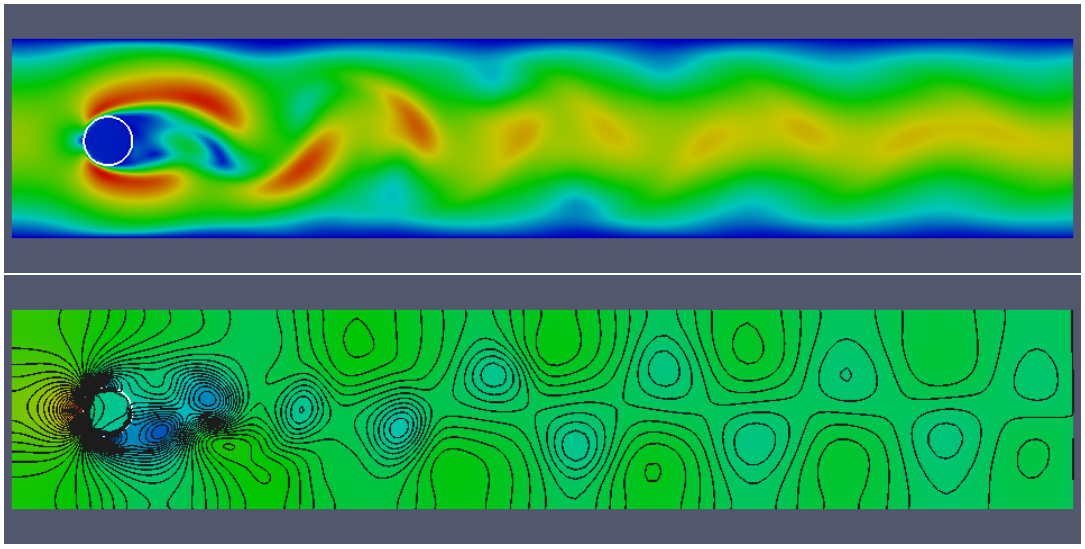

Figure 5.7: Velocity magnitude (above) and pressure-contours (below) at final time $T = 5$ in case of Application II.

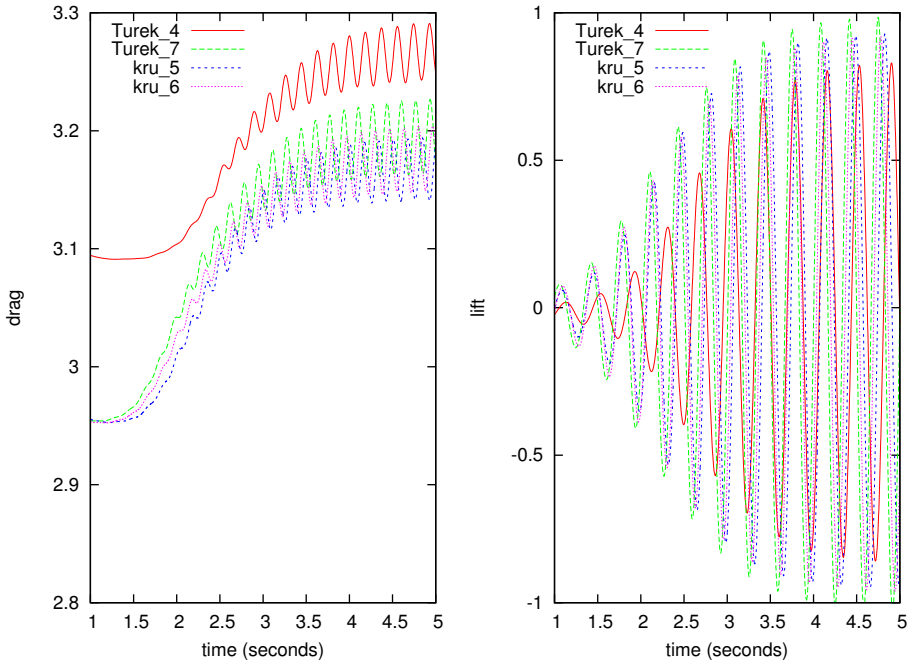

Figure 5.8: Drag and lift coefficient time plots indicate that the FD based methods give good results, without reaching the reference solution by Turek (Turek_7). The drag coefficient is slightly underestimated compared to the reference solution, but in a better range compared to the level-4 (Turek_4) solution by Turek. Here kru_5 indicates the result on the coarser and kru_6 on the finer computational mesh, the latter being superior to the kru_5 result by itself. Analogous things are valid in case of the lift.

5.3 Application III: Boussinesq equations on multi-connected domains.

Another application is the numerical treatment of the so called Boussinesq equations, meaning without much going into detail, that the Navier-Stokes equations are coupled with an equation for temperature.
At first we give a short review on what this system of equations is describing physically, followed by the illustration of a test case on the unit rectangle, in order to show the standard solution of the problem on a very simple domain for increasing Rayleigh numbers.
The highlight then is the presentation of results from exploring the possibilities of the proposed methods on the field of Boussinesq equations on geometrically complicated domains, i.e. placing obstacles inside the unit-rectangle, while changing the boundary conditions.

5.3.1 Description of the problem

As a basis for the model treated in this part of the work we assume $\tilde{\Omega} \subset \mathbb{R}^2$, with $\tilde{\Gamma} := \partial\tilde{\Omega}$ being partitioned into a Neumann- and a Dirichlet-part as usual. The Boussinesq equations then can be written in the non-dimensional form (see [Ran08]):

$$\partial_t \boldsymbol{u} - \frac{1}{Re}\triangle \boldsymbol{u} + (\boldsymbol{u}\cdot\nabla)\boldsymbol{u} + \nabla p = -\frac{Ra}{Re^2 Pr}\boldsymbol{g}T \quad \text{in } \tilde{\Omega}\times I, \tag{5.8}$$

$$\nabla\cdot\boldsymbol{u} = 0 \quad \text{in } \tilde{\Omega}\times I, \tag{5.9}$$

$$\partial_t T - \frac{1}{RePr}\triangle T + \boldsymbol{u}\cdot\nabla T = 0 \quad \text{in } \tilde{\Omega}\times I, \tag{5.10}$$

$$\boldsymbol{u} = \boldsymbol{0} \quad \text{on } \partial\tilde{\Omega}\times I, \tag{5.11}$$

$$T = T_D \quad \text{on } \tilde{\Gamma}_D\times I \quad , \quad \partial_n T = T_N \quad \text{on } \tilde{\Gamma}_N\times I \tag{5.12}$$

$$T = 0 \quad , \quad \boldsymbol{u} = \boldsymbol{0} \quad \text{in } \tilde{\Omega}\times\{0\}. \tag{5.13}$$

In this system, the triple of unknowns $(\boldsymbol{u}, p, T)$ consists of the usual pair $(\boldsymbol{u}, p)$ describing the flow pattern, which is driven only by the right hand side and thus by (normalized) gravity $\boldsymbol{g} = (0, -1)$ and the remaining unknown, the scalar temperature field T, as can be seen from equations (5.8),(5.11) and (5.13).

The temperature T is described by the heat equation (5.10), where the velocity $\boldsymbol{u}$ is part of the equation data driving the heat flow.

Besides the *Reynolds* number Re the relevant parameters appearing are:

- the *Prandtl* number Pr, being a material constant, more exact the ratio of kinematic viscosity and thermal conductivity. We set $Pr = 0.71$, which is the *Prandtl* number for atmospheric air,

- the *Rayleigh* number Ra, taking effectively the place of the Reynolds number, as it is the relevant factor for stability of the system. It is known that in the range $Ra < 10^8$ the resulting flow stays laminar, see [Has01]. Moreover, it can be written $Re = \frac{\sqrt{Ra}}{Pr}$.

The Boussinesq equations in this form circumstantiate a slowly evolving temperature field with constant density, while the temperature differences are relatively small, such that the overall description of the in general far more complicated heat-transfer process can be simplified, as several non-linear terms can be skipped for being (nearly) constant or very small. Besides that we are treating a form of so called natural convection, i.e. external sources influencing the system, besides the ones already given, are neglected. For more information see e.g. [Ran08].

What happens from the physically point of view is, that due to thermal expansion next to a heat source a buoyancy force appears, acting on the gas or fluid, transporting material upward, while next to a heat sink the material is transported downward. This interaction together with gravity causes a flow, in our case modelled by system (5.8)-(5.13).

In order to demonstrate and explore the ability of the proposed methods to deal with multi-connected domains, the Boussinesq equations and other akin ones, we concentrate on the following basic setting, see Figure 5.9: The (in general fictitious) domain $\tilde{\Omega}$ is the unit rectangle $\tilde{\Omega} := (0,1)^2$, with its left and right hand sides being heated or cooled, while no-heat-flux (perfect thermal insulation) conditions are supposed on the upper and lower sides. Such configurations are very common in the heat transfer community, and besides show a lot of interesting effects although the underlying geometry is very simple.

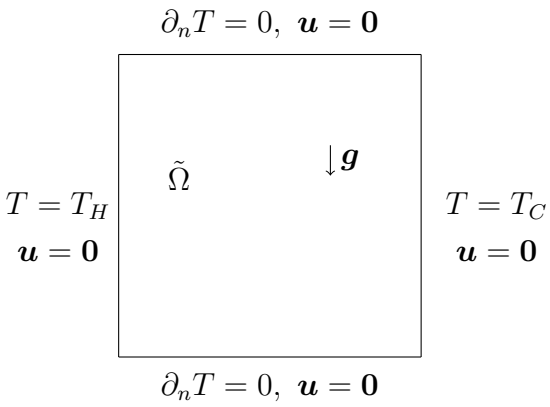

Figure 5.9: Original geometry and boundary conditions of the third application, it is $\tilde{\Omega} = (0,1)^2$. The left boundary is heated, while the right one is cooled. Perfect insulation takes place at upper and lower boundary.

5.3.2 Numerical details

The whole system is treated in a fully implicit monolithic manner, meaning that a non-linear defect-correction iteration, see Section 4.3, is applied in order to get an approximate solution for the whole system describing $(\boldsymbol{u}_h, p_h, T_h)$, while using the techniques developed in this work.

The common Oseen linearisation, introduced in the last subsections, together with substituting $\boldsymbol{u}_h^{i+1} \cdot \nabla T_h^{i+1}$ by $\boldsymbol{u}_h^{i} \cdot \nabla T_h^{i+1}$ in case of the heat equation, was used. In all cases i being the iteration index of the non-linear scheme. The system matrix is assembled completely new only as long as the non-linear residual is bigger than 10^{-3} in order to spare computation time, while getting adequate numerical solutions.

Time discretization happened by using the BDF2 scheme, with one implicit Euler step in the beginning for construction of a second starting value.

After experimentations with four, five and six times globally refined grids, with additional local refinement next to the Dirichlet boundaries, we choose a nearly Cartesian grid with 4480 elements and 18956 degrees of freedom for discretization in space as a basis for all computations, see left picture of Figure 5.10. As rather big temperature gradients appear on the left and right side of the domain, the elements on these sides are refined one time more then the rest, in order to avoid possible numerical oscillations due to the boundary layers, as well as for better resolution of the discontinuities in the boundary conditions. For the more complicated implicitly given domains the meshes are based on the original one, but one time locally re-

finement took place next to the inner boundary components additionally, see Figure 5.10, right picture, for the case of Application III.2 as an example. In all cases it is $h_{min} = \sqrt{2}/2^7 \approx 0.011$ and the time step is set to $\triangle t = 2/100$.

As criterion for reaching the steady-state we define:

$$\frac{\|(\boldsymbol{u}_h^n, p_h^n, T_h^n) - (\boldsymbol{u}_h^{n-1}, p_h^{n-1}, T_h^{n-1})\|_\infty}{\triangle t \cdot \|(\boldsymbol{u}_h^n, p_h^n, T_h^n)\|_\infty} \leq 2 \cdot 10^{-6},$$

where as always n is the time step number.

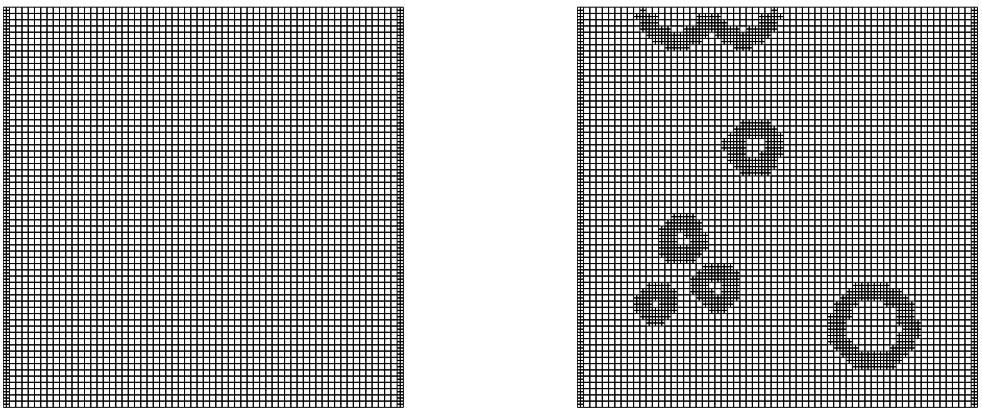

Figure 5.10: The heuristic refined rectangular meshes for the computations regarding Application III. Left: Grid for computations on the simple domain consisting of 4480 elements, refinement took place next to the left and right sides in order to prevent oscillations due to mild boundary layers. Right: Computational mesh for computations due to the multiple-connected domain of Application III.2, consisting of 5659 elements, originating from the left one by a single additional refinement next to the inner boundaries. These boundary components are described only by a characteristic level set function.

The FE formulations $(3.28)^+$ and $(3.2)^+$ with the underlying adjusted discrete spaces

$$\begin{aligned}
\mathbf{V}_h &:= \left\{ \boldsymbol{v}_h \in \left(C^0(\overline{\tilde{\Omega}}) \right)^d : \ \boldsymbol{v}_h|_K \in \ (Q_1(K))^d \ \forall K \in T_h \right\} \cap \left(H_0^1(\tilde{\Omega}) \right)^d, \\
Q_h &:= \left\{ q_h \in C^0(\overline{\tilde{\Omega}}) : \ \ q_h|_K \in Q_1(K) \ \forall K \in T_h \right\} \cap L_0^2(\tilde{\Omega}), \\
W_h &:= \left\{ T_h \in C^0(\overline{\tilde{\Omega}}) : \ \ T_h|_K \in Q_1(K) \ \forall K \in T_h \right\} \cap V_0(\tilde{\Omega}),
\end{aligned}$$

with respect to the triangulation T_h described above, are used for the numerical solution process.

The complicated multi-connected domains $\Omega := \tilde{\Omega} \setminus \overline{\omega}$ can be seen in the results-section: A set of convex obstacles ω in each case is cut out of the fictitious domain $\tilde{\Omega}$, but only by describing these sets by characteristic level set functions.

In the standard case the regularization-terms in $(3.2)^+$ and $(3.28)^+$ are suppressed, along with setting $\Gamma := \partial\Omega = \emptyset$.

The author is aware of a potential mass-conservation problem due to the utilization of stabilized FE, but this factor shall be not addressed here.

5.3.3 Results and observations

The grids described above are sufficient to resolve the instabilities within the given range of laminar non-steady problems, while qualitative good solutions result from the method. Streamline diffusion was disabled during the computations in case of the temperature equation.
In case of the Navier-Stokes part the Galerkin least squares stabilization was used nevertheless, as the discrete inf-sub condition still has to be circumvented, while the divergence-free constraint has to be resolved most properly. By using a space and time step of approximate the same order, an equal choice for the stabilization parameters δ_K and γ_{div}, as in the steady case, has been made, along with the well established choice $\delta_0 = 0.1$.

Now the results regarding several tasks are presented, first in text-form, followed by graphical output of the steady-state solutions found by our solver. The Rayleigh number is varied in case of the simple domain, while being fixed to $Ra = 10^5$ when treating the complex domains.

Application III.1

At first a look upon the "trivial domain" problem, that is $\omega = \emptyset$, see Figure 5.9. This on the one hand serves as a qualitative check whether the solver gives sufficient results, and on the other hand to get a feeling for effects appearing in context of the Boussinesq equations. Boundary conditions for the temperature are set to $T_H = 1/2$ and $T_C = -1/2$. Steady-state results are presented in Figure 5.11 in form of streamlines and temperature contours, with $Ra \in \{10^3, 10^4, 10^5\}$. The pictures show the typical behaviour in case of the chosen Rayleigh numbers, as can be seen from the literature (see e.g. [Ran08, Has01, KVL03]). The more Ra increases, the more complex the flow pattern gets, along with the temperature contours getting more and more distorted in flow direction.

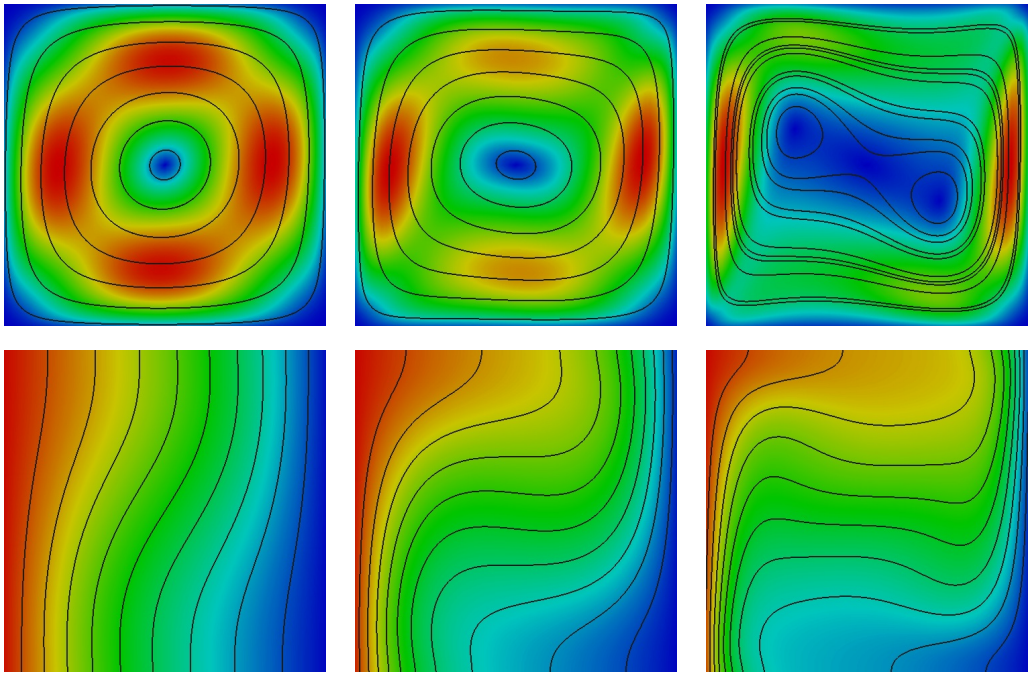

Figure 5.11: Results for velocity field (streamlines and magnitude, first line) and temperature distribution (contours and magnitude, second line) are presented in case of Application III.1 with $Ra = 10^3, 10^4, 10^5$ (from left to right column). Flow and temperature distribution show an increasing complexity for growing Rayleigh number Ra. The results shown are in very good qualitative agreement to those found in the literature.

Application III.2
This is the first task in order to deal with a complex multi-connected domain. The updated configuration is sketched in Figure 5.12. The original boundary conditions on $\partial\tilde{\Omega}$ are adopted from Application III.1, but a number of obstacles, described by the techniques developed in this work, have been placed within the domain. On each inner boundary component $\partial_n T = 0$ and $\boldsymbol{u} = \mathbf{0}$ are imposed weakly. The results are shown is Figure 5.13.

Velocity field and temperature contours are presented, showing the expected behaviour. The velocity field shows a more complex, mainly clockwise, rotation compared to the standard case in the first subapplication; including a shift of the recirculation zones. The obstacles are resolved well, while the weakly imposed non-slip conditions for $\boldsymbol{u}$ can be observed. The temperature contours show the influence of the perfect insulation at the implicitly given inner boundaries.

Application III.3
The next task deals with a non-slip/heated inner boundary, see Figure 5.14. The original boundary conditions of Application III.1 on $\partial\tilde{\Omega}$ are adopted again. The steady-state results can be observed in Figure 5.15.

What we see is a pretty symmetrical flow pattern as expected, along with two recirculation zones next to the inner boundary, and near the area of maximal velocity magnitude. The zero-boundary conditions $\boldsymbol{u} = \mathbf{0}$ are matched very good. The same is true for the inner Dirchlet conditions $T = 1/10$, which in interplay with the strongly imposed conditions on $\partial\tilde{\Omega}$ drive the flow, for his part deforming the temperature field.

Application III.4
At last we take a look on a situation where both left and right boundaries are cooled to zero, with perfect insulation on the upper and lower sides. The main task is that the only heat source now is at the implicitly given inner boundary. So the flow caused by the inner boundary conditions has to drive the system mainly. The situation is sketched in Figure 5.16, with three elliptical boundaries heated to $+1/10$.

The steady-state solution shows the expected slightly asymmetric flow behaviour caused by the heated inner boundary, with recirculation zones resulting from the interplay with the cooled outer boundary components, also reflected by the asymmetric temperature contours. At the inner ellipses the Dirchlet conditions are matched with high accuracy in case of both the temperature and the velocity.

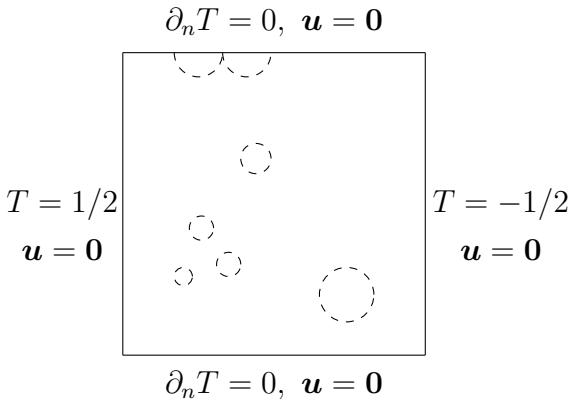

Figure 5.12: Geometry and boundary conditions of Application III.2, it is still $\tilde{\Omega} = (0,1)^2$. The left boundary is heated, while the right one is cooled. Perfect insulation takes place at upper and lower boundary, as well as on the inner boundary components. The latter are indicated by dashed lines.

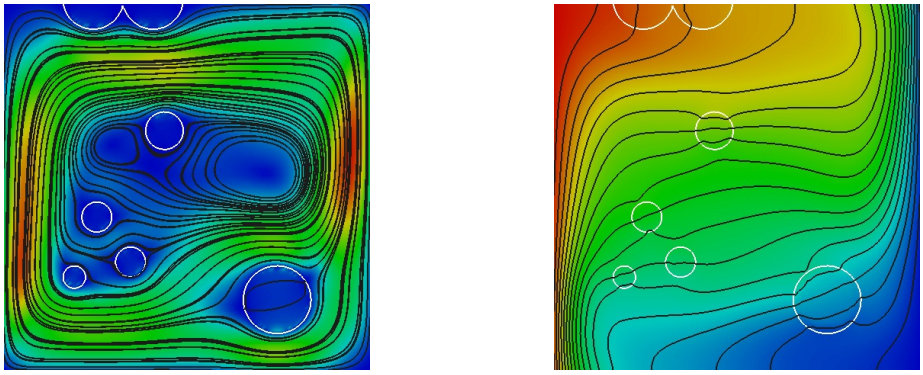

Figure 5.13: Velocity field (left) and temperature (right) at steady-state are presented in case of application III.2. The flow shows a more complex behaviour than in the undisturbed case, with the obstacle placed in the domain being flown around. The temperature contours show the influence of the perfect insulation at the inner boundaries, while the weakly imposed non-slip conditions for $\boldsymbol{u}$ can be observed.

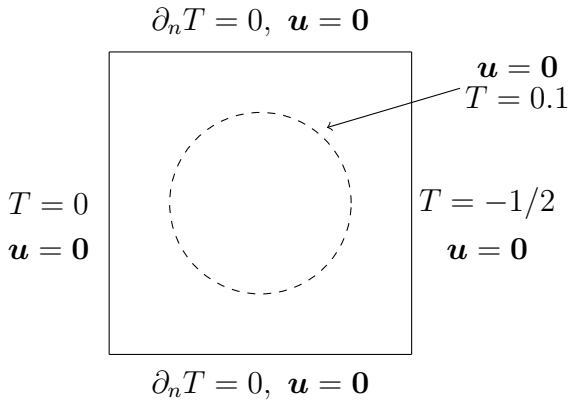

Figure 5.14: Geometry and boundary conditions of Application III.3. The left and right boundary components are cooled, while the inner boundary is heated. Perfect insulation takes place at upper and lower boundary. Non-slip conditions in case of velocity and a heated boundary for the temperature are imposed weakly at the inner boundary component.

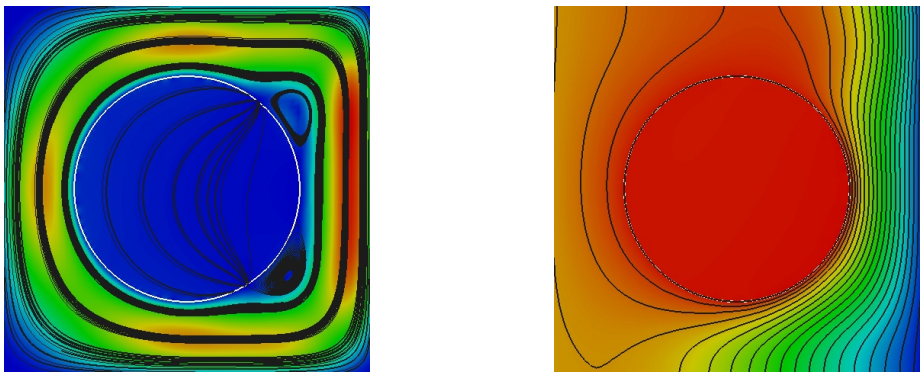

Figure 5.15: Steady-state velocity field (left) and temperature contours (right) are presented in case of Application III.3. The flow shows a mainly clockwise circulation as expected, with small recirculation zones next to the right side of the heated cylinder. The temperature contours are distorted in flow direction; the temperature 0.1-isoline matches nearly perfect with the cylinder boundary, while the weakly imposed non-slip conditions for $\boldsymbol{u}$ can be observed.

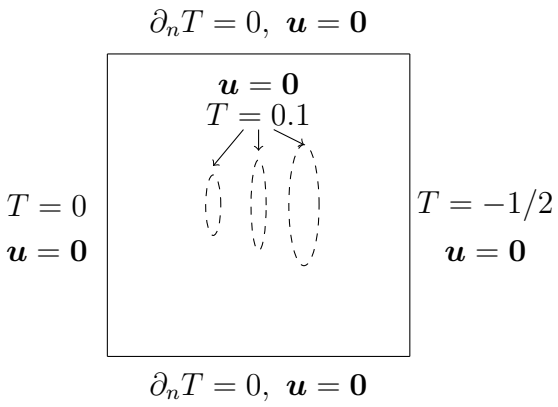

Figure 5.16: Geometry and boundary conditions of Application III.4. Heated inner boundaries and cooled left and right outer boundaries, the upper and lower components, as in all cases, being supposed as perfectly insulated.

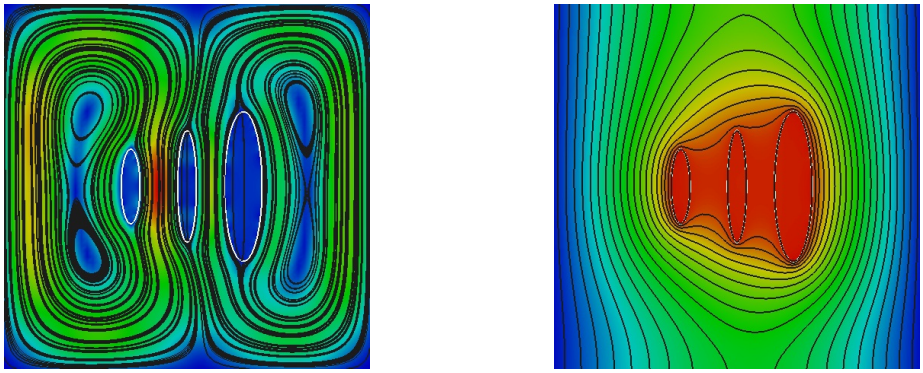

Figure 5.17: Steady-state results in case of Application III.4. Three heated ellipses within the domain and cooled left and right outer boundaries causing a flow and temperature variation in time, with the slightly asymmetric steady state shown in this picture. As always the complex flow pattern to the left and the temperature distribution to the right. The results make sense from the physical point of view, along with the inner boundary conditions regarding velocity and temperature are imposed with high accuracy.

5.4 Application IV: Incompressible viscous flow around a moving plain cylinder

As a non-steady application and experiment dealing with moving inner boundary, and thus in essence with a time-dependent domain, we estimate numerically the incompressible viscous flow around a moving plain cylinder in a box.

5.4.1 Problem setting

We follow Glowinski et al. [GPP96, GPP98], where the same configuration has been used in order to test fictitious domain techniques based on boundary and volume distributed Lagrange multipliers. The box is given by

$$\tilde{\Omega} := (-0.35, 0.9) \times (-0.5, 0.5),$$

the center $(x_c(t), y_c(t))$ of the disk

$$\omega = \omega(t) := \big\{(x, y) \in \mathbb{R}^2 : \ (x - x_c)^2 + (y - y_c)^2 \leq R^2; \ R = 0.125\big\},$$

representing the cylinder, is moving between $(0, 0)$ and $(0.5, 0)$ with period four along an a priori specified trajectory defined by

$$x_c(t) := 0.25 \left(1 - \cos\left(\frac{\pi t}{2}\right)\right), \quad y_c(t) := -0.1 \sin\left(\pi \left(1 - \cos\left(\frac{\pi t}{2}\right)\right)\right). \quad (5.14)$$

The geometry is sketched in Figure 5.18.

The mathematical formulation of the problem at hand on $\Omega = \Omega(t) := \tilde{\Omega} \setminus \omega(t)$ can be stated as:

$$\begin{aligned}
\partial_t \boldsymbol{u} - \nu \triangle \boldsymbol{u} + (\boldsymbol{u} \cdot \nabla)\boldsymbol{u} + \nabla p = \boldsymbol{0} \quad &\text{in} \quad \Omega \times I, \\
\nabla \cdot \boldsymbol{u} = 0 \quad &\text{in} \quad \Omega \times I, \\
\boldsymbol{u} = \boldsymbol{0} \quad &\text{on} \quad \Gamma_0 := \partial\tilde{\Omega} \times I, \\
\boldsymbol{u} = \boldsymbol{g} \quad &\text{on} \quad \Gamma := \partial\omega \times I, \\
\boldsymbol{u} = \boldsymbol{0} \quad &\text{in} \quad \Omega \times \{0\}.
\end{aligned} \quad (5.15)$$

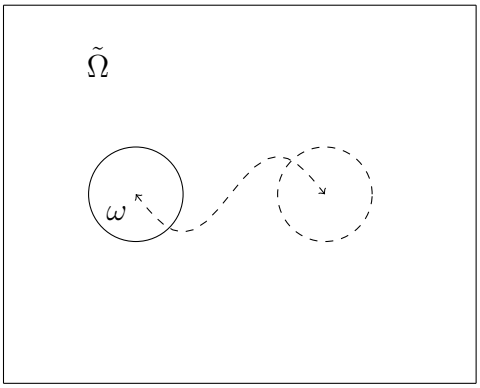

Figure 5.18: Geometry of the fourth application: Plain rectangular box $\tilde{\Omega} := (-0.35, 0.9) \times (-0.5, 0.5)$ with moving disk ω inside. The given periodic trajectory of the disk midpoint between $(0, 0)$ and $(0.5, 0)$ is indicated by dashed lines. The plain cylinder boundary is described only implicitly by a characteristic zero level set.

The inhomogeneous Dirichlet boundary-condition is given by

$$\boldsymbol{g} = \big(\dot{x}_c, \dot{y}_c\big) + \big(-(y - y_c)\pi, (x - x_c)\pi\big) \text{ on } \Gamma, \tag{5.16}$$

where $\dot{x}_c, \dot{y}_c$ indicate the time derivatives, such that $\boldsymbol{u}|_\Gamma$ coincides with the disk velocity while rotating counterclockwise at angular velocity π. This together with setting $\nu = 1/100$ gives a maximum Reynolds number of about 25.6. The only sources causing a non-trivial solution are disk movement and the time-dependent condition on the moving inner boundary.

5.4.2 Numerical details

For obvious reasons the FD techniques described in this work based on the asymmetric Nitsche method $(3.28)^+$ are used for the simulations. More exact, we will use formulation $(3.28)^+$ with the underlying FE spaces

$$\begin{aligned} \mathbf{V}_h &:= \left\{ \boldsymbol{v}_h \in \left(C^0(\overline{\tilde{\Omega}}) \right)^d : \ \boldsymbol{v}_h|_K \in \ (Q_1(K))^d \ \forall K \in T_h \right\} \cap \left(H_0^1(\tilde{\Omega}) \right)^d, \\ Q_h &:= \left\{ q_h \in C^0(\overline{\tilde{\Omega}}) : \ \ q_h|_K \in Q_1(K) \ \forall K \in T_h \right\} \cap L_0^2(\tilde{\Omega}), \end{aligned}$$

with respect to a Cartesian mesh based triangulation T_h, where the pressure space has been adjusted to the problem at state.

We prefer the asymmetric Nitsche method for its better stability purposes compared to the symmetric version, as the inner boundary of the cylinder cuts the unfitted grid in an uncontrolled manner, while moving in time. No additional geometrical regularization has been used. This approach is closer to the first mentioned paper [GPP96], where boundary distributed Lagrangian multipliers have been used in order to enforce the boundary condition on Γ.
A more adequate description would be to enforce the rigid body motion on the whole domain covered by the cylinder in each time step, which in fact is done for example in [GPP98], using a second moving triangulation of the disk.
More on volume Lagrange multiplier based fictitious domain methods can be found for example in [Glo03] and the literature therein. Alternatively, in Bönisch [Bön06] a single mesh is used along with a projection technique, after solving suitable ersatz problems with discontinuous coefficients on the whole domain, and adaptive refinement in each time step.

5.4.3 Results and observations

Several computations took place on four and five times globally refined grids, using adequate time steps. The implicit Euler and BDF2 2 schemes have been utilized for semi-discretization in time. The common defect correction based Oseen linearisation was used in order to solve the problem in each time step. For stabilization, after some experiments, the parameters for stabilization and penalization have been set to $\gamma_{div} = \delta_K = 0.1 \min\{h, h^2/\nu\}$, $\gamma_D = 40$, $\gamma_1 = 5$ and $\rho = 0.1h^2$. This is next to the choice in Application I, and in case of the stabilization parameter feasible, as the time step is chosen to be an $\mathcal{O}(h)$-term.
The results are in very good qualitative agreement to the ones in [GPP96], using this problem in order to get a feeling for such kinds of tasks, and to the ones in [GPP98], where volume and boundary distributed Lagrangian multiplier based methods have been compared on the same test configuration.
Thus, again following Glowinski [GPP96, GPP98], results in form of pressure contours along with the streamlines for the discrete times $4.5, 5, 5.5, 6, 6.5, 7, 7.5, 8$ are shown within the next figures, resulting from computations using the implicit Euler scheme with a time step $\triangle t = 1/64 \approx 0.0156$ on the five times uniformly refined grid, with $h \approx 0.041$. In case of the higher order time stepping scheme, the time parameter was doubled, while the results look similar to the ones from the Euler scheme.

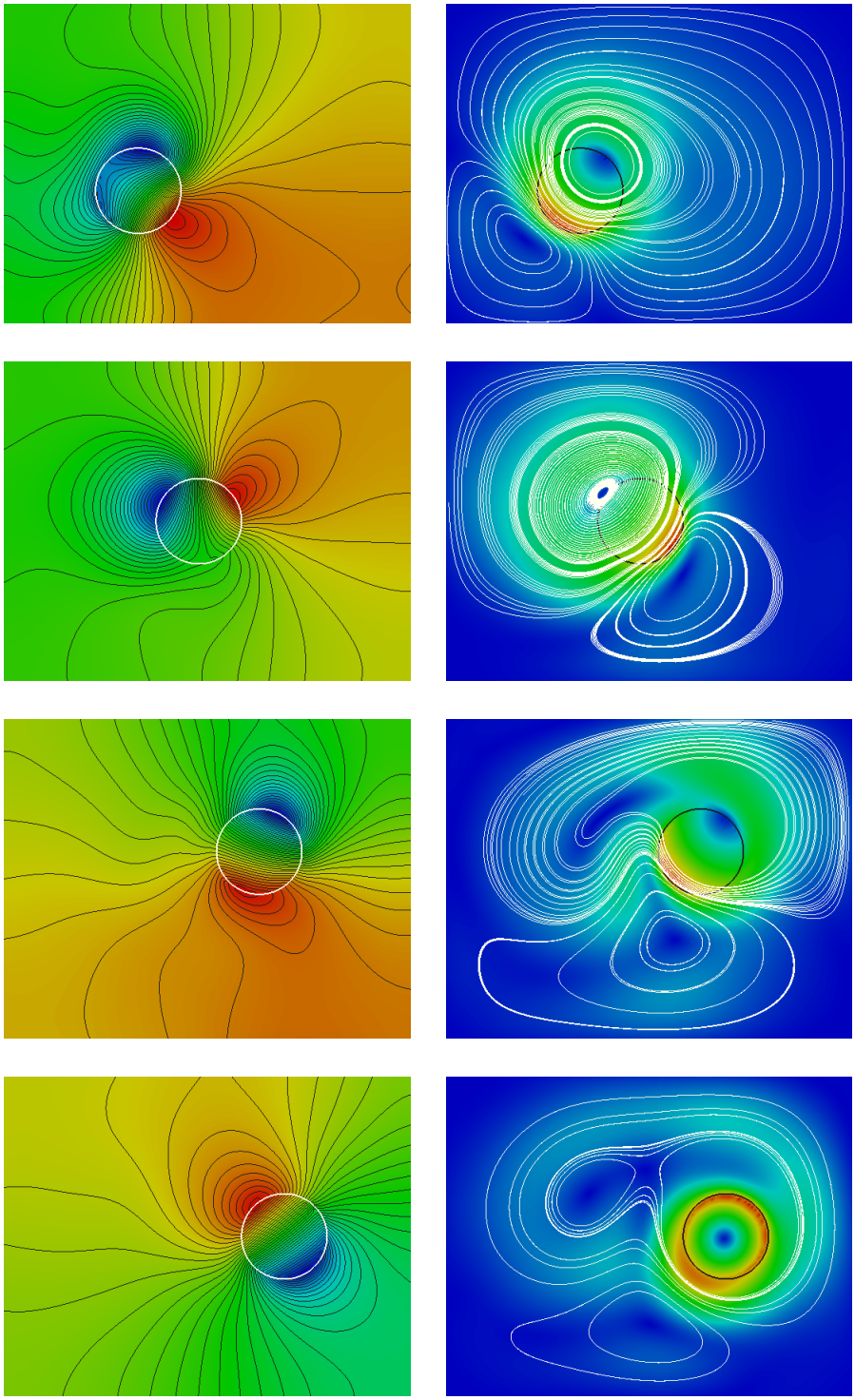

Figure 5.19: Resulting pressure contours (left column) and streamlines (right column) at times $t = 4.5, 5, 5.5, 6$ (from top to bottom) in case of Application IV. The disk is moving from left to right. The colour scale is from blue (low pressure/velocity magnitude) to red (high pressure/velocity magnitude).

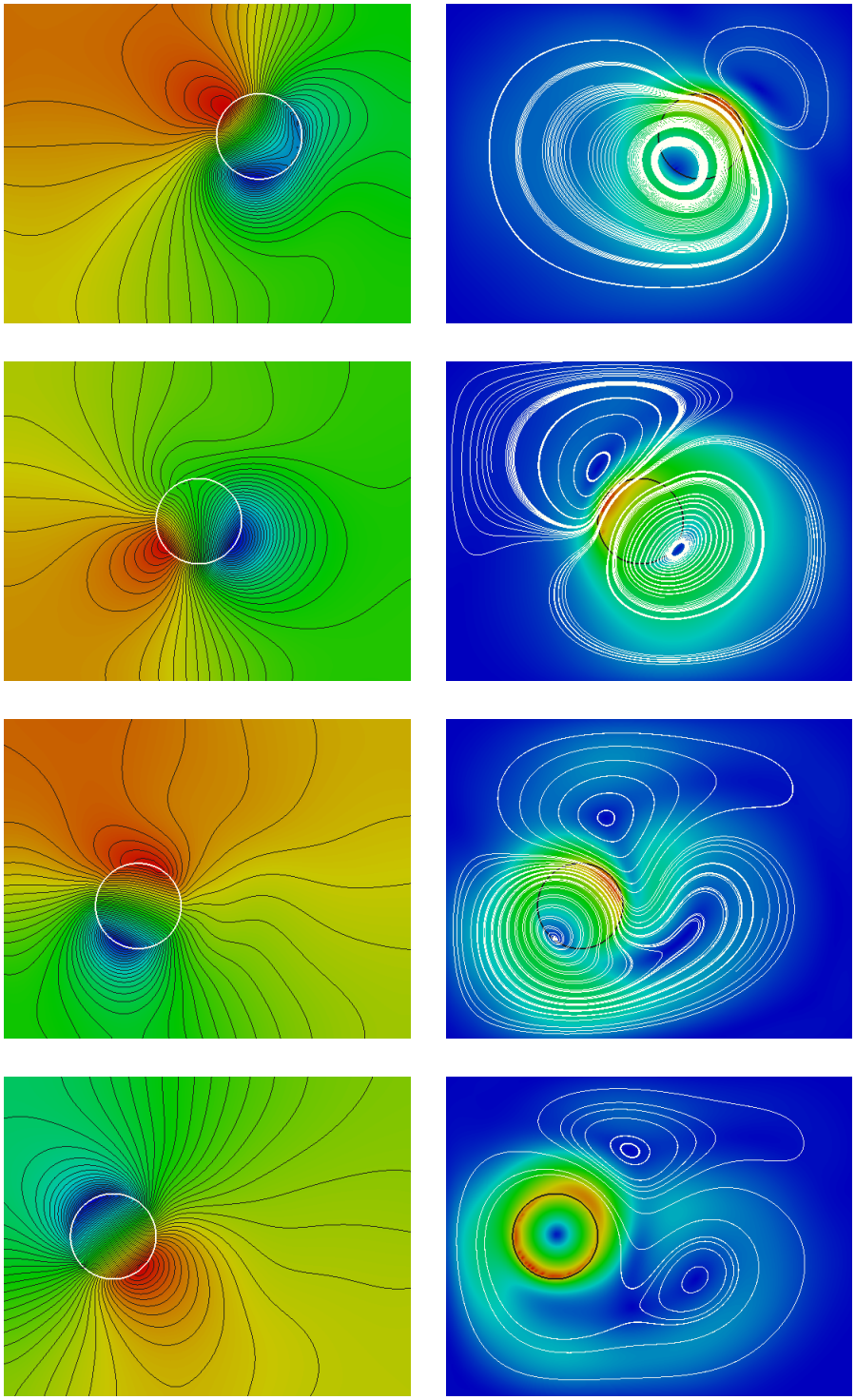

Figure 5.20: Resulting pressure contours (left column) and streamlines (right column) at times $t = 6.5, 7, 7.5, 8$ (from top to bottom) in case of Application IV. The disk is moving from right to left. The colour scale is from blue (low pressure/velocity magnitude) to red (high pressure/velocity magnitude).

6 Discussion and Outlook

New methods belonging to the fictitious domain context based on the results and ideas of Glowinski et al. have been introduced and analyzed, both from the continuous and the discrete numerical level. In two dimensions, symmetric and asymmetric variants of Nitsches method have been used in order to impose essential boundary conditions in case of the discrete methods.

The level set method was utilized in order to describe the underlying geometry the equations are defined on. The new methods are able to handle very general nonlinear, time-dependent and asymmetric problems of second order, including saddle point problems in form of Stokes and Navier-Stokes equations.

Numerical analysis took place regarding different special cases, separated with respect to the typical aspects causing trouble, as to mention dominant convection and circumventing a discrete inf-sub condition in case of the Stokes and Navier-Stokes equations. Streamline diffusion/Galerkin least squares stabilization was used to resolve such kind of problems.

From the practical point of view, the asymmetric versions of Nitsches method turn out to be preferable in view of their better stability properties, when used in the FD context, while numerical tests suggest, that not too much loss regarding the error reduction rates happens compared to the symmetrical versions.

The methods have been utilized successfully in view of several applications, after the task of numerical accuracy was addressed. In the field of laminar and unsteady plain flow problems, slow thermal convection on multi-connected domains, as well as in rigid body motion, the methods seem to have a lot of potential; at least in two dimensions, while it of course would be possible to generalize the method to three dimensions as well.

Among the advantages of the developed methods are the usage of standard FE spaces, along with the usage of Cartesian and near Cartesian grids, and high flexibility regarding the underlying geometry.

Drawbacks should be mentioned also: A lot of parameters for stabilization, regularization and so on have to be fitted. Besides that, the condition of the resulting discrete problems requires special care by a good pre-conditioner, in case of using an iterative solver.

Obvious possibilities for extensions and interesting future tasks would be in the field of three dimensional problems. In view of the last point, but also independent, exploration in the area of better local refinement strategies would be desirable. Especially strategies based on dual weighted residual techniques, in order to produce economical grids, could be a great enrichment.
Moreover, economical pre-condition techniques, for example from the multi-grid section, would be of interest.

Another obvious task to be mentioned is the exploration of fluid-structure interaction problems, like numerical simulation of glacier motion or droplet evaporation, using the methods at hand. In addition to that, fictitious domain approaches similar to the ones used in this work could potentially be applied to other common fields of continuum mechanics besides the Navier-Stokes equations.

Bibliography

[ABCM02] Douglas N Arnold, Franco Brezzi, Bernardo Cockburn, and L Donatella Marini. Unified analysis of discontinuous galerkin methods for elliptic problems. *SIAM Journal on Numerical Analysis*, 39(5):1749, 2002.

[AH09] K. Atkinson and Weimin H. *Theoretical Numerical Analysis*. Springer, 3. edition, 2009.

[Bab73a] I. Babuška. The Finite Element Method with Lagrangian Multipliers. *Numer Math.*, **20**:179–192, 1973.

[Bab73b] I. Babuška. The Finite Element Method with Penalty. *Mathematics of Computation*, **27**(122), April 1973.

[BBH10] R. Becker, E. Burman, and P. Hansbo. A hierarchical NXFEM for fictitious domain simulations. *CHALMERS PREPRINT 2010:24*, , 2010.

[BE86] J. W. Barrett and C. M. Elliott. Finite Element Approximation of the Dirichlet Problem Using the Boundary Penalty Method. *Numer. Math*, **49**:343–366, 1986.

[Bec02] R. Becker. Mesh adaption for Dirichlet flow control via Nitsche's method. *Commun. Numer. Meth. Engng*, **18**:669–680, 2002. (DOI: 10.1002/cnm.529).

[BF91] F. Brezzi and M. Fortin. *Mixed and hybride finite element methods*. Springer, 1991.

[BF09] Erik Burman and Miguel A. Fernández. Stabilization of explicit coupling in fluid–structure interaction involving fluid incompressibility. *Computer Methods in Applied Mechanics and Engineering*, 198(5–8):766 – 784, 2009.

[BH91] H. J. C. Barbosa and T. J. R. Hughes. The finite element method with Lagrangian multipliers on the boundary: circumventing the Babuska-

Brezzi condition. *Computer Methods in Mechanics and Engineering*, **85**(1):109–128, 1991.

[BH10a] E. Burman and P. Hansbo. Fictitious domain finite element methods using cut elements: I. A stabilized Lagrange multipier method. *Comput. Methods Appl. Mech. Eng.*, 2010. (2010), doi:10.1016/j.cma.2010.05.011.

[BH10b] E. Burman and P. Hansbo. Fictitious domain finite element methods using cut elements: II. A stabilized Nitsche method. *CHALMERS PREPRINT 2010:25*, 2010.

[BHK] W. Bangerth, T. Heister, and G. Kanschat. `deal.II` *Differential Equations Analysis Library,Technical Reference*. `http://www.dealii.org`.

[BHK07] W. Bangerth, R. Hartmann, and G. Kanschat. deal.II – a general purpose object oriented finite element library. *ACM Trans. Math. Softw.*, 33(4):24/1–24/27, 2007.

[BHS01] Roland Becker, Peter Hansbo, and Rolf Stenberg. A finite element method for domain decomposition with non-matching grids. Technical report, MATH. MODEL. ANAL. NUMER, 2001.

[BM97] I. Babuška and J. Melenk. The Partition of Unity Method. *International Journal for Numerical Methods in Engineering*, **40**:727–758, 1997.

[Bön06] S. Bönisch. *Adaptive Finite Element Methods for Rigid Particulate Flow Problems*. PhD thesis, Universität Heidelberg, 2006.

[BR06] M. Braack and T. Richter. Solutions of 3D Navier-Stokes benchmark problems with adaptive finite elements. *Computers and Fluids*, **35**(4):372–392, 2006.

[Bra98] M. Braack. *An Adaptive Finite Element Method for Reactive-Flow Problems*. PhD thesis, University of Heidelberg, 1998.

[Bra03] D. Braess. *Finite Elemente*. Springer, 3. edition, 2003.

[CB03] J. Chessa and T. Belytschko. An enriched finite element method and level sets for axisymmetric two-phase flow with surface tension. *Internat. J. Numer. Methods Engrg.*, **43**:50–67, 2003.

[CB09] R. Codina and J. Baiges. Approximate imposition of boundary conditions in immersed boundary methods. *International Journal for Numerical Methods in Engineering*, 2009.

[Dav04] Timothy A. Davis. Algorithm 832: Umfpack v4.3—an unsymmetric-pattern multifrontal method. *ACM Trans. Math. Softw.*, 30(2):196–199, June 2004.

[DBDV10] G. Dupire, J. P. Boufflet, M. Dambrine, and P. Villon. On the necessity of Nitsche term. *Applied Numerical Mathematics*, 60:888–902, 2010.

[Düc10] M. Dücker. *Numerical analysis of Cauchy-type problem arising in electrical engineering.* PhD thesis, University of Siegen, 2010.

[EB05] C. Engwer and P. Bastian. A Discontinuous Galerkin method for simulations in complex domains. *IWR-Preprint*, 2005.

[EGK08] C. Eck, H. Garcke, and P. Knabner. *Mathematische Modellierung.* Springer, 2008.

[GG95] V. Girault and R. Glowinski. Error Analysis of a Fictitious Domain Method Applied to a Dirichlet Problem. *Japan J. Indust. Appl. Math.*, (12):487–514, 1995.

[Glo03] R. Glowinski. *Numerical Methods for Fluids (Part 3).* North-Holland, 2003.

[GP92] R. Glowinski and W. T. Pan. Error estimates for fictitious domain/penalty/finite element methods. *Calcolo*, **29**(125), 1992.

[GPH+99] Roland Glowinski, Tsorng-Whay Pan, Todd I. Hesla, Daniel D. Joseph, and Jacques Périaux. A distributed lagrange multiplier/fictitious domain method for flows around moving rigid bodies: Application to particulate flow. *International Journal for Numerical Methods in Fluids*, 30(8):1043–1066, 1999.

[GPP96] R. Glowinski, T. W. Pan, and J. Periaux. Fictitious Domain Methods for Incompressible Viscous Flow around Moving Rigid Bodies. *Proceedings of MAFELAP 1996*, 1996.

[GPP98] R. Glowinski, T. W. Pan, and J. Periaux. Distributed Lagrange multiplier methods for incompressible viscous flow around moving rigid bodies. *Comput. Methods Appl. Mech. Engrg.*, **151**, 1998.

[GPWZ96] R. Glowinski, W. T. Pan, R. O. Wells, and X. Zhou. Wavelet and Finite Element Solutions for the Neumann Problem Using Fictitious Domains. *JOURNAL OF COMPUTATIONAL PHYSICS*, (126):40–51, 1996.

[GR94] C. Grossmann and H.-G. Roos. *Numerik partieller Differentialgleichungen*. Teubner Studienbücher, 2. edition, 1994.

[GR07] S. Gross and A. Reusken. An extended pressure finite element space for two-phase incompressible flows with surface tension. *Journal of Computational Physics*, (224):40–58, 2007.

[GT83] D. Gilbarg and N. S. Trudinger. *Elliptic Partial Differential Equations of Second Order*. Springer, 1983.

[Hac86] W. Hackbusch. *Theorie und Numerik elliptischer Differentialgleichungen*. Teubner, 1986.

[Han05] P. Hansbo. Nitsches method for interface problems in computational mechanics. *GAMM-Mitt*, 2005. 28/2 (2005) 183-206.

[Has01] H. Haschke. *Splitting-Techniken zur spektralen Approximation der Navier-Stokes- und Boussinesq-Gleichungen*. PhD thesis, Universität Essen, 2001.

[Hei08] C.-J. Heine. Finite element methods on unfitted meshes. *ISSN 1439-962-X, Preprint Nr. 9/2008-28.10.2008*, 2008. Universität Freiburg.

[HH03] Peter Hansbo and Joakim Hermansson. Nitsche's method for coupling non-matching meshes in fluid-structure vibration problems. *Computational Mechanics*, 32(1-2):134–139, 2003.

[HN81] C. W. Hirt and B. D. Nichols. Volume of fluid (vof) method for the dynamics of free boundaries. *J. Comp. Phys.*, 39:301–225, 1981.

[HS97] W. Hackbusch and S. A. Sauter. Composite Finite Elements for the approximation of PDEs on domains with complicated micro-structures. *Numer. Math.*, **75**(4), 1997.

[HY09] J. Haslinger and Renard Y. A new fictitious domain approach inspired by the extended finite element method. *SIAM Journal on Numerical Analysis*, **47**(2):1474–1499, 2009.

[Jim04] P. K. Jimack. Adaptive Algorithms for Free-Surface Flow Problems. 2004. http://www.scs.leeds.ac.uk/pkj/Papers/Conf-I/J04a.pdf.

[Joh90] C. Johnson. *Numerical solution of partial differential equations by the finite element method*. Cambridge University Press, 3. edition, 1990.

[JS08] M. Juntunen and R. Stenberg. Nitsches method for general boundary conditions. *Mathematics of Computation*, (S 0025-5718(08)02183-2), 2008.

[KVL03] Khalil Khanafer, Kambiz Vafai, and Marilyn Lightstone. Buoyancy-driven heat transfer enhancement in a two-dimensional enclosure utilizing nanofluids. *International Journal of Heat and Mass Transfer*, 46(19):3639 – 3653, 2003.

[LB08] A. J. Lew and G. C. Buscaglia. A discontinuous-Galerkin-based immersed boundary method. *Int. J. Numer. Meth. Engng.*, **76**(4), 2008.

[LGT81] J. L. Lions, R. Glowinski, and R. Tremolieres. *Numerical Analysis of Variational Inequalities*. North Holland, 1981.

[LN11] A. Lew and M. Negri. Optimal convergence of a discontinuous-alerkin-based immersed boundary method. *ESAIM:Mathematical Modelling and Numerical Analysis*, (45):651–674, 2011.

[LP00] M. Lai and C. S. Peskin. An immersed boundary method with formal second-order accuracy and reduced numerical viscosity. *Journal of Computational Physics*, **160**:705–719, 2000.

[MDB99] N Moes, J. Dolbow, and T. Belytschko. The Partition of Unity Method. *International Journal for Numerical Methods in Engineering*, **46**(1):131–150, 1999.

[Nit71] J. Nitsche. Über ein Variationsprinzip zur Lösung von Dirichlet-Problemen bei der Verwendung von Teilrämen, die keinen Randbedingungen unterworfen sind. *Abhandlungen aus dem mathematischen Seminar der Universität Hamburg*, **36**:9–15, Springer, 1971.

[OS88] S. Osher and J.A. Sethian. Front propagating with curvature-dependent speed: algorithms based on hamilton-jacobi formulations. *J. Comput. Phys.*, **79**:1–49, 1988.

[Pes72] C. S. Peskin. *Flow patterns around heart valves: A digital computer method for solving the equations of motion*. PhD thesis, Albert Einstein College of Medicine, 1972.

[Pes02] C. S. Peskin. The immersed boundary method. *Acta Numerica*, pages 479–517, 2002. DOI: 10.1017/S0962492902000077.

[PS08] Daniel Peterseim and Stefan A. Sauter. The composite mini element - coarse mesh computation of stokes flows on complicated domains. *SIAM J. Numer. Anal.*, 46:3181–3206, September 2008.

[PS09] D. Peterseim and S. Sauter. Finite Element Methods for the Stokes Problem on Complicated Domains. , 2009.

[QV94] A. Quarteroni and A. Valli. *Numerical approximation of partial differential equations*. Springer Verlag, Berlin, 1994.

[QV05] A. Quarteroni and A. Valli. *Domain Decomposition Methods for Partial Differential Equations*. Clarendon Press, Oxford, 2005.

[Ran06] R. Rannacher. Numerische Mathematik 2. *Vorlesungsskriptum SS 2006*, 2006.

[Ran08] R. Rannacher. Numerische Mathematik 3. *Vorlesungsskriptum WS2004/2005*, 2008.

[Rec06] M. Rech. *An adaptive two-scale approach to the non-conforming approximation of Dirichlet problems on complicated domains*. PhD thesis, Universität Zürich, 2006.

[RST08] H.-G. Roos, M. Stynes, and L. Tobiska. *Robust Numerical Methods for Singularly Perturbed Differential Equations*. Springer, 2. edition, 2008.

[SCMB01] N. Sukumar, D. L. Chopp, N. Moes, and T. Belytschko. Modeling holes and inclusions by level sets in the extended finite-element method. *Computer Methods in Applied Mechanics and Engineering*, **190**(46-47):6183–6200, 2001.

[Set99] J.A. Sethian. *Level Set Methods and Fast Marching Methods*. Cambridge University Press: Cambridge, UK, 2. edition, 1999.

[SFSO97] Mark Sussman, Emad Fatemi, Peter Smereka, and Stanley Osher. An improved level set method for incompressible two-phase flows. *Computers and Fluids*, 27:663–680, 1997.

[SGW11] Shadan Shahmiri, Axel Gerstenberger, and Wolfgang A. Wall. An xfem-based embedding mesh technique for incompressible viscous flows. *International Journal for Numerical Methods in Fluids*, 65(1-3):166–190, 2011.

[ST96] M. Schäfer and S. Turek. Benchmark computations of laminar flow around a cylinder. *Technical report, Universität Heidelberg*, **Preprint SFB 359**, 1996.

[Ste95] R. Stenberg. On some techniques for approximating boundary conditions in the finite element method. *Journal of Computational and Applied Mathematics*, (63):139–148, 1995.

[Ste98] R. Stenberg. MORTARING BY A METHOD OF J.A. NITSCHE. *Computational Mechanics*, 1998.

[Str71] A.H. Stroud. *Approximate calculation of multiple integrals*. Prentice-Hall, 10. edition, 1971.

[SZ90] Ridgway L. Scott and Shangyou Zhang. Finite Element Interpolation of Nonsmooth Functions Satisfying Boundary Conditions. *Mathematics of Computation*, 54(190):483–493, 1990.

[Tur98] S. Turek. The 'DFG-Benchmark 1995/6': Channel flow around a circle at Re=100, 1998. http://www.mathematik.uni-dortmund.de/ featflow.

[Win07] C. Winkelmann. *INTERIOR PENALTY FINITE ELEMENT APPROXIMATION OF NAVIER-STOKES EQUATIONS AND APPLICATION TO FREE SURFACE FLOWS*. PhD thesis, Ecole Polytechnique Federale de Lausanne, 2007.

[YMUS99] T. Ye, R. Mittal, H.S. Udaykumar, and W. Shyy. An Accurate Cartesian Grid Method for Viscous Incompressible Flows with Complex Immersed Boundaries. *J. Comp. Phys.*, **156**:209–240, 1999.

[Zho97] G. Zhou. HOW ACCURATE IS THE STREAMLINE DIFFUSION FINITE ELEMENT METHOD? *Mathematics of Computation*, **66**(217):31–44, January 1997.